Spring 2014

Synthesis of radioactive and nonradioactive nanostructures through radiolytic and wet chemistry

Jessika Viviana Rojas Marin

Department: Mining and Nuclear Engineering

SYNTHESIS OF RADIOACTIVE AND NONRADIOACTIVE NANOSTRUCTURES THROUGH RADIOLYTIC AND WET CHEMISTRY

by

JESSIKA VIVIANA ROJAS MARIN

A DISSERTATION

Presented to the Faculty of the Graduate School of the

MISSOURI UNIVERSITY OF SCIENCE AND TECHNOLOGY

In Partial Fulfillment of the Requirements for the Degree

DOCTOR OF PHILOSOPHY

in

NUCLEAR ENGINEERING

2014

Approved by
Carlos H. Castano, Advisor
Hyoung-Koo Lee
Saed Mirzadeh
Shoaib Usman
Xin Liu

PUBLICATION DISSERTATION OPTION

This dissertation consists of five papers that have been prepared in the style utilized by the CRC Press, Journal Radiation Physics and Chemistry, Materials Letters, Journal of Radioanalytical and Nuclear Chemistry and Radiochimica Acta. The first article, Production of metal nanoparticles on carbon nanotubes by gamma irradiation, has been published Chapter 22 in Radiation Synthesis of Materials and Compounds, Kharisov, Ed(s) B. I. Kharissova, O. V., Mendez, U. Pages 491 to 505, February 6, 2013 by CRC Press. The second, synthesis of rhenium oxide nanoparticles (RexOy) by gamma irradiation has been published in the Journal of Radiation physics and Chemistry,volume 99, June 2014, Pages 1–5. The third, radiation-assisted synthesis of iridium and rhodium nanoparticles supported on Polyvinylpyrrolidone, has been submitted for publication to the Journal of Radioanalytical and Nuclear Chemistry. The fourth, radiolytic synthesis of iridium nanoparticles onto carbon nanotubes, was submitted for publication in the Journal of Nanoparticle Research. Finally, the fifth, synthesis and characterization of lanthanum phosphate nanoparticles as carriers for radium isotopes, will be submitted to the Journal of Radiochimica Acta.

ABSTRACT

In this work the synthesis of non radioactive and radioactive nanoparticles (NPs) through radiolytic and wet chemistry was studied. Non radioactive NPs of rhenium, iridium, and rhodium were synthesized from aqueous solutions containing the metal salt precursors by gamma irradiation. The solutions were irradiated to generate reducing species that led to the nucleation and growth of the nanoparticles. Amorphous rhenium oxide nanoparticles with average sizes ranging from 10 nm to 55 nm were obtained. Metallic iridium and rhodium nanoparticles were produced in polyvinyl-pyrrolidone (PVP) having narrow particle size distributions and average particle sizes from 2 nm to 6 nm. The stability of the NPs in PVP was explained based on the interaction of the metal with both of the functional groups, C-N and C=O, of the PVP. Iridium NPs supported on carbon nanotubes were also synthesized by gamma irradiation. The NPs were finely distributed on the surface of the nanotubes. The nanoparticle yield was found to increase with the radiation dose and the precursor concentration.

The synthesis of radioactive NPs, specifically lanthanum phosphate containing ^{223}Ra and ^{225}Ra isotopes, was carried out in aqueous media using a precipitation method. The NPs crystallized in rhabdophane structure with a mean particle size of 3.4 nm and 6.3 nm for core and core-2shells respectively. The ability of $LaPO_4$ NPs to retain the isotopes within their structure was investigated. It was found that core NPs retained up to 88% of the activity over a period of 35 days. It was also found that the addition of two $LaPO_4$ shells to the core NPs increases the retention ability up to 99.99%. This fact suggests that $LaPO_4$ NPs are potential carriers of radium isotopes for targeted alpha therapy.

ACKNOWLEDGMENTS

I would like to express a sincere gratitude to my advisor Dr. Carlos H. Castano for his guidance and support during the development of this project. I would also like to thank the members of the committee Dr. Shoaib Usman, Dr. Saed Mirzadeh, Dr. Xin Liu, and Dr. Hyoung-Koo Lee for all the advice they provided me for the completion of this work. I would further like to thank Dr. Stoyan Toshkov from University of Illinois Urbana-Champain, Nuclear Engineering Department who kindly helped me with the sample irradiation.

This dissertation could not have been done without funding opportunities from Nuclear Engineering Department, the Energy Research and Development Center (ERDC), the Materials Research Center (MRC) and the Research Board at the Missouri University of Science and Technology. Additional funding by the Medical Radioisotope Program, Nuclear Security and Isotopes Technology Division and the Center for Nanophase Materials Sciences (CNMS) at Oak Ridge National Laboratory is gratefully acknowledged.

Most especially, I owe my husband Carlos E. and my family members for the encouragement that enabled me to complete this process. Thanks to my friends in Rolla all those who accompanied me during this time.

TABLE OF CONTENTS

LIST OF ILLUSTRATIONS

Page

PAPER I

PAPER II

PAPER III

PAPER IV

PAPER V

SECTION

LIST OF TABLES

Page

SECTION

1. INTRODUCTION

1.1. SCOPE OF THE WORK

The current applications of ionizing radiation and its relationship with nanotechnology is an area that has gained special attention in the recent years. Figure 1.1 shows some of the fields where ionizing radiation and nanotechnology are combined for specific applications. On one side, the use of ionizing radiation is becoming a potential alternative for the controlled synthesis of nanostructures, modification of nanostructure properties, and development of new nanomaterials characterization techniques. On the other side, the application of nanomaterials in nuclear waste management, nuclear medicine as isotope carriers, and radiation detection is of growing interest. The main two topics of this work are framed in Figure 1.1: the use of ionizing radiation for the controlled synthesis of nanostructures and the use of nanomaterials as isotope carriers for nuclear medicine.

The synthesis of supported and unsupported transition metals nanoparticles with accurate control on nanoparticles size and distribution is an important area in nanotechnology. Since their chemical and physical properties are highly dependent of their final geometry. Among the transition metal nanoparticles, rhenium (Re), iridium (Ir), and rhodium (Rh) are being actively investigated in catalysis. Current synthesis methods involve the reduction of transition metal salt precursors, electrochemical synthesis, and physical vapor deposition, among others. These methods involve the use of

specific chemicals as reducing agents and/or controlled atmospheres. The use of gamma irradiation may provide a straightforward strategy to synthesize transition metal nanoparticles.

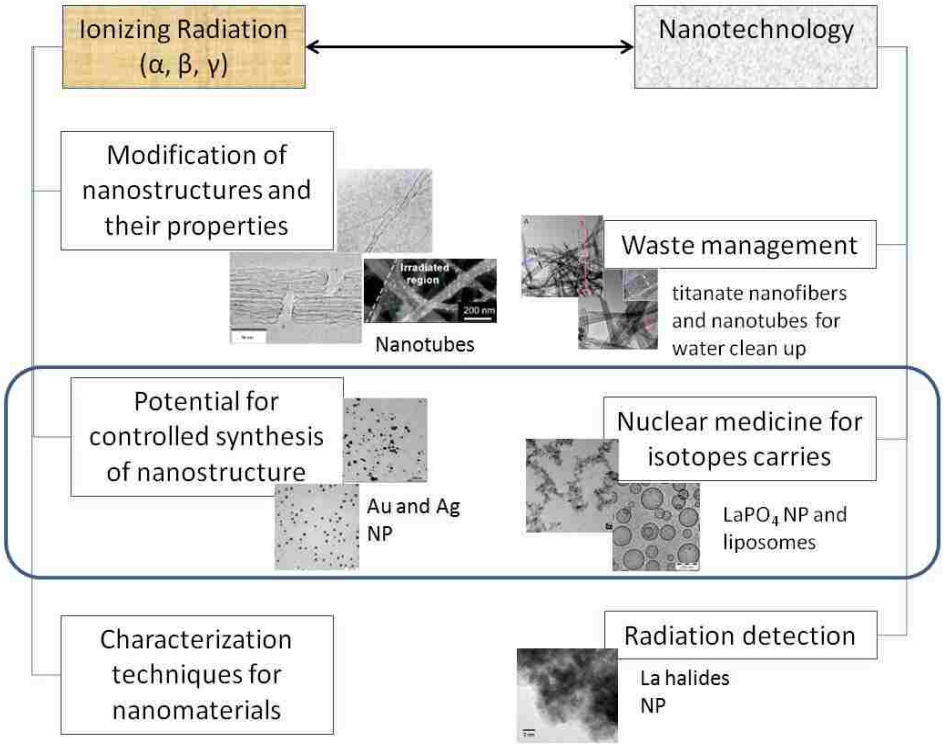

Figure 1.1. Ionizing radiation and nanotechnology: methods and applications.

The use of nanomaterials as carriers for radioisotopes have shown potential applications in targeted radioimmunotherapy (RIT), targeted alpha therapy (TAT), and medical diagnostic imaging. This approach aims to overcome the global radiotoxicity of the radionuclides and associated daughters, one of the main limitations of TAT. If the

decay products are not sequestered at the target site, they can travel and deliver a potentially toxic dose to unwanted tissues and organs. Among several isotopes, ^{223}Ra is currently used to treat symptomatic bone metastases due to its high affinity with calcium, the main constituent of bone tissue. However, this fact also limits the use of ^{223}Ra to target other tissues. Hence, the development of appropriate carriers to deliver ^{223}Ra to other sites is required.

Synthesis of biocompatible nanomaterials has become essential for the design and fabrication of drug delivery and imaging systems. Inorganic nanomaterials are of special importance due to their size-shape dependent properties that make them suitable for a variety of applications. In this group of nanomaterials, lanthanide phosphates possess remarkable physical and chemical properties that are well-suited for biomedical applications. These materials are also known for their high resistance to radiation damage. Lanthanide phosphate NPs are therefore promising candidates as carriers for α and β emitters in RIT, TAT, and imaging applications.

1.2. RESEARCH OBJECTIVES

From the research topics previously described, two main goals were addressed. Initially, a new method to synthesize supported and unsupported Re, Rh, and Ir nanoparticles was developed using gamma irradiation. In addition, lanthanum phosphate nanoparticles containing ^{225}Ra and ^{223}Ra were produced by wet chemistry. Also, their ability to retain the isotopes within their structure was evaluated *in vitro*.

1.3. SUMMARY OF RESULTS

The results of this research have been described in detail in following sections of this dissertation which consist of five manuscripts. A brief description of the manuscripts included in this document is presented below.

- *PAPER I. Production of metal nanoparticles on carbon nanotubes by gamma irradiation*. In this chapter, the use of gamma irradiation as a promising technique to decorate carbon nanotubes with metal nanoparticles is discussed in detail. The influence of parameters such as dose, dose rate, and stabilizer concentration on particle size is addressed. Carbon nanotubes are a good option as solid supports for metallic nanoparticles as they have a high chemical and thermal stability. Numerous methods have been designed to synthesize metallic nanoparticles on the surface of carbon nanotubes. These methods often involve the use of chemicals that serve as reducing agents of metal precursors and the need for controlled atmospheres, temperature and Pressure. Gamma irradiation however, has shown several advantages for the synthesis of nanomaterials, more specifically, metallic nanoparticles. First, it is a single step process and the synthesis is carried out in water, avoiding the need for specific solvents. Second, gamma irradiation of water generate powerful reducing species, thus no additional chemicals are needed to reduce metal ions. Third, the process is carried out at ambient temperature and pressure.

- *PAPER II. Synthesis of rhenium oxide nanoparticles (RexOy) by gamma irradiation.* Rhenium, as part of the transition metals group is of great interest in the areas of catalysis, electronics, and coatings. In this study, radiolytic reduction of perrhenate ions in a mixture of water-isopropanol led to nucleation and growth of nanoparticles in the form of Re_xO_y with average sizes between 10 nm and 55 nm. The size and size distribution of the resulting nanoparticles were investigated as a function of the precursor concentration and irradiation dose. The nanoparticles were found to be amorphous.

- *PAPER III. Radiation-assisted synthesis of iridium and rhodium nanoparticles supported on polyvinylpyrrolidone (PVP).* Iridium (Ir) and rhodium (Rh), similar to rhenium, have gained significant attention for catalytic applications. The control over their particle size and distribution is essential for their catalytic performance. The controlled synthesis of rhodium and iridium nanoparticles carried out by gamma irradiation of aqueous solutions of metal precursor salts in the presence of PVP as stabilizer is reported in this section. The nanoparticles were synthesized at various precursor and stabilizer concentrations and doses of 20, 40 and 60 kGy. It was found that irradiation of the solutions at 60 kGy evidenced a complete reduction of the ionic species. Nanoparticles with narrow particle size distributions were obtained at metal precursor/PVP concentrations of 6 mM / 0.3 mM and 6 mM / 3 mM for iridium and rhodium nanoparticles irradiated at 60 kGy. At these conditions, the formation of iridium and rhodium nanoparticles, having average sizes of 2.4 nm and 2.6 nm respectively, was

accomplished. The interaction of the nanoparticles with the polymeric matrix was found to be through the functional groups, C-N and C=O, of the PVP.

- *PAPER IV. Radiolytic synthesis of iridium nanoparticles onto carbon nanotubes.* In this section, a method to deposit iridium nanoparticles on multiwalled carbon nanotubes using gamma irradiation is presented. Carbon nanotubes were found to be an appropriate support to synthesize iridium nanoparticles with average particle size from 4.5 nm to 3.4 nm. The particles, prepared at various absorbed doses, precursor and surfactant concentration were found to be homogeneously distributed on the nanotubes surface. The concentration of nanoparticles was found to increase with increasing the absorbed dose from 0 to 60 kGy. Increasing the precursor concentration from 3 mM to 6 mM did not have a significant effect on the particle size; instead, it led to a higher concentration of nanoparticles on the nanotubes. Ir-C bonds were not detected, thus, the interaction between the nanoparticles and the nanotubes may be through oxygenated sites on the nanotubes surface.

- PAPER V. *Synthesis and characterization of lanthanum phosphate nanoparticles as carriers for radium isotopes.* In this work, the ability of core and core-shell nanoparticles of lanthanum phosphate nanoparticles ($LaPO_4$) to retain radium isotopes within their lattice structure was studied. Both ^{223}Ra and ^{225}Ra were used for this purpose. The nanoparticles were found to increase their size from 3.4 nm to 6.3 nm with the subsequent addition of 2 shells of $LAPO_4$. Core nanoparticles

were found to retain in ~88% of the activity over a period of 35 days. The subsequent addition of 2 shells on the core nanoparticles was found to increase the isotope retention up to 99.9%.

2. LITERATURE REVIEW

2.1. TRANSITION METAL NANOPARTICLES: SYNTHESIS AND APPLICATIONS

Transition metals at the nanoscale regime have shown a unique combination of physical and chemical properties. This fact has opened a wide range of possible applications in diverse fields such as of information storage, optoelectronics, sensors, fuel cell technology and catalysis among others [1-10]. The control over the particle size, particle size distribution and shape plays an important role on the properties of these types of nanomaterials [1, 2]. Therefore, there has been a tremendous interest on developing methods that allow a controlled synthesis [11, 12]. Various chemical and physical synthesis methods have been reported such as reduction of metal salt precursors [13, 14], electrochemical synthesis [15], microemulsions [16, 17], laser ablation [18], microwave assisted synthesis [19] etc. In these methods the control over the particle size and shape is carried out by the use of stabilizers and/or solid supports.

Supports are often used for the synthesis of nanoparticles which lead a better distribution of the nanoparticles and avoid aggregation [20]. They may also provide mechanical strength and offer additional desired properties for certain applications. In this context, different preparation methods on various supports such as γ-Al_2O_3, TiO_2, MgO, CeO_2, carbon, carbon nanotubes, etc. has been reported [21-23]. Among the various types of supports, carbon nanotubes, in the form of single walled (SWCNT) and multiwalled (MWCNT), have several advantages such as chemical stability and thermal stability over a wide temperature range [23-26]. Also, they can be synthesized with a high

purity level. The decoration of CNTs with nanoparticles has been carried out by diverse methodologies: electroless deposition, thermal decomposition, impregnation using an aqueous solution, and electrodeposition [27]. Polymeric stabilizers can also be used as support for metallic nanoparticles. They also serve as diffusion barriers to the growth species during synthesis [28-31].

2.2. RADIATION CHEMISTRY OF METAL COLLOIDS

2.2.1. Radiolysis of Water. The process of radiolysis of water has been a matter of substantial investigation as it plays an important role in a wide variety of applications. The initial phenomenon of ionization of water requires 13eV and it leads to the formation of abnormal ions that are very unstable, having lifetimes around 10-10 s [32]. These ions produce very reactive species (H+ and OH•). In addition to unstable ions, electrons are also generated. Their initial kinetic energy allows them to travel approximately 15 nm. These electrons lose their energy by collisions and, when they have lost the majority of their energy, they are captured by strongly polarized molecules of water. These electrons are called solvated electrons or electrons in aqueous solution [33].

During radiolysis of water a number of reactions take place and would finally lead to species such as H•, OH•, H+, H_2O_2, H_2 and electrons in aqueous solution (e_{aq}^-). The concentration of species created in this process is given by the G factor which is the number of molecules or radicals produced per 100 eV of radiation energy absorbed. The product yield or G factor depends of the linear energy transfer of the radiation, the pH

and purity level of the water. The values are summarized in Table 2.1for various linear energy transfers (LET) of the particles [33, 36].

Table 2.1. Radical and molecular product yield in for various LET of the particles [33].

LET ($keV\ \mu m^{-1}$)	Radical and molecular product yield (G factor)				
	e_{aq}^-	OH•	H•	H_2	H_2O_2
0.23	2.63	2.73	0.55	0.45	0.68
12.3	1.48	1.78	0.62	0.68	0.84
61	0.72	0.91	0.42	0.96	1.00
108	0.42	0.54	0.27	1.11	1.08

2.2.2. Radiation Synthesis of Metal Clusters. The species formed during radiolysis of water, H•, e-aq, and OH•, are very reactive. The first two have strong redox potentials of E° (H+/ H•) =-2.3 VNHE, and E° (H2O/ e-aq) =-2.87 VNHE, respectively. Therefore, both of them can reduce metal ions present in the solution to a state of zero-valence as shown in equations 1 and 2, where M+ represents monovalent ions [35].

$$M^+ + e_{aq}^- \rightarrow M^0 \qquad (1)$$

$$M^+ + H^\bullet \rightarrow M^0 + H^+ \qquad (2)$$

On the contrary, hydroxyl radicals ($OH^{\bullet}$), are also strong oxidizing agents with $E^0 = (OH^{\bullet}/H_2O) = +2.8\ V_{NHE}$, thus it would bring the ions or the atoms to a higher oxidation state. Secondary alcohols or formate ions are used as $OH^{\bullet}$ radical scavenger, and, as a result, more reducing species are generated. Thus in the presence of the scavenger a highly reducing environment is promoted. The use of ionizing radiation (eg. γ, β) for the reduction of metal ions eliminates the need of additional chemicals for the reduction of metal precursors [34-36].

Figure 2.1 depicts the process of nanoparticles synthesis under irradiation [35]. Initially, the reducing agents generated during radiolysis of water reduce the ions to a zero valence state. This can be a rather complex process where the ions are reduced by to intermediate valence states. Once the atoms uniformly generated in the solution, they tend to form dimers (M_2) or interact with ionic species becoming a nucleation center as expressed in equations (3) to (6), where m, n and p represent the nuclearities and x, y, z the number of associated ions. This occurs as a result of the interaction of metal- metal atom and metal-ion which is stronger than atom-solvent or atom-ligand interaction.

$$M^0 + M^+ \rightarrow M_2^+ \qquad (3)$$

$$M_2^+ + M_2^+ \rightarrow M_4^{2+} \qquad (4)$$

$$M_m + M^+ \rightarrow M_{m+1}^+ \qquad (5)$$

$$M_{m+x}^{x+} + M_{p+y}^{y+} \rightarrow M_{n+z}^{z+} \qquad (6)$$

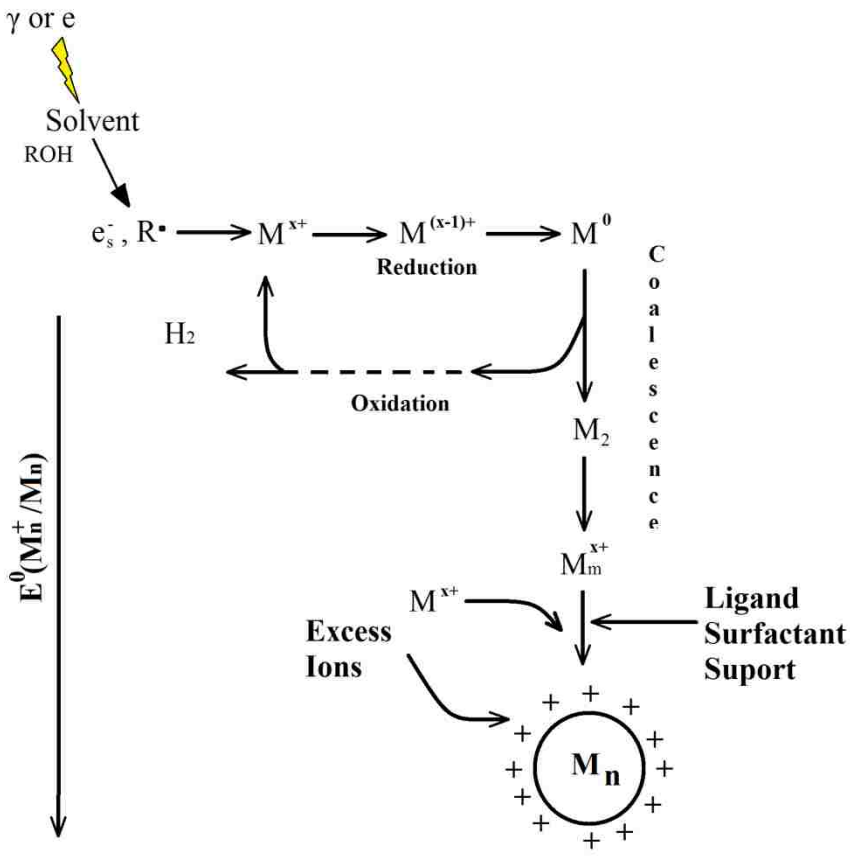

Figure 2.1. Metal nanoparticle formation under irradiation. Figure adapted from the reference [35].

2.2.3. Metal Cluster Stabilization. When nanoparticles are dispersed in a solvent, van der Waals forces and Brownian motion play an important role on the stability of the nanoparticles. Van der Waals forces become significant only at short distances and Brownian motions ensure that the nanoparticles are in continuous collision with each other. Thus, the combination of these two aspects would result in agglomeration of the nanoparticles. In order to avoid this, polymers with functional groups having high affinity for the metal surface are used. In addition the polymeric

chain protects the cluster though steric stabilization. Thus, the stabilizer inhibits the coalescence of the nuclei at the early stage and control the growth process. Stabilizers that are commonly used for the synthesis of metal nanoparticles include: poly vinyl alcohol (PVA), polyvinyl pyrolidone (PVP), sodium polyvinyl sulfate (PVS), polyacrylamide (PAM), poly N-methylacrylamide (PNMAM), poly ethyleneimine, and surfactants such as sodium dodecylsulfate (SDS). These materials have to be selected so that they do not reduce the ions before irradiation.

Dose rate is also a factor that has to be considered with special attention since it controls the rate at which the ion reduction is occurring. The radiation-induced radicals are generated randomly in the bulk sample with a quite homogeneous distribution. When the samples are irradiated with a high dose rate (pulse regime), all the reducing species are produced and scavenged in a very short time, which is followed by the cluster formation of atoms separately created. On the other hand, if samples are irradiated with a low dose rate (continuous radiation regime), the production of reducing radicals is slower than the association of ions with atoms, thus the reduction process occurs mostly in the surface of the aggregates. In this case, the reduction of atoms does not contribute to the formation of new clusters but to the growth of the ones already formed [35, 38].

2.2.4. Irradiation Techniques. Irradiation of aqueous solutions for nanoparticles synthesis is often carried out with the isotopes ^{60}Co and ^{137}Cs. The dose rate can be controlled in the range of 0.25 kGy/h to 35 kGy/h [35]. In this study, the samples were irradiated at the University of Illinois, Urbana-Champaign Nuclear Radiation Facility. The facility has a Gammacell 220 Excell Cobalt irradiator [MDS

Nordion 447, Ontario, Canada, K2K 1 × 8], shown in Figure 2.2 with a cylindrical irradiation chamber of 203 mm (high) by 152 mm (diameter). The absorbed dose can be controlled by adjusting the irradiation time. The system provides a dose rate of 10 kGy/hr (10 kGy/hr = 1 Mrad/hr).

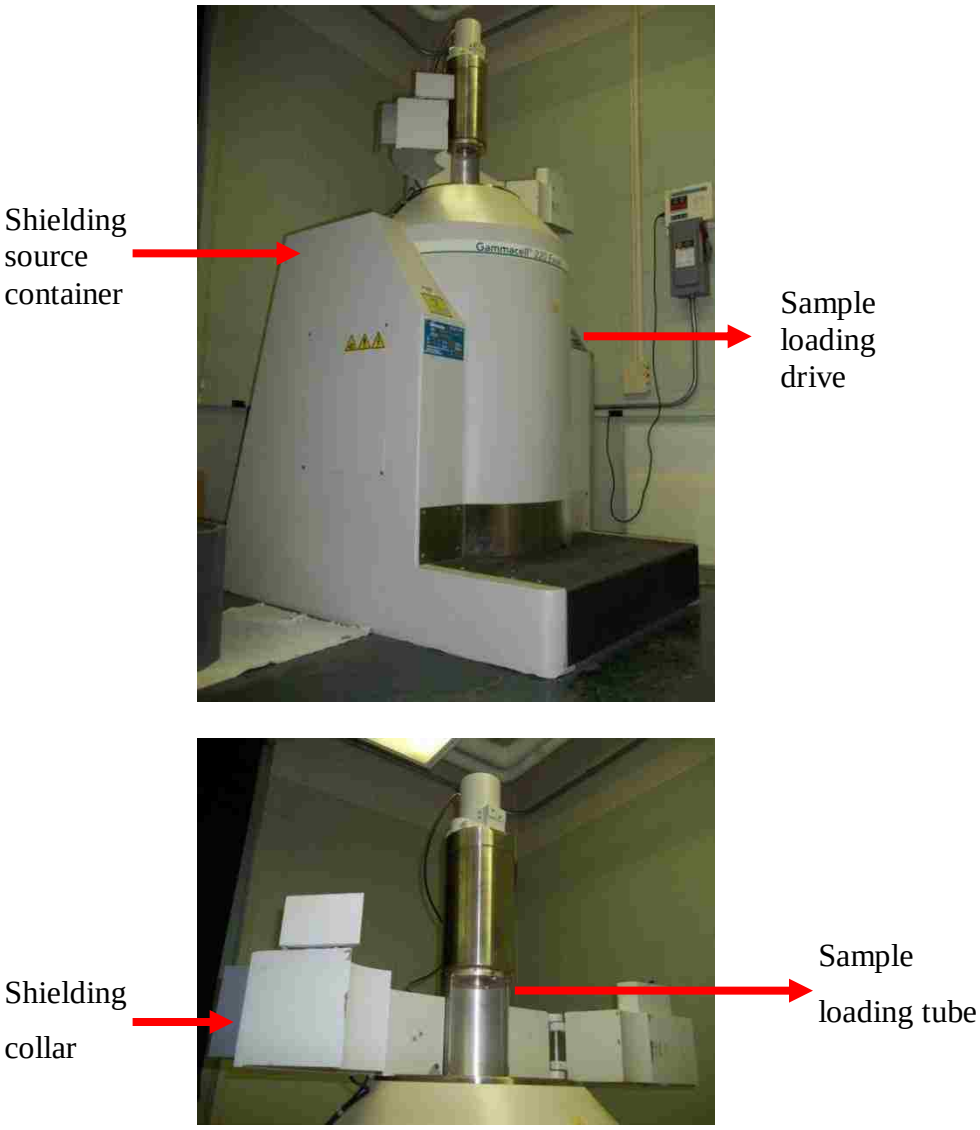

Figure 2.2. The external features of Gammacell 220 Excel.

2.3. NANOMATERIALS AND THEIR POTENTIAL USE FOR CANCER IMAGING AND TREATMENT

The application of nanomaterials in the medicine has increased tremendously since the past two decades. The ability of organic and inorganic nanostructures for drug delivery, cancer imaging and therapy has offered excellent prospects for the development of new non-invasive strategies for the diagnosis and treatment of cancer [40-42].

Success of cancer treatment can be improved by early diagnosis. However, detection of tumors at early stages is challenging. Several imaging techniques are currently being used as standard tools for visualization of tumors such as Computed Tomography (CT), Magnetic Resonance (MR), Positron Emission Tomography (PET), Single Photon emission CT (SPECT), Ultrasound (US), and optical imaging. A wide variety of nanomaterials may be engineered with different functionalities to allow nanoparticles inserted in the body to absorb preferentially in tumors, helping locate and image cancer at the earliest stages. Clever use of nanomaterials coupled with conventional imaging techniques could lead to synergistic detection effectiveness [41-44].

According to the World Cancer Research Fund International, the number of cancer cases around the world in 2012 was estimated to be 14.1 million, of these 52% were in men and 48% in women. This number is expected to increase to 24 million by 2035. By definition, Cancer is the uncontrolled growth and spread of cells. It can affect almost any part of the body. The growth often invades surrounding tissue and can metastasize to distant sites. There are four major characteristics of cancer cells which are, uncontrolled growth (uncontrolled division), invasion of adjacent tissue, metastasis

(spreading to other locations in the body), and immortality (protection against programmed cell death uncontrollable) [41].

The abnormalities present in tumor cells results in an extensive leakage of blood plasma components and other macromolecules. The general explanation given for this phenomenon is that, in order for tumor cells to grow quickly, they stimulate the formation of new blood vessels from pre-existing ones. This physicochemical process is referred to as angiogenesis. As a result, nanoparticles and macromolecules in the size range of 10-100 nm accumulate preferentially within many of these solid tumors. This phenomenon is called enhanced permeability and retention (EPR) effect [40-42]. Passive targeting of tumors can be achieved by exploiting this effect using macromolecules and nanoparticles (NPs) for imaging and/or drug release instead of conventional small-molecule drugs, which, unless bound to tumor specific molecules, can also interact with and affect normal tissue. Drug delivery systems are nowadays designed based on the EPR effect for passive targeting [41]. Active targeting of tumors is an alternative path for drug delivery. This method involves the conjugation of a targeting ligand or an antibody to the nanoparticles. The targeting molecules are selected so that they specifically bind to antigens or receptors that present on the tumor cell surface. This approach may have the potential to selectively deliver the nanoparticles to tumor tissues with high efficiency [40-43].

Cancer is currently treated with conventional methods such as chemotherapy and external radiotherapy. In both cases, the treatment also affects healthy cells, thus side effects are observed due to the appreciable destruction of normal tissue. In order to decrease side effects, new methods are being developed such as targeted radiation therapy, where the isotopes are loaded in a carrier designed to seek for specific cells [43].

Using this delivery approach, only cancer cells are specifically targeted based on their abnormality, while normal cells are largely unaffected.

The radioisotopes for targeted radiation therapy are selected based on their physical and chemical properties, technical feasibility, among others. They are categorized in alpha (α), beta (β) and auger particle emitters and they are used for specific applications. Alpha α-particles deposit most of their energy within 50 to 100 μm. Thus these isotopes are best suited for treatment of small tumors, micro metastasis or residual tumors [44, 53-55]. Beta particles have a longer radiation range (few millimeters) which makes the more suitable for the irradiation of large volume tumors. Auger particles deposit all their energy over an extremely short range (<150 nm), therefore they are most effective when located in the cytoplasm [43, 44].

Nanoparticles as carriers for radioisotopes are being explored as an alternative for both targeted cancer treatment and imaging. This alternative is in the early stages of investigation. Further research needs to be done regarding the synthesis methods, toxicology, and therapeutic efficiency of different radioactive nanoparticles [45-55].

2.4. TARGETED ALPHA THERAPY

In order to decrease side effects during treatment of cancer, new methods involving nanostructures for targeted drug delivery are being developed [43, 44]. In these methods, only cancer cells are specifically targeted based on their abnormality, while normal cells are unaffected. Among these methods, targeted alpha therapy (TAT) has the potential for specific tumor cells treatment with minimum damage to surrounding tissue [43-55]. Alpha particles are of special interest because they have greater biological

effectiveness than beta emitters due to their higher linear energy transfer. In addition, alpha particles deposit their energy within a few cell diameters. The most relevant isotopes with potential for therapeutic use are listed in Table 2.2 [43].

Table 2.2.Characteristic of some alpha emitters for therapeutic applications.

Isotope	Particle(s) emitted	Half-life	Energy of α-particle (MeV)
^{225}Ac	4 α and 2 β	10 d	5-8
^{225}Ra	4 α and 2 β	11.4	6-8
^{224}Ra	4 α and 2 β	3.6	6-7
^{223}Ra	4 α and 2 β	15	6-7
^{213}Bi	1 α and 2 β	46 min	6
^{212}Bi	1 α and 1 β	60.6 min	6
^{212}Pb	1 α and 2 β	10.6 h	7.8
^{211}At	1 α	7.2 h	6

From the isotopes listed in Table 1, ^{225}Ac and $^{223\text{-}225}$Ra isotopes have received attention as *in vivo* generators, which release several alpha particles during their decay (see Figure 2.3). One of the challenges when using these isotopes in TAT is the migration of their daughters during circulation. If they are not retained in the target site they can

migrate and deliver a toxic dose to non-targeted tissue [48-55]. Thus, the use of appropriate carriers is essential for the isotope delivery to the tumor site.

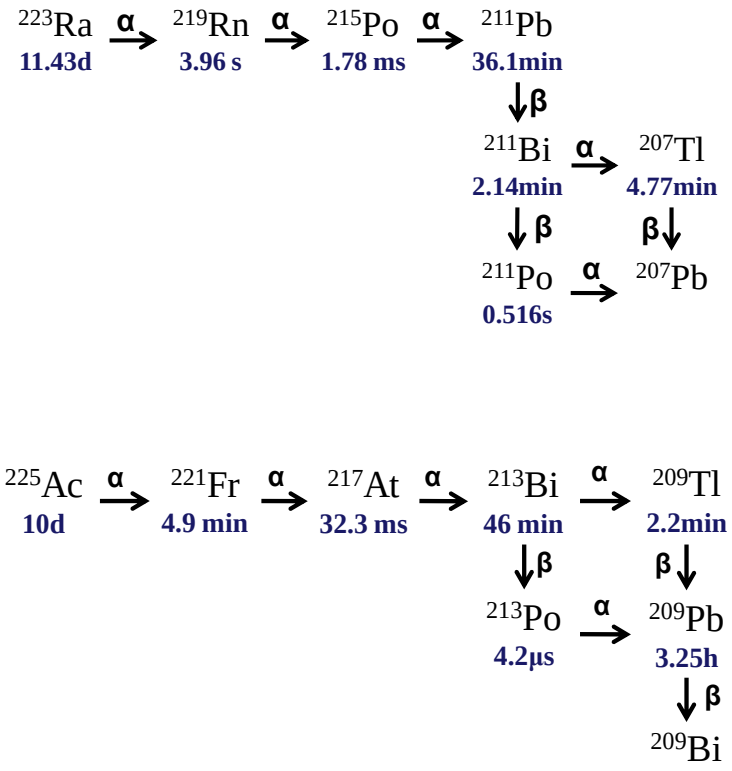

Figure 2.3. ^{223}Ra and ^{225}Ac decay schemes.

2.5. POTENTIAL NANOMATERIALS AS ISOTOPE CARRIERS

The use of nanoparticles to retain the daughters of *in vivo* alpha generator at the target site is a relatively new area. Some approaches using liposomes [50] and nanozeolites [51] to encapsulate ^{225}Ac and radium isotopes have been previously reported. Also, recent work on the use of Lanthanum phosphate ($LaPO_4$) nanoparticles

has been reported [52-55]. Nanoparticles of approximately 5 nm in diameter retained more than 99.9% of ^{225}Ac while retaining about 50% of the daughters. Further work in this system, has shown the ability of further increase the retention of the daughters. Adding 2 shells increased retention of the ^{221}Fr daughter from 50% for the $LaPO_4$ core to 70%. With four shells of $GdPO_4$, the initial retention of the ^{221}Fr daughter was 98%. Daughter retention decreased by roughly 2% per day over the course of a week, and stabilized at 88%.

The isotope ^{223}Ra, in the form of radium-223 dichloride, has already been approved by the Food and Drug Administration (FDA) for the treatment of patients with symptomatic bone metastases. Its effectiveness is based on the affinity of the isotope with bone tissue. Thus, in order to extend the use of this isotope to other type or targeted treatment, appropriate carriers need to be selected.

2.6. REFERENCES

[1] Pachon, L.D., Rothenberg, G. Transition-metal nanoparticles: synthesis, stability and the leaching issue. Appl. Organometal.Chem. 2008. 22, 288–299.

[2] Guisbiers, G., Abudukelimu, G., Hourlier, D. Size-dependent catalytic and melting properties of platinum-palladium nanoparticles. Nanoscale research letters. 2011. 6: 396.

[3] Roldan Cuenya, B. Synthesis and catalytic properties of metal nanoparticles: Size, shape, support, composition, and oxidation state effects. Thin Solid Films. 2010. 518, 3127–3150.

[4] Rueping, M., Koenigs, R.M., Borrmann, R., Zoller, J., Weirich, T.E., Mayer, J. Size-Selective, Stabilizer-Free, Hydrogenolytic Synthesis of Iridium Nanoparticles Supported on Carbon Nanotubes. Chem. of Mater. 2011.23, 2008-2010.

[5] Shim, J.H., Kim, J.E., Cho, Y.B., Lee, C., Lee, Y. Oxidation-state dependent electrocatalytic activity of iridium nanoparticles supported on graphene nanosheets. Phys Chem Chem Phys. 2013.15, 15365-15370.

[6] Evangelisti, C., Panziera, N., Pertici, P., Vitulli, G., Salvadori, P., Battocchio, C., et al. Palladium nanoparticles supported on polyvinylpyridine: Catalytic activity in Heck-type reactions and XPS structural studies. J. of Catal. 2009. 262, 287-293.

[7] Bernas, H., Simakova, I., Prosvirin, I.P., Mäki-Arvela, P., Leino, R., Murzin, D.Y. Hydrogenation of Citral Over Carbon Supported Iridium Catalysts. Catal. Letters. 2012. 142,690-697.

[8] Yuan, Y., Yan, N., Dyson, P.J. Advances in the Rational Design of Rhodium Nanoparticle Catalysts: Control via Manipulation of the Nanoparticle Core and Stabilizer. ACS Catalysis. 2012. 2, 1057-1069.

[9] Challa, S.S.R. Kumar (Editor). Nanomaterials for cancer therapy. ISBN: 9783527313860. Wiley, John & Sons, Incorporated.

[10] Fonseca, G. S., Machado, G., Teixeira, S.R., Fecher, G.H., Morais, J., Alves, M.C., et al. Synthesis and characterization of catalytic iridium nanoparticles in imidazolium ionic liquids. J Colloid Interface Sci. 2006. 301, 193-204.

[11] Hei, H. Controlled Synthesis and Characterization of Nobel Metal Nanoparticles. Soft Nanoscience Letters. 2012. 2, 34-40.

[12] Zhou, J., Ralston, J., Sedev, R., Beattie, D.A., Functionalized gold nanoparticles: Synthesis, structure and colloid stability, Journal of Colloid and Interface Science. 2009. 331(2), 251-262.

[13] Wenlong, C., Shaojun, D., Erkang, W. Studies of electrochemical quantized capacitance charging of surface ensembles of silver nanoparticles. Electrochemistry Communications. 2002. 4, 412–416.

[14] James, C. The Preparation of Palladium Nanoparticles: Controlled particle sizes are key to producing more effective and efficient materials. Platinum Metals Rev. 2012. 56 (2), 83-98.

[15] Starowicz, M., Stypuła, B., Banaś, J. Electrochemical synthesis of silver nanoparticles. Electrochemistry Communications. 2006. 8 (2), 227-230.

[16] Ignác, C. Preparation of metal nanoparticles in water-in-oil (w/o) microemulsions. Advances in colloid and interface science. 2004. 110(1), 49-74.

[17] Hoefelmeyer, J.D., Liu, H., Somorjai, G.A., Tilley, T.D. Reverse micelle synthesis of rhodium nanoparticles. J Colloid Interface Sci. 2007. 309, 86-93.

[18] Amendola,V. Meneghetti, M. Laser ablation synthesis in solution and size manipulation of noble metal nanoparticles Phys. Chem. Chem. Phys. 2009. 11, 3805-3821.

[19] Liu, Z., et al. "Physical and electrochemical characterizations of microwave-assisted polyol preparation of carbon-supported PtRu nanoparticles." Langmuir. 2004. 20.1, 181-187.

[20] Lu J., Aydin, C., Browning, N.D., Wang, L., Gates, B.C. Sinter-Resistant Catalysts: Supported Iridium Nanoclusters with Intrinsically Limited Sizes. Catalysis Letters. 2012. 142, 1445-1451.

[21] Djeddi, A., Fechete, I., Garin, F. Selective ring opening of methylcyclopentane over Pt/γ-Al2O3, Ir/γ-Al2O3 and Pt-Ir/γ-Al2O3 catalysts with hydrogen at atmospheric pressure. Applied Catalysis A: General. 2012. 340(9) 413-414.

[22] Vuori, H., Pasanen, A., Lindblad, M., Valden, M., Niemelä, M.V., Krause, A.O.I. The effect of iridium precursor on oxide-supported iridium catalysts prepared by atomic layer deposition. Applied Surface Science. 201. 257, 4204-4210.

[23] Hayeka, K., Gollerb, H., Penner, S., Rupprechterc, G., Zimmermannd, C. Regular alumina-supported nanoparticles of iridium, rhodium and platinum under hydrogen reduction: structure, morphology and activity in the neopentane conversion. Catalysis Letters. 2004. 92, 1-9.

[24] Kuznetsova, L.I., Kuznetsova, N.I., Koscheev, S.V., Zaikovskii, V.I., Lisitsyn, A.S., Kaprielova, K.M., et al. Carbon-supported iridium catalyst for reduction of chlorate ions with hydrogen in concentrated solutions of sodium chloride. Applied Catalysis A: General. 2012. 427-428, 8-15.

[25] Yoon, B., Wai, C.M. Microemulsion-Templated Synthesis of Carbon Nanotube-Supported Pd and Rh Nanoparticles for Catalytic Applications. Journal of the Americal Chemical Society. 2005. 127, 17174-5.

[26] Pan, H-B, Wai, C.M. Sonochemical One-Pot Synthesis of Carbon Nanotube-Supported Rhodium Nanoparticles for Room-Temperature Hydrogenation of Arenes. J Phys Chem C. 2009. 113, 19782-19788.

[27] Rojas, J.V., Castano, C.H. Production of metal nanoparticles on carbon nanotubes by gamma irradiation. In: Kharisov, B.I., Kharissova, O.V., Mendez, U.O., editors. Radiation Synthesis of Materials and Compounds: CRC Press; 2013. 491-503.

[28] Xian, J., Hua, Q., Jiang, Z., Ma, Y., Huang, W. Size-dependent interaction of the poly(N-vinyl-2-pyrrolidone) capping ligand with Pd nanocrystals. Langmuir. 2012. 28, 6736-6741.

[29] Gniewek, A., Trzeciak, A., Ziolkowski, J., Kepinski, L., Wrzyszcz, J., Tylus, W. Pd-PVP colloid as catalyst for Heck and carbonylation reactions: TEM and XPS studies. Journal of Catalysis. 2005. 229, 332-343.

[30] Ichikuni, H.T.N, Sakurai, H., Tsukuda, T. Effect of Electronic Structures of Au Clusters Stabilized by Poly(N-vinyl-2-pyrrolidone) on Aerobic Oxidation Catalysis. J Am Chem Soc. 2009. 131, 7086-7093.

[31] Borodko, Y., Humphrey, S.M., Tilley, T.D., Frei, H., Somorjai, G.A. Charge-Transfer Interaction of Poly(vinylpyrrolidone) with Platinum and Rhodium Nanoparticles. J Phys Chem C. 2007. 111, 6288-6295

[32] Appleby, A., Schwarz, H.A. Radical and Molecular Yields in Water Irradiated by y Rays and Heavy Ions. J Phys Chem. 1969. 79, 1937-1941.

[33] Tubiana, M., Dutreix, J., Wambersie, A., Bewley, D.K. Introduction to Radiobiology CRC Press, Sep 1, 1990. 371.

[34] Belloni, J., Mostafavi, M. Radiation chemistry of nanocolloids and clusters. In: Jonah. CD, Rao BSM, editors. Radiation chemistry: present status and future trends: Elsevier. 2001. 411-452.

[35] Belloni, J., Mostafavi, M., Remita, H., Marignier, J-L., Delcourt, M-O. Radiation-induced synthesis of mono-and multi-metallic clusters and nanocolloids. New J. Chem., 1998. 1239-1255.

[36] Belloni J. Nucleation, growth and properties of nanoclusters studied by radiation chemistry. Catalysis Today. 2006. 113, 141-156.

[37] Zhang, X., Ye, Y., Wang, H., Yao, S. Deposition of platinum–ruthenium nano-particles on multi-walled carbon nano-tubes studied by gamma-irradiation. Radiation Physics and Chemistry. 2010. 79, 1058-1062.

[38] Naghavi, K., Saion, E., Rezaee, K., Yunus, W.M.M. Influence of dose on particle size of colloidal silver nanoparticles synthesized by gamma radiation. Radiation Physics and Chemistry. 2010. 79, 1203-1208.

[39] Misra, N., Biswal, J., Gupta, A., Sainis, J.K., Sabharwal, S. Gamma radiation induced synthesis of gold nanoparticles in aqueous polyvinyl pyrrolidone solution and its application for hydrogen peroxide estimation. Radiation Physics and Chemistry. 2012. 81, 195-200.

[40] Huang, H. C., Barua, S., Sharma, G., Dey, S.K., Rege, K. Inorganic nanoparticles for cancer imaging and therapy. J Control Release, 2011. 155, 344-357.

[41] Barreto, J. A., O'Malley, W., Kubeil, M., Graham, B., Stephan, H., Spiccia, L. Nanomaterials: Applications in Cancer Imaging and Therapy. Adv. Mater., 2011. 23, 18-40.

[42] Nadejda, R., Zhong, Z. Photothermal ablation therapy for cancer based on metal nanostructures. J. Sci China Ser B-Chem. 2009. 52, 1559-1575.

[43] Wang, X., Yang, L., Chen, Z.G., Shin, D.M. Application of nanotechnology in cancer therapy and imaging. CA Cancer J Clin. 2008. 58, 97-110.

[44] Zhang, L., Chen, H., Wang, L., Liu, T., Yeh, J., Lu, G., et al. Delivery of therapeutic radioisotopes using nanoparticle platforms: potential benefit in systemic radiation therapy. Nanotechnol Sci Appl. 2010. 3, 159-70.

[45] National Research Council (US) and Institute of Medicine (US) Committee on State of the Science of Nuclear Medicine. Advancing Nuclear Medicine Through Innovation. Washington (DC): National Academies Press (US); 2007. 4, Targeted Radionuclide Therapy

[46] Chanda, N. et al. Radioactive gold nanoparticles in cancer therapy: therapeutic efficacy studies of GA-198AuNP nanoconstruct in prostate tumor–bearing mice. Nanomedicine: Nanotechnology, Biology, and Medicine. 2010. 6, 201-209.

[47] Kannan, R., Zambre, A., Chanda, N., Kulkarni, R., Shukla, R., Katti, K., Upendran, A., Cutler, C., Boote, E., Katti, K. V. Functionalized radioactive gold nanoparticles in tumor therapy. Nanomed Nanobiotechnol. 2012. 4, 42-51.

[48] Woodward, J., Kennel, S.J., Stuckey, A., Osborne, D., Wall, J., Rondinone, A.J., Standaert, R.F., Mirzadeh, S. Bioconjugate Chem. 2011. 22, 766-76.

[49] Di Pasqua, A.J., Huckle, J.E., Kim, J.K., Chung, Y., Wang, A. Z., Jay, M., Lu, X. Preparation of Neutron-Activatable Holmium Nanoparticles for the Treatment of Ovarian Cancer Metastases. Small. 2012. 8 (7), 997–1000.

[50] Henriksen, G., Schoultz, B.W., Michaelsen, T.E., Bruland, O.S., Larsen, R.H. Sterically stabilized liposomes as a carrier for alpha-emitting radium and actinium radionuclides. Nucl Med Biol. 2004. 31, 441-449.

[51] Piotrowska, A., Leszczuk, E., Bruchertseifer, F., Morgenstern, A., Bilewicz, A. Functionalized NaA nanozeolites labeled with Ra for targeted alpha therapy. J Nanopart Res. 2013. 15, 2082.

[52] Woodward, J., Kennel, S.J., Stuckey, A., Osborne, D., Wall, J., Rondinone, A.J., et al. $LaPO_4$ nanoparticles doped with actinium-225 that partially sequester daughter radionuclides. Bioconjug Chem. 2011. 22, 766-776.

[53] McLaughlin, M.F., Robertson, D., Pevsner, P.H., Wall, J.S., Mirzadeh, S., Kennel, S.J. LnPO4 nanoparticles doped with Ac-225 and sequestered daughters for targeted alpha therapy. Cancer Biother Radiopharm. 2014. 29, 34-41.

[54] McLaughlin, M.F., Woodward, J., Boll, R.A., Rondinone, A.J., Mirzadeh, S., Robertson, J.D. Gold-coated lanthanide phosphate nanoparticles for an 225Ac in vivo alpha generator. Radiochim Acta 2013. 101, 595-600.

[55] McLaughlin, M.F., Woodward, J., Boll, R.A., Wall, J.S., Rondinone, A.J., Kennel S.J., et al. Gold Coated Lanthanide Phosphate Nanoparticles for Targeted Alpha Generator Radiotherapy. Plos One. 2013. 8, 1-8.

PAPER

I. PRODUCTION OF METAL NANOPARTICLES ON CARBON NANOTUBES BY GAMMA IRRADIATION

Rojas, J.V., Castano, C. H.

Production of Metal Nanoparticles on Carbon Nanotubes by Gamma Irradiation. CRC press 2013.

Chapter 22 in Radiation Synthesis of Materials and Compounds, Kharisov, B. I. Kharissova, O. V., Mendez, U.

Introduction

Carbon nanotubes (CNTs) are being studied for a variety of applications due to their outstanding mechanical, chemical, electrical, and optical properties (Baughman et al. 2002; Popov 2004, Belin and Epron 2005). In addition, CNTs structures are being modified to expand their use in new applications (Baughman et al. 2002; Hirsch 2002; Makala et al. 2006; Hou et al. 2008). Decorating carbon nanotubes with certain metal nanoparticles is a promising option for catalysis (Wildgoose et al. 2006), hydrogen storage (Cheng et al. 2001; Hou et al. 2003; Chen et al. 2008; Rakhi et al. 2008, Zacharia et al. 2005; Yuruma et al. 2009, Suttisawat et al. 2009; Strobel 2006; Sarkar et al. 2004), and sensing (Star et al. 2006; Vairavapandian et al. 2008).

The decoration of CNTs with nanoparticles has been carried out by many electrochemical, chemical, and physical methods (Xue et al. 2001; Quinn et al. 2005; Qu and Dai. 2005; Sun et al. 2006; Georgakilas et al. 2007; Ren and Xing 2006; Wildgoose et al. 2006; Karousis et al. 2009). Ionizing radiation is currently being investigated both as a new alternative to create defects in the surface of the nanotubes and as a method for the production of metallic nanoparticles (Belloni et al. 1998; Joshi et al. 1998; Doudna et al. 2003; Skakalova et al. 2003; Skakalova et al. 2004; Guo et al. 2005; Hulman et al. 2005; Sarkany et al. 2005; Krasheninnikov and Nordlund 2010; Remita and Remita 2010). The Gamma (γ) irradiation has shown significant advantages over others methods since radiation parameters such as energy, dose, and dose rate can be finely controlled.

In addition, reducing agents are generated uniformly throughout the aqueous solution. The reduction potential of these agents makes them able to reduce free ions at each encounter. Successful attempts have been made to directly deposit metallic nanoparticles such as gold, platinum, and ruthenium on carbon nanotubes by gamma irradiation with a homogeneous distribution. Nonetheless, several factors must be considered to obtain the desired results (Liu et al. 2003; Oh et al. 2005; Lee et al. 2007; Zhang et al. 2010; Rojas and Castano 2012).

In this chapter, we present gamma irradiation as a promising technique to decorate carbon nanotubes with metal nanoparticles. The influence of parameters such as dose, dose rate, and stabilizer concentration on particle size will be discussed.

Radiation Effects on Carbon Nanotubes

A common misconception is that radiation (ions, electrons, gamma rays, etc.) have exclusively detrimental effects on the properties of materials. To the contrary, irradiation can also induce positive effects on materials, particularly for nanostructured systems under controlled irradiation conditions. For example, both ion and electron beams have been used to synthesize both nanoclusters and nanowires, modifying in a controllable manner their morphology, as well as altering their electronic, mechanical, and magnetic properties (Krasheninnikov and Nordlund 2004). In addition, irradiation of CNTs with energetic particles (electrons or ions) can successfully create molecular junctions between nanotubes (forming cross and Y- shaped structures) (Terrones et al. 2002). Ion irradiation has also been used to the production of CNT-amorphous diamond nanocomposites and as a technique to improve adherence of nanotubes to both metallic and graphite substrates (Krasheninnikov and Nordlund 2004).

Functionalization of CNTs is of special importance for diverse applications as it can lead not only to the improvement of their solubility but also, to their ability to be coupled with other materials creating composites with fascinating characteristics (Hircsh 2002). Irradiation-induced defects normally increase the reactivity of nanotubes at the surface. Thus, functional groups can be attached to both graphene and nanotubes in specific areas (Guo et al. 2005; Salah et al. 2009; Fedoseeva et al. 2010). The induced defects in the sp2-bonded carbon systems due to focused electron and ions beams are governed by the knock-on displacement of carbon atoms, creating vacancies and interstitials in the nanotubes (Krasheninnikov and Nordlund 2010).

Although the effects of highly energetic particles (both electrons and ions) on carbon nanotubes have been extensively studied (Krasheninnikov and Nordlund 2010), limited attention has been given to the effects of gamma irradiation on CNTs. Recent studies have been published on the improvement of both Young's modulus and the electrical conductivity of gamma irradiated paper made of single walled carbon nanotubes (SWNT). It was found that these two properties reached a maximum value at a dose of 170 kGy. It has been suggested that highly energetic photons create defects on the nanostructure leading to the formation of bonds between the nanotubes. Once a critical defect concentration is reached at a certain dose, some of the previously created bonds might be broken, thus affecting the final mechanical and electrical properties of the nanotubes. In addition, it was also observed that the effect of irradiation was much stronger for samples irradiated in the air in comparison to those in a vacuum (Skakalova 2003).

Gamma irradiation of SWNTs has been used as a pretreatment for chemical functionalization with thionyl chloride ($SOCl_2$). This process was based on the premise that the concentration of defects is likely to influence the concentration of functional groups attached to the nanotubes (Skakalova 2004). This study showed that further functionalization with $SOCl_2$ after irradiation enhances even more both the Young's modulus and the electrical conductivity.

The Functionalization of multiwalled carbon nanotubes (MWCNTs) with both thionyl chloride and decylamine has also been studied after gamma irradiation. The

concentration of functional groups attached to the nanotubes was found to increase monotonically, with increasing irradiation doses in the range of 50 to 250 kGy. This happens due to a significant increase in defects on the sidewall of the nanotubes created by the gamma photons. Finally, more stable dispersions of MWCNTs in organic solvents, such as both acetone and tetrahydrofuran (TFT), were observed, indicating a better solubility of the nanostructure after gamma irradiation (Guo et al. 2005). Irradiated MWCNTs have also shown a modification of their original structural characteristics, such as inter-wall distance, which seem to be dependent on the surrounding medium (Xu et al. 2011). These results have indicated that gamma irradiation might be an effective pretreatment for further functionalization on the structural modification of CNTs (Guo et al. 2005).

Synthesis of Metallic Nanoparticles Supported on Carbon Nanotubes

The decoration of CNTs with nanoparticles has been carried out by diverse methodologies: electroless deposition (Qu and Dai 2005), thermal decomposition (Xue et al. 2001), chemical reduction in supercritical CO2 solutions (Sun et al. 2006), impregnation using an aqueous solution (Tessonnier et al. 2005), and electrodeposition (Quinn et al. 2005). These techniques commonly use noble metal salts as precursors for the preparation of the nanoparticles, which are obtained by a reduction process.

Applications of the electroless deposition methodology are limited by the fact that only metal ions with redox potential higher than that of the nanotubes can be reduced. For example, Au ($AuCl^{-4}$/Au, +1.002 V vs SHE) and Pt ($PtCl_4^{2-}$/Pt, +0.775 vs SHE)

nanoparticles have been successfully synthesized by a spontaneous reduction of the metal ions by SWCNTs. On the contrary, neither Cu^{2+} ($Cu(NO_3)_2/Cu$, +0.340 V vs SHE) nor Ag^{+} ($Ag(NH_3)^{2+}/Ag$, +0.373 V vs SHE) can be reduced without the presence of a reducing agent (Choi et al. 2002). This problem was solved by placing the nanotubes on a metal substrate with a redox potential lower than that for the metal ions. With this method, ions can be reduced into nanoparticles onto the carbon nanotubes surface even if their redox potential is lower that of the carbon nanotubes. This method refers to as substrate enhanced electroless deposition (Qu and Dai 2005).

Thermal decomposition has been used for the synthesis of nanoparticles of Pd, Pt, Au and Ag, on CNTs. In the process, CNTs are dispersed in either water or acetone by the addition of a metal salt. A subsequent evaporation of the solvent is carried out at a temperature of approximately 100°C. As a final step, both decomposition and a reduction of the mixture are conducted at temperatures between 300°C and 700°C under an H_2 atmosphere. Using this method, nanoparticles with sizes between 8 to 20 nm were obtained on the surface of the nanotubes (Xue et al. 2001).

Nanoparticles such as Pd-Rh have been successfully attached to MWCNTs by a chemical reduction in supercritical CO_2 solutions (SC CO_2). Supercritical fluids (SCFs) have a combination of properties, such as low viscosity, high diffusivity, near zero surface tension, and strong solvent power for some small molecules that make them applicable in different areas in material science. Although inorganic salts are not generally soluble in SC CO_2, some polar solvents, such as ethanol, methanol, and

acetone, can act as co-solvents to enhance the solubilization of inorganic precursors in supercritical solutions. After reactions, dry and high-purity products are easily obtained by in-situ extraction using SC CO_2 as a solvent (Sun et al. 2006).

Electrodeposition is another method used to produce metal nanoparticles on CNTs. This process was performed in a two electrode arrangement in a solution containing the CNTs with either $HAuCl_4$, K_2PtCl_4 or $(NH_4)_2PdCl_4$. As a result of this study, Au, Pt, and Pd nanoparticles were deposited on the CNTs by controlling the deposition potential, duration of the pulse, and the concentration of the metal salt in the electrochemical system (Quinn et al 2005).

Radiochemical methods have also been recently explored as a promising technique to both produce and deposit metallic nanoparticles of CNTs. In addition to the ability to create defect sites on the sidewall of carbon nanotubes, gamma irradiation is proven to provide other advantages in the synthesis of nanoparticles such as: fine control of energy of radiation, dose, and dose rate. Also, reducing agents are generated uniformly within the solution. These reducing agents' strong reduction potential makes them able to reduce free ions at each encounter. Finally, the controlled reduction of metal ions can be made with no need of any excess of additional reducing agents. Thus, no undesired oxidation products from the reactants are produced (Belloni et al 1998; Liu et al 2003; Lia et al 2007).

Radiation Chemistry for the Production of Metallic Nanoparticles

During water radiolysis, radicals such as H•, OH•, H+, H_2O_2, H_2, and electrons in aqueous solution (e_{-aq}) are produced. The concentration of species created in this process is given by the G factor. This factor represents the number of molecules, or radicals, produced per 100 eV of radiation energy absorbed. The normally accepted values of product yields in a Co-60 gamma irradiated aqueous solution, with both neutral pH and ambient temperature, are presented in Table 1 (Appleby and Schwarz 1969).

Table 1. Radical and molecular product yield in gamma irradiated aqueous solutions (Appleby and Schwarz 1969).

Product	H•	OH•	H+	H_2O_2	H_2	e_{-aq}
G factor (#species/100ev)	0.61	2.86	2.70	0.61	0.43	2.70

The species H•, e_{-aq}, and OH• are very reactive. Both H• and e-aq are strong reducing agents with redox potentials of E° (H+/ H•) =-2.3 VNHE and E° (H2O/ e_{-aq}) =-2.87 VNHE, respectively. Therefore, both can reduce metal ions present in the solution to a state of zero-valence. This process takes place through the direct reaction of the metal ion with either H• or e_{-aq} in the case of monovalent ions. In contrast, the reduction of multivalent metal ions in aqueous solutions is a multistep process where atoms in unusual valence states are initially formed. This initial reduction is followed by further reduction and agglomeration until a stable nanoparticle is obtained (Belloni et al. 1998).

OH• radicals, however, are strong oxidizing agents, with E° (OH•/ H_2O) =+2.8VNHE. Thus, metal atoms are brought to a higher oxidation state. A scavenger of OH• radicals, such as primary alcohols, secondary alcohols, or formate ions, are required in the solution prior to irradiation for the reduction of metal ions to proceed. The secondary radicals, produced by the reaction between the scavenger and radiolysis species H• and OH•, are also strong reducing agents. The corresponding reactions are summarized in Table 2 (Belloni et al. 1998).

Table 2. Reactions of scavenger with radicals and the respective redox potentials of the radical products.

Scavenger	Radical	Products	Redox potential
$(CH_3)_2CHOH$	OH•	$(CH_3)_2C•OH + H_2O$	$E°((CH_3)_2CO/(CH_3)2C•OH)= -1.8V_{NHE}$
	H•	$(CH_3)_2C•OH + H_2$	
HCOO-	OH•	$COO- + H_2O$	$E°(CO_2/ COO-)= -1.9V_{NHE}$
	H•	$COO- +H_2$	

Effects of the Stabilizer, Gamma Dose, and Dose Rate on the Synthesis of Nanoparticles

During the reduction process of the metal ions that takes place with gamma irradiation, the atoms tend to dimerize when they either encounter or combine with ions. This occurs because the binding energy between either atoms or clusters with unreduced ions is stronger than either the atom-solvent or the atom-ligand energy. In order to limit

the coalescence process of the aggregates, polymeric molecules, or cluster stabilizers, are added to the solution to be irradiated. Functional groups, such as carboxyl groups, that have a high affinity for the metal ions, ensure the anchoring of the molecule at the cluster surface. At the same time, the polymeric chain of the molecule protects the cluster from coalescing with another at the early stage by means of electrostatic repulsion, or steric hindrance (Belloni et al. 1998).

When nanoparticles are to be prepared by irradiation, the stabilizer must be selected in such a way that it does not reduce the ions before irradiation. Polymers, such as poly vinyl alcohol (PVA) (Eisa et al. 2011), polyvinyl pyrolidone (PVP) (Gasaymeh et al. 2011), sodium polyvinyl sulfate (PVS), polyacrylamide (PAM) (Zhu 1998), poly N-methylacrylamide (PNMAM), poly ethyleneimine, and surfactants such as sodium dodecylsulfate (SDS) (Joshi et al. 1998), do not affect the electronic state of the ions but fulfill the conditions for stabilization.

Figure 1 (a) shows a scanning electron microscope image (SEM) of MWCNT-Pd produced in a solution containing water and isopropanol in a ratio of 2:1 and 0.015M of SDS as stabilizer. The sample was irradiated at 40 kGy. At a very low SDS concentration, less than the critical micelle concentration (CMC) of the SDS in water (approximately 18mM), either few or no nanoparticles were obtained after irradiation. Instead, large agglomerates were formed due to the lack of dispersion stability. By increasing the amount of surfactant, even at low doses, some nanoparticles were observed in the sample, as shown in Figure 1 (b). The right amount of SDS allows palladium

nanoparticles to form a homogeneous dispersion, leading to the formation of nanoparticles, with different sizes at different doses (Rojas and Castano 2011).

Previous studies on the deposition of palladium nanoparticles on MWCNTs using $PdCl_2$ as the metal precursor at different doses between 10 kGy to 40 kGy have demonstrated a noticeable variation of the nanoparticles yield. Also, a decrease in the nanoparticles size with the increase in dose has been observed (see Figure 2). The proposed mechanism with this study implies that the increase in dose leads to a larger amount of reducing agent produced in the solution. This causes a rapid Pd^{+2} reduction thus forming numerous Pd seeds, that then generate separate smaller particles, rather than a few big ones (Rojas and Castano 2012). In addition to the nanoparticles obtained on the surface of the carbon nanotubes, bigger particles where also obtained from the process. Histograms with size distribution of the palladium nanoparticles at the different doses and the curve of average size vs. dose are shown in Figure 3. Two remarkable features are observed with increasing dose: (i) the frequency of big particles gradually decreases and (ii) the peaks position gradually shifts to a smaller diameter. Both the average size (μ) and the standard deviation (σ) of the Pd nanoparticles are shown, where $\mu 1$, $\sigma 1$ and $\mu 2$, $\sigma 2$ correspond to the first and second peak in the histogram, respectively (Rojas and Castano 2012).

Dose rate is also a factor that must be considered as it controls the rate at which the ions are being reduced. As previously mentioned, the radiation-induced radicals are generated homogeneously within the bulk sample. When the samples are irradiated with a

high dose rate (pulse regime), all of the reducing species are produced and scavenged within a few seconds. This is followed by the clustering of the atoms created separately. The pulse regime can be achieved with electron accelerators where mean dose rates of 2.2 kGy/s or higher are reached. If, however, samples are irradiated with a low dose rate, continuous radiation regime, the production of reducing radicals is slower than the clustering of atoms. The isotopes ^{60}Co and ^{137}Cs are frequently used for the continuous radiation regime, as the dose rate can be controlled to stay within the range of 0.25 kGy/h to 35 kGy/h (Belloni et al. 1998; Wishart 2008). In the latter situation, the reduction process occurs primarily on the surface of already formed aggregates. In this case, the reduction of atoms does not contribute to the formation of new clusters but instead to the growth of the ones initially formed (Remita and Remita 2010).

Interaction Mechanisms between CNTs and Nanoparticles

There are two primary methods used to both synthesize and deposit nanoparticles on carbon nanotubes. The first method consists of growing growth of nanoparticles in the presence of CNTs directly onto the CNTs' surface. In this instance, a metal precursor, such as salts, is used and, together, with the nanotubes, are dissolved in a specific amount in a solution containing water, an OH• scavenger, and a stabilizer. This mixture is then irradiated with gamma rays so that the metal ions can be reduced by radicals produced by the irradiation. During irradiation, not only are the ions reduced but the generation of new defects on the surface of the carbon nanotubes is also promoted. These defects are beneficial as they serve as preferred nucleation sites for the reduced metal ions. With this process, nanoparticles can be deposited onto the CNT walls primarily through van der

Waals interactions. These appear to be strong enough to assure significant adhesion of the nanoparticles to the nanotubes (Georgakilas et al 2007). Suitable examples of the results obtained by this method are presented in Figure 4 a-c, where a) and b) are TEM images of palladium nanoparticles on MWCNTs by gamma-irradiation using palladium chloride ($PdCl_2$) (Rojas and Castano 2012). Figure 4 c) corresponds to a SEM image of platinum–ruthenium nanoparticles using hexachloroplatinic acid hexahidrate (H_2PtCl_6) with ruthenium (III) chloride hydrate (RuCl as metal precursor (Zhang et al. 2010). In these two experiments, the solutions containing both a salt and the nanotubes with water/isopropanol and a suitable stabilizer were irradiated at a dose of 40 kGy.

The second method consists of generating nanoparticles separately from the nanotubes and, subsequently, modifying them with the appropriate functional groups for linkage to the carbon nanotubes' surface. These links can be such that either the functional groups create covalent bonds with the functional groups present on the CNT surface or they can simply get attached to the CNT surface through weak intermolecular interactions such as π-π stacking, hydrophobic, or electrostatic attractions (Georgakilas et al. 2007). Using this method, gold nanoparticles, synthesized by the citrate method, have been attached to SWCNTs (Salah et al. 2009). In this second method, the nanoparticles, as well as the nanotubes, were irradiated separately in order to create active sites. Only later where they mixed together, producing the results shown in Figure 4(d).

Summary

Carbon nanotubes decorated with metallic nanoparticles are currently being studied for a wide variety of applications. This arises from the fact that the properties of

raw nanotubes are substantially modified with the addition of the nanoparticles. Different methods have been developed to synthesize metallic nanoparticles on carbon nanotubes, each one with their own advantages and disadvantages. Gamma irradiation has several advantages over others such as a fine control over the dose and dose rate. Additionally, the radical that are created during the process are distributed homogeneously in the solution, they have a strong reducing potential and there are no unwanted residues after the reaction. The overall control of the irradiation parameters, in combination with the right amount of both, metal precursor and stabilizer, lead to a fine control of the nanoparticles' size. Gamma irradiation has also shown to have beneficial effects over both the electrical and mechanical properties of carbon nanotubes. It is also a potential technique that can be use as pretreatment for their further functionalization.

References

[1] Appleby, A., Schwarz, H. A.1969 Radical and molecular yields in water irradiated by gamma.-rays and heavy ions. J. Phys. Chem. 73 (6): 1937–1941

[2] Baughman, R. H., Zakhidov, A. A., De Heer, W. A. 2002. Carbon Nanotubes—the Route toward Applications. Science 297: 787-792.

[3] Belin T., Epron F. Characterization methods of carbon nanotubes: a review. 2005. Mater. Sci. Eng., B 119: 105–118.

[4] Belloni, J., Mostafavi, M., Remita, H., Marignier, J.L. Delcourt, M.O.1998. Radiation-induced synthesis of mono-and multi-metallic clusters and nanocolloids. New J. Chem: 1239-1255.

[5] Chen, Y.L., Liu, B., Wu, J., Huang, Y., Jiang, H., Hwang, K.C. 2008 Mechanics of hydrogen storage in carbon nanotubes. J. Mec Phys Solids 56: 3224–3241.

[6] Cheng H. M., Yang, Q.H., Liu, C. 2001. Hydrogen Storage in Carbon Nanotubes. Carbon 39: 1447–1454.

[7] Choi, H. C., Shim, M., Bangsaruntip, S., Dai, H. 2002. Spontaneous reduction of metal ions on the sidewalls of carbon nanotubes. J. Am. Chem. Soc. 124 (31): 9058–9059

[8] Doudna, C. M., Bertino, M. F., Blum, F. D., Tokuhiro, A. T. Lahiri-Dey, D., Chattopadhyay S., Terry, J. 2003. Radiolytic Synthesis of Bimetallic Ag-Pt Nanoparticles with a High Aspect Ratio. J. Phys. Chem. B 107: 2966-2970

[9] Eisa, W. H., Abdel-Moneam, Y. K., Shaaban, Y., Abdel-Fattah, A. A., Amira M. A. Z. 2011. Gamma-irradiation assisted seeded growth of Ag nanoparticles within PVA matrix. Mater. Chem. Phys. 128(1–2): 109–11

[10] Fedoseeva Y. V., Bulusheva, L. G., Okotrub, A. V., Vyalikh, D. V., Fonseca, A. 2010. High reactivity of carbon nanotubes and fluorinated carbon nanotubes irradiated by Ar+ ions. Phys. Status Solidi B 247(11–12): 2691–2694

[11] Gasaymeh, S. S., Radiman, S., Heng, L.Y., Saion, E. Saeed, G.H. M. 2010. Synthesis and Characterization of Silver/Polyvinilpirrolidone (Ag/PVP) Nanoparticles Using Gamma Irradiation Techniques. Am. J. Applied Sci. 7 (7): 892-901

[12] Georgakilas, V., Gournis, D., Tzitzios, V., Pasquato L., Guldie, D. M., Prato, M. 2007. Decorating carbon nanotubes with metal or semiconductor nanoparticles. J. Mater. Chem. 17: pp. 2679–2694.

[13] Guo, J., Li, Y., Wu, S. Li, W. 2005. The effects of γ-irradiation dose on chemical modification of multi-walled carbon nanotubes. Nanotechnology 16: 2385–2388.

[14] Hirsch, A. 2002. Functionalization of Single-Walled Carbon Nanotubes, minireview. Angew. Chem. Int. Ed. 41 (11): 1853-1859.

[15] Hou, P.X., Xu, S.T., Ying, Z., Yang, Q.H., Liu, C., Cheng, H.M. 2003. H ydrogen adsorption / desorption behavior of multi-walled carbon nanotubes with different diameters. Carbon 41: 2471–2476.

[16] Hulman, M., Skakalova, V., Kuzmany, S. R. H. 2005. Raman spectroscopy of single-wall carbon nanotubes and graphite irradiated by γ rays. J. Appl. Phys. 98 (024311): 1-6.

[17] Joshi, S.S., Patil, S.F., Iyer, V., Mahumuni, S. 1998. Radiation induced synthesis and characterization of copper nanoparticles. Nanostruct Mat 10(7): 1135–1144

[18] Karousis, N, Tsotsou, G.E., Evangelista, F., Rudolf, P., Ragoussis, N., Tagmatarchis, N. 2008. Carbon Nanotubes Decorated with Palladium Nanoparticles: Synthesis, Characterization, and Catalytic Activity J. Phys. Chem. 112: 13463–13469.

[19] Krasheninnikov, A. V., Nordlund, K. 2010. Ion and electron irradiation-induced effects in nanostructured materials. J. Appl. Phys. 107 (071301): 1-70

[20] Krasheninnikov, A.V. Nordlund, K. Irradiation effects in carbon nanotubes. 2004. Nucl. Instr. and Meth. in Phys. Res. B 216: 355–366

[21] Lee, K.P., Gopalan, A. I., Santhosh, P., Lee, S. H., Nho, Y. C. 2007. Gamma radiation induced distribution of gold nanoparticles into carbon nanotube-polyaniline composite. Compos Sci Technol 67: 811–816.

[22] Lia, T., Parka, H. G., Choib S.H. 2007. γ-Irradiation-induced preparation of Ag and Au nanoparticles and their characterizations. Mater. Chem. Phys 105: 325–330

[23] Liu, F.K., Hsu, Y. C., Tsai, M.H., Chu, T.C. 2003. Using γ-irradiation to synthesize Ag nanoparticles. Radiat Phys Chem 67: 517–521.

[24] Makala S. Raghuveer, Ashavani Kumar, Matthew J. Frederick, Gregory P. Louie, P. Gopal Ganesan, and Ganapathiraman Ramanath. "Site-Selective Functionalization of Carbon Nanotubes". Adv. Mater. 18, 2006, pp 547–552.

[25] Oh, S.D., So, B.K., Choi, S.H., Gopalan, A., Lee, K.P., Yoon, K. R., Choi, I. S. 2005. Dispersing of Ag, Pd, and Pt–Ru alloy nanoparticles on single-walled carbon nanotubes by g-irradiation. Mater. Lett. 59: 1121–1124.

[26] Popov, V. N. 2004. Carbon nanotubes: properties and application. Mat Sci Eng R 43: 61-102.

[27] Quinn, B.M., Dekker, C., Lemay, S. G. 2005. Electrodeposition of Noble Metal Nanoparticles on Carbon Nanotubes. J. Am. Chem. Soc., 127 (17): 6146–6147.

[28] Qu, L. Dai, L.2005. Substrate-Enhanced Electroless Deposition of Metal Nanoparticles on Carbon Nanotubes. J. AM. CHEM. SOC. 127: 10806-10807

[29] Rakhi, R.B., Sethupathi, K., Ramaprabhu, S. 2008. Synthesis and hydrogen storage properties of carbon nanotubes. Int. J. Hydrogen Energy 33: 381 – 386.

[30] Rashidi, A.M., Nouralishahi, A., Khodadadi, A.A., Mortazavi, Y., Karimi, A., Kashefi, K. 2010. Modification of single wall carbon nanotubes (SWNT) for hydrogen storage. Int. J. hydrogen energy 35: 9489-9495.

[31] Remita, H., Remita, S. 2010. Metal cluster and Nanomaterials: Contribution of radiation chemistry. In Recent trends in radiation chemistry, ed. James F. Wishart, B. S. M. Rao, 347-383. World scientific publishing Co.

[32] Ren, G., Xing, Y. 2006. Deposition of metallic nanoparticles on carbon nanotubes via a fast evaporation process. Nanotechnology 17(22): 5596–5601

[33] Rojas, J., Castano, C. H.2011. Production and characterization of supported transition metal nano-particles on multi-walled carbon nanotubes functionalized by gamma irradiation and chemical processes. Supplemental proceedings: volume 1: materials processing and energy materials TMS (the minerals, metals & materials society). John Wiley & Sons, Inc.

[34] Rojas, J. V. Castano, C. H. 2012. Production of palladium nanoparticles supported on multiwalled carbon nanotubes by gamma irradiation. Radiat. Phys. Chem. 81 (1): 16-21.

[35] Salah, N., Habib, S.S., Khan, Z. H., Al-Hamedi, S. Djouider, F. 2009. Functionalization of gold and carbon nanostructured materials using gamma-ray irradiation. Rad. Phys. Chem. 78: 910–913

[36] Sarkany, A., Papp, Z., Sajo, I., Schay, Z. 2005. Unsupported Pd nanoparticles prepared by gamma-radiolysis of PdCl2. Solid State Ionics 176: 209–215.

[37] Sarkar, A. Banerjee, R. 2004. A quantitative method for characterization of carbon nanotubes for hydrogen storage. Int. J. Hydrogen Energy 29: 1487 – 1491.

[38] Skakalova, V., Dettlaff-Weglikowska, U., Roth, S. 2004. Gamma-irradiated and functionalized single wall nanotubes". Diamond Relat. Mater. 13: 296–298

[39] Skakalova, V., Hulman, M., Fedorko, P., Lukac, P., Roth, S. 2003. Effect of Gamma-Irradiation on Single-Wall Carbon Nanotube Paper. AIP Conf. Proc. 685: 143-147.

[40] Strobel, R., Garche J., Moseley, P.T., Jorissen, L., Wolf, G. 2006. Hydrogen storage by carbon materials. J. Power Sources 159: 781–801.

[41] Star, A., Joshi, V., Skarupo, S., Thomas, D., Gabriel, J.C. P. 2006. Gas Sensor Array Based on Metal-Decorated Carbon Nanotubes. J. Phys. Chem. B 110: 21014-21020

[42] Sun, Z., Liu, Z., Han, B., Miao, S., Miao, Z., An,G. 2006. Decoration carbon nanotubes with Pd and Ru nanocrystals via an inorganic reaction route in supercritical carbon dioxide–methanol solution. J. Colloid Interface Sci. 304: 323–328.

[43] Suttisawat, Y., Rangsunvigit, P., Kitiyanan, B., Williams, M., Ndungu, P., Lototskyy, M.V., Nechaev, A., Linkov, V., Kulprathipanja, S. 2009. Investigation of hydrogen storage capacity of multi-walled carbon nanotubes deposited with Pd or V. Int. J. hydrogen energy 34: 6669–6675.

[44] Tessonnier, J.-P., Pesant, L., Ehret, G., Ledoux, M. J., Pham-Huu C. 2005. Pd nanoparticles introduced inside multi-walled carbon nanotubes for selective hydrogenation of cinnamaldehyde into hydrocinnamaldehyde. Appl. Catal., A (1-2): 203-210

[45] Terrones, M., Banhart f., Grobert N., Charlier J.-C., Terrones, H., Ajayan, P. M. 2002. Molecular junctions by joining single-walled carbon nanotubes. Phys. Rev. Lett 89 (7): 075505-1-4

[46] Vairavapandian, D., Vichchulada, P., Lay, M. D. 2008. Preparation and modification of carbon nanotubes: Review of recent advances and applications in catalysis and sensing. Anal. Chem. Acta 626 (2): 119–129

[47] Wang, H., Sun, X., Ye, Y., Qiu, S. 2006. Radiation induced synthesis of Pt nanoparticles supported on carbon nanotubes. J. Power Sources 161: 839–842

[48] Wildgoose, G. G., Banks, C.E., Compton R. G. 2006. Metal Nanoparticles and Related Materials Supported on Carbon Nanotubes: Methods and Applications. Small 2(2): 182 – 193

[49] Wishart, J. F. 2008. Tools for radiolysis studies. In Radiation chemistry: from basics to applications in material and life sciences, ed. Mélanie Spotheim-Maurizot, Mehran Mostafavi, Jacqueline Belloni, Thierry Douki, 17-34. EDP sciences.

[50] Xue, B., Chen, P., Hong, Q, Lin, J. Tan, K.L. 2001. Growth of Pd, Pt, Ag and Au nanoparticles on carbon nanotubes. J. Mater. Chem. 11: 2378-2381.

[51] Xu, Z., Chen, Lei; Liu, L. Wu, X., Chen, L. 2011. Structural changes in multi-walled carbon nanotubes caused by γ-ray irradiation. Carbon 49(1): 350-351

[52] Yuruma, Y., Taralp, A., Veziroglu, T. N. 2009. Review Storage of hydrogen in nanostructured carbon materials. Int. J. hydrogen energy 34: 3784–3798.

[53] Zacharia, R., Kim, K.Y., Fazle, A.K.M., Nahm, K. S.2005. Enhancement of hydrogen storage capacity of carbon nanotubes via spill-over from vanadium and palladium nanoparticles. Chem. Phys. Lett. 412: 369–375.

[54] Zhang, X., Ye, Y., Wang, H., Yao, S. 2010. Deposition of platinum–ruthenium nano-particles on multi-walled carbon nano-tubes studied by gamma-irradiation. Radiat Phys Chem. 79: 1058–1062.

[55] Zhu, Y., Qian, Y., Li, X., Zhang, M. 1998. A nonaqueous solution route to synthesis of polyacrylamide-silver nanocomposites at room temperature. Nanostruct. Mater. 10(4): 673-678

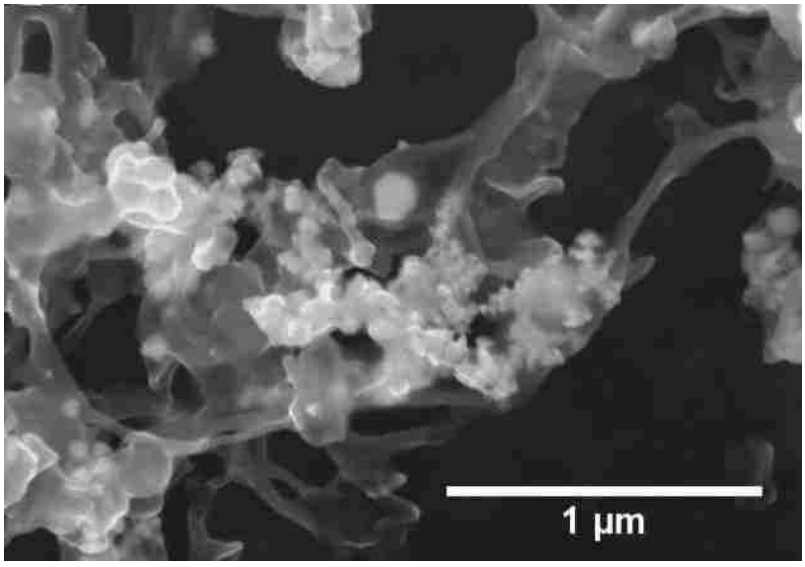

(a)

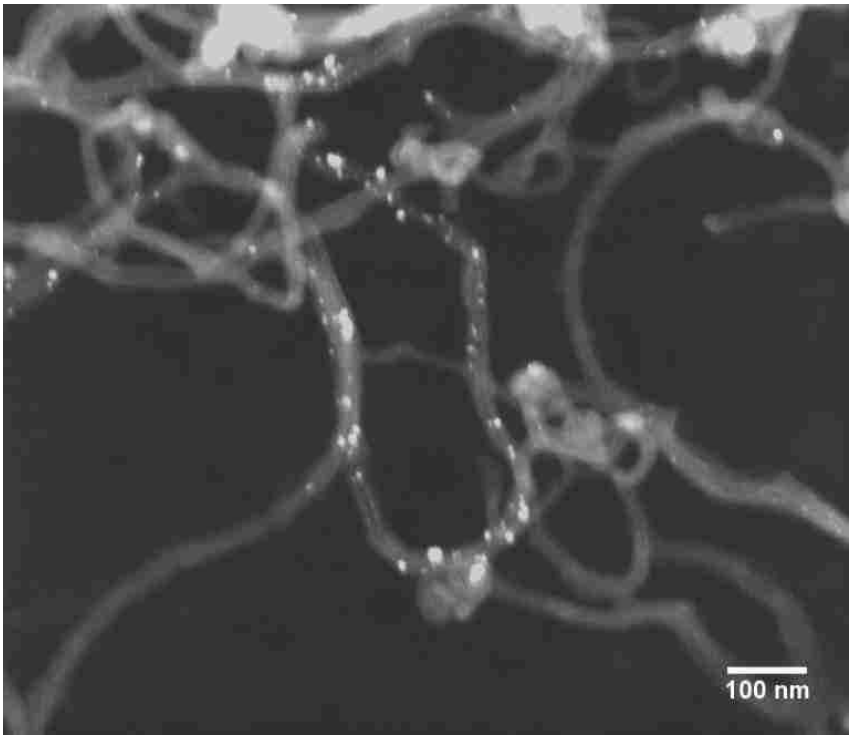

(b)

Figure 1. Images of MWCNTS-Pd after gamma irradiation a)SEM of sample irradiated at 30 kGy containing SDS at 15mM, b) STEM of sample irradiated at 40 kGy containing SDS at 0.05M.

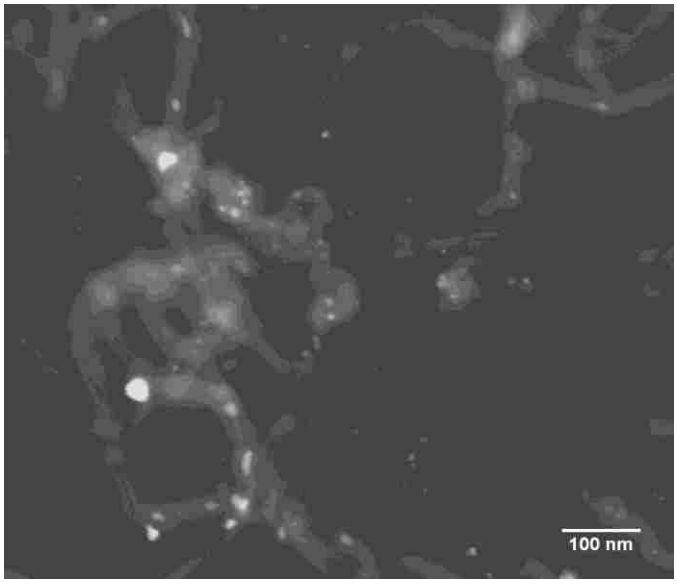

(a)

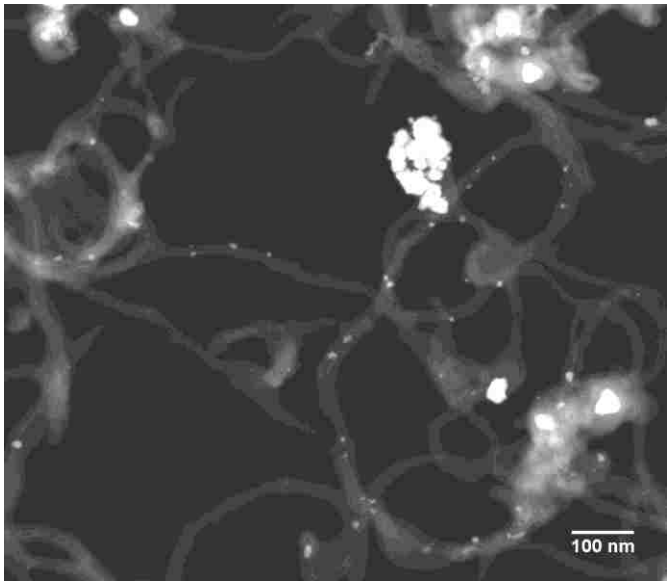

(b)

Figure 2. STEM images of MWCNTs decorated with Pd nanoparticles with 0.07M SDS irradiated at a dose rate of 10 kGy/h and different doses at a) 10 kGy, b) 20 kGy, c) 30 kGy, d) 40 kGy. Reprinted with permission from Rojas and Castano 2012. Radiat. Phys. Chem. 81 (1): 16-21

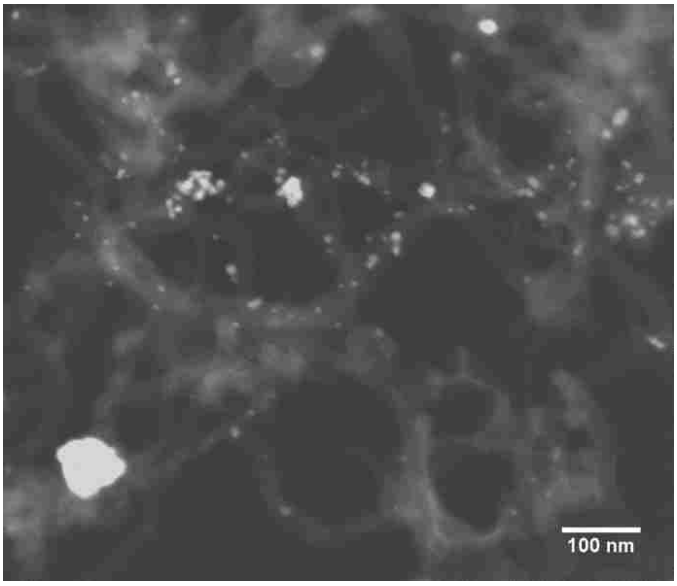

(c)

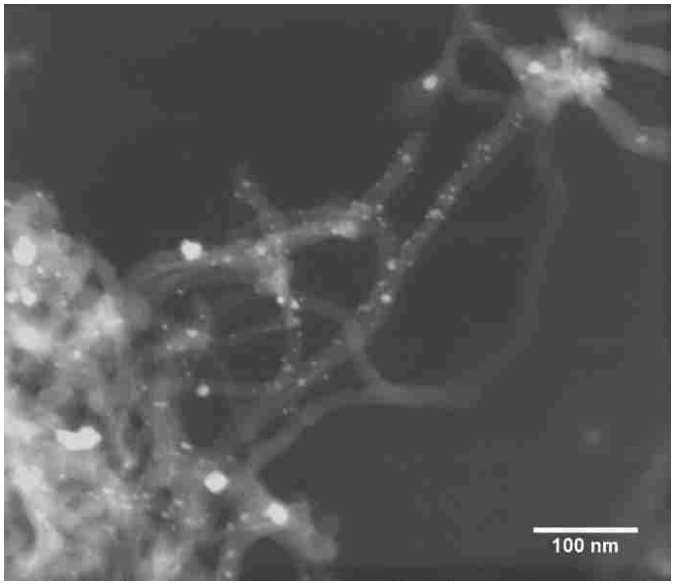

(d)

Figure 2. STEM images of MWCNTs decorated with Pd nanoparticles with 0.07M SDS irradiated at a dose rate of 10 kGy/h and different doses at a) 10 kGy, b) 20 kGy, c) 30 kGy, d) 40 kGy. Reprinted with permission from Rojas and Castano 2012. Radiat. Phys. Chem. 81 (1): 16-21 (cont).

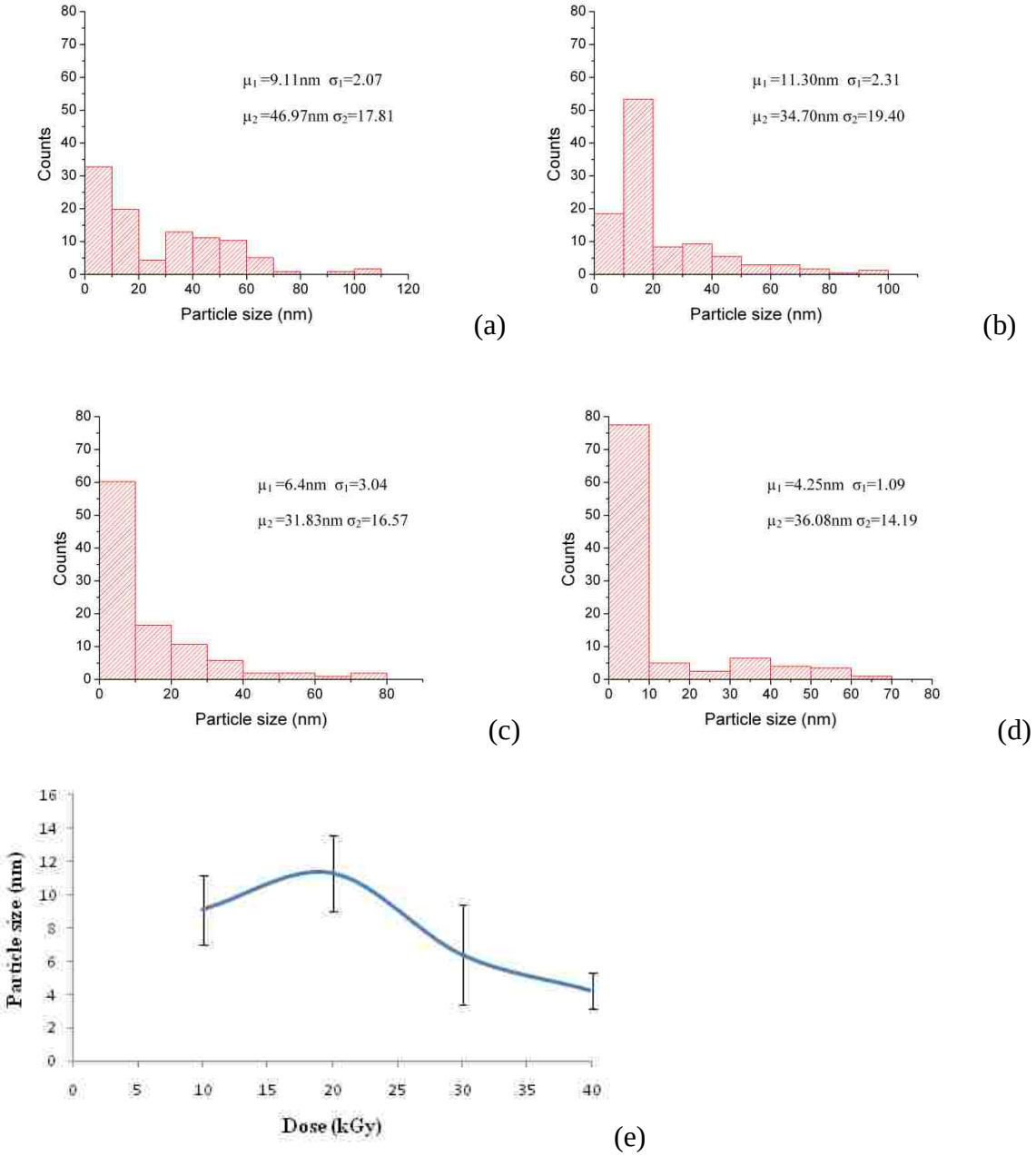

Figure 3. Particle size distribution (diameter in nm) of Pd nanoparticles on MWCNTs with 0.07M SDS irradiated at a dose rate of 10 kGy/h and different doses at a) 10 kGy, b) 20 kGy, c) 30 kGy, d) 40 kGy and e) Plot of particle size vs. dose. Reprinted with permission from Rojas and Castano 2012. Radiat. Phys. Chem. 81 (1): 16-21.

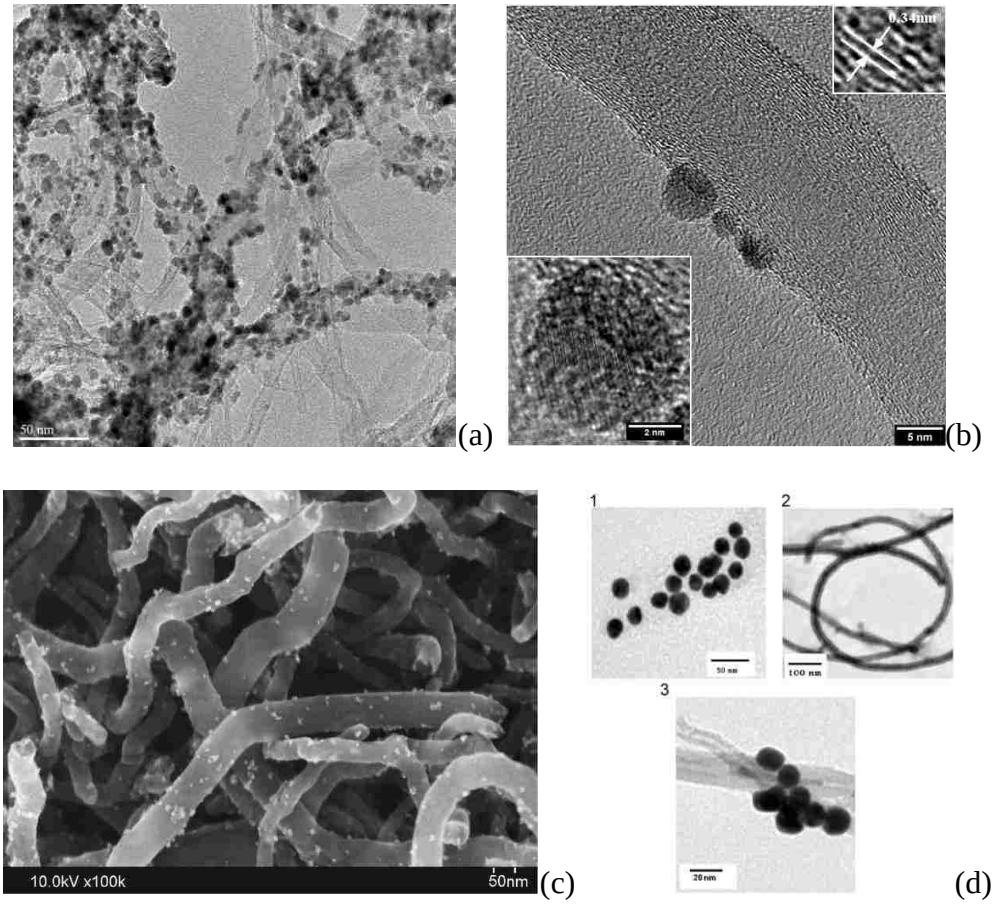

Figure 4. a) TEM images of MWCNT decorated with Pd nanoparticles at 40 kGy and 0.07M SDS (Reprinted with permission from Rojas and Castano 2012. Radiat. Phys. Chem. 81 (1): 16-21) b) High resolution TEM image of MWCNT decorated with Pd nanoparticles showing the d spacing of Pd ((d_{111}) of 0.2246 nm) and interwall space of a MWCNT, c) SEM image of the Pt/Ru nanoparticles on MWCNTs prepared in aqueous solution with a water/isopropanol ratio of 60:40(v/v) irradiated to 40 kGy (Reprinted with permission from Zhang et al 2010. Radiat Phys Chem. 79: 1058–1062) and d) TEM images of (1) gold nanoparticles reduced from 0.17mM$HAuCl_4$ using 1%solution of $Na_3C_6H_5O_7.2H_2O$, (2) carbon nanotubes (2mg/ml), (3) attached gold nanoparticles on the surface sites of carbon nanotubes in aerated solutions due to gamma rays irradiation in air (Reprinted with permission from Salah et al 2009. Rad. Phys. Chem. 78: 910–913).

II. SYNTHESIS OF RHENIUM OXIDE NANOPARTICLES (Re_xO_y) BY GAMMA IRRADIATION

J. V. Rojas [a], C. H. Castano [a*]

[a] Department of Mining and Nuclear Engineering, Missouri University of Science and Technology, 301 W. 14th ST, Rolla, MO 65409 USA. jvr45d@mst.edu

[a*] Corresponding author. Department of Mining and Nuclear Engineering, Missouri University of Science and Technology, 301 W. 14th St. Rolla MO 65409 USA. castanoc@mst.edu. Tel: +1 – (573) 341 – 6766. Fax: +1 – (573) 341 – 6309

Abstract

Rhenium nanoparticles in the form of Re_xO_y were synthesized by gamma irradiation. A solution of sodium perrhenate in a mixture of water-isopropanol with a volume ratio of 2:1 was prepared. The solution was irradiated with a cobalt-60 gamma source with absorbed doses of 10, 20, 30 and 40 kGy. During gamma irradiation of water, strong oxidizing and reducing species are produced, thus isopropanol was primarily added in order to scavenge the oxidizing species. Radiolytic reduction of perrhenate ions leads to nucleation and growth of nanoparticles with average sizes between 10 and 55 nm. The size and size distribution of the resulting nanoparticles were investigated at three different concentrations of sodium perrhenate, 1, 3, and 5mM, without the addition of any surfactant or stabilizer. Morphological and structural characteristics of the nanoparticles were performed with STEM, TEM, and UV-vis spectroscopy. Average particle size was

found to increase in general with increased absorbed dose and initial concentration of sodium perrhenate. Nonetheless, for the 5mM solution of sodium perrhenate, the particle size increased from 10 to 30 kGy and a decrease was observed at 40 kGy. The nanoparticles were found to be amorphous.

Keywords: Rhenium, nanoparticles, perrhenate ions, gamma irradiation, radiation induced chemistry

1. Introduction

The synthesis of transition metals nanostructures and their oxides has been widely explored due to their fascinating physical and chemical properties. Diverse methodologies for the synthesis of transition metals nanoparticles such as gold (Grzelczak et al., 2008; Zhao et al., 2013), platinum (Kim et al., 2011; Boneta et al., 1999), palladium (James, 2012; Rojas and Castano, 2012), rhodium (Hoefelmeyer et al., 2007), and silver (Sun, 2013) and transition metal oxides (Vijaya et al., 2000; Alrehaily et al., 2013) have been developed. The applications of these nanomaterials in different areas such as optics, electronics, catalysis, and medicine have been broadly studied holding promising results.

Rhenium, being part or the transition metals group, has gained significant attention as it poses a unique combination of properties that position it as a high performance engineering material. Rhenium has the second highest melting point (3157 °C) surpassed only by tungsten. It also has a low friction coefficient and high hardness which makes it a suitable material for wear resistance applications. Rhenium also has

found applications in aircraft and aerospace, catalysis, electronics, and coatings (Carlen and Bryskin, 1994; Bryskin, 1992). In biomedical applications, rhenium isotopes $^{188}Re/^{186}Re$ have been considered as candidate for radiotherapy as it has a short half-life of 16.9 h which minimizes the toxicity to the body; beta emissions of 1.069 and 2.12 MeV, suitable for radiotherapy; and gamma emission of 155 keV which allows imaging distribution in the body (Conzone et al., 1998; Häfeli et al., 2001). However, given the rarity and elevated price of rhenium, limited research has been done regarding its synthesis and applications in nanostructures.

The controlled synthesis of rhenium compounds, such as rhenium oxides, has become special interest due to their remarkable catalytic activity (Broadbent, et al., 1962; Chong et al., 2012) and electrical properties (Biswas and Rao, 2006) which make them potential candidates for production of electronic components such as solid oxide fuel cells, solid state batteries, liquid crystal cells, catalyst among others (Cazzanelli et al., 2009; Vargas-Uscateguia et al., 2013).

Mucalo and Bullen reported the synthesis of rhenium hydrosol system. It was produced by the reduction of aqueous potassium hexachlororhenate with hydrazine using a gum arabic as protecting agent. The particles were found to have an average size of 316 nm. However, their stability was hindered by the fact that they slowly dissolve in water over time to form the highly stable perrhenate ion (Babu and Mucalo, 2003; Mucalo and Bullen, 2001).

Rao and Biswas synthesized ReO_3 nanoparticles with a particle size between 8.5 and 32.5 nm. The nanoparticles were prepared by decomposition of the Re_2O_7-dioxane complex under solvothermal conditions. ReO_3 is one of the most interesting transition metal oxides as its electrical conductivity is close to that of copper (Biswas and Rao, 2006). The preparation of Re nanoparticles by means of pulsed-laser decomposition methods was recently reported by Chong et al. Starting from a ammonium perrhenate or dirhenium decacarbonyl as the precursor and 3-ercaptopropionic acid (MPA) as the capping agent nanoparticles with an average size of 40 nm were obtained (Chong et al., 2012).

Radiation chemistry has contributed to the advances in the synthesis of nanostructures since the reduction of metal precursors may also be achieved by the species generated during irradiation of aqueous solutions (Rojas and Castaño, 2012, 2013). This process has the advantage of simple physicochemical conditions that leads to homogeneous reduction and nucleation of the nanoparticles (Belloni et al., 1998; Belloni et al., 2001; Remita et al., 2010). In this work the synthesis of rhenium nanoparticles in the form of Re_xO_y by gamma irradiation is reported. The resulting nanoparticles were characterized with STEM, TEM and UV-vis spectroscopy.

2. Experimental Procedure

2.1 Materials

Sodium perrhenate (99.95% metals basis) and isopropanol (99.5% high purity) were purchased from Alfa Aesar and were used without any further purification. Deionized water was used to prepare the solutions.

2.1.1 Samples preparation

Initially, solutions containing sodium perrhenate in concentrations of 1, 3 and 5mM were prepared in a mixture of deionized water-isopropanol (2:1 v/v) (approximate pH of 5). Next, the samples were placed in an ultrasonic bath during 30 minutes to obtain a homogeneous dispersion. Then, the solutions were distributed in 2ml glass vials and degassed with argon to remove oxygen. Lastly, the samples were irradiated in a Cobalt 60 Gammacell 220 Excel (MDS, Nordion) with absorbed doses of 10, 20, 30 and 40 kGy (dose rate 10 kGy/hr).

2.1.2 Characterization

The morphology and crystalline structure of the resulting nanoparticles were evaluated with a Helios NanoLab 600 in STEM mode at 30kV and a TEM TECNAI F20 at 200kV. The suspensions were initially sonicated for 30 minutes and a drop was directly placed on a formvar-carbon coated copper grid. The UV-VIS absorption spectra of the suspensions were recorded on a Thermo Scientific *GENESYS 10S* spectrophotometer in a wavelength interval between 200 and 800 nm. Quartz square spectrophotometer cuvettes, with 10mm pathlength, and 3.5ml capacity were used.

3. Results and discussion

Radiolysis of water leads to highly reactive species such as H•, OH•, H^+, H_2O_2, H_2 and electrons in aqueous solution (e^-_{aq}) that are produced due to high energy radiation. These species are uniformly generated in water and the concentration is given by the G factor, representing the number of molecules or radicals produced per 100 eV of radiation energy absorbed. Product yields are well known for gamma irradiated aqueous solution and the values are G(H•)=0.61, G(OH•)=2.86, G(H^+)=2.70, G(H_2O_2)=0.61, G(H_2)=0.43, G(e^-_{aq})=2.7 (Appleby and Schwarz, 1969).

The species e^-_{aq}, H• and OH• are reactive, being the first two strong reducing agents with redox potentials: E° (H_2O/e^-_{aq}) = -2.87 V_{NHE} and E° (H^+/ H•) = -2.3 V_{NHE}, respectively. They can reduce the perrhenate ions. On the other hand, OH• radicals are strong oxidizing agents with E° (OH•/H_2O) = +2.8 V_{NHE}, thus, bringing the reduced species to a higher oxidation state. Primary or secondary alcohols or formate ions are added to the solution prior to irradiation as scavengers of OH• radicals. The secondary radicals, generated as a result of the reaction between the scavenger and radiolysis species H• and OH•, are also strong reducing agents; the reactions are summarized in Table 1 (Belloni et al., 1998; Remita and Remita, 2010).

The standard potential of the Re/ ReO_4^- and Re_2O_3/ReO_4^- couple in acidic and solutions has been previously reported as (Bard et al., 1985)

$$Re + 4H_2O \rightarrow ReO_4^- + 8H^+ + 7e^- \qquad E^0 = -0.34V \qquad (1)$$

$$Re_2O_3 + 5H_2O \rightarrow 2ReO_4^- + 10H^+ + 8e^- \qquad E^0 = -0.476V \qquad (2)$$

In the case of ReO_2/ReO_4^- and ReO_3/ReO_4^-, the standard potentials of the couples have been reported and are summarized in Standard Potentials in Aqueous Solutions. ReO_2/ReO_4^- couple was measured by Hugs (Z. Z. Hugs, cited in Bard et al, 1985):

$$ReO_2 + 2H_2O \rightarrow ReO_4^- + 4H^+ + 3e^- \qquad E^0 = -0.51V \qquad (3)$$

Likewise, King and Cobble measured the electrode potentials of ReO_3/ReO_4^- (King and Cobble, 1957; Bard et al., 1985):

$$ReO_3 + H_2O \rightarrow ReO_4^- + 2H^+ + e^- \qquad E^0 = -0.765 \pm 0.008V \qquad (4)$$

According to these reactions, the four different species are likely to be present after gamma irradiation of the aqueous solutions containing perrhenate ions. Nonetheless, given the perrhenate concentrations and slightly acidic solutions studied here, the oxides Re_2O_3 and ReO_2 are thermodynamically the most stable species.

The solution of water, alcohol and, sodium perrhenate was initially transparent as shown in Figure 1 a). After irradiation the samples turned brown and the color change was more prominent with increasing absorbed dose and concentration of perrhenate ions. This can be seen in Figure 1 b) which shows the 3mM perrhenate samples after irradiation with absorbed doses of 10, 20, 30, and 40 kGy. The darkening of the solution is due to an increase in reduced species, either by the formation of new nuclei or the growth of existing particles (probably both). The color change of sodium perrhenate

solutions has been previously reported as a consequence of borohydride reduction of perrhenate ions resulting in Re_2O_3 species (Broadbent and Johnson, 1962).

Nanoparticles synthesized by radiolytic reduction of perrhenate ions are shown in Figure 2. STEM images of the nanoparticles obtained at absorbed doses of 10, 20, 30 and 40 kGy revealed their spherical shape and the variation of size as a function of dose and salt concentration. In order to study the dependence of these two factors in the particle size and distribution, a set of images was acquired for each of the samples. Subsequently, the particle size was measured by using the software ImageJ. Figure 3 summarizes the results obtained for the average size and standard deviation of the nanoparticles as a function of dose at the concentration of 1mM, 3mM, and 5mM. The particle size was found to increase as a function of absorbed dose for the concentrations of 1mM and 3mM. Since the binding energy between two reduced species is stronger than the atom-solvent or atom-ligand bond energy, the species tend to dimerize when they encounter or associate with an excess of ions (Belloni et al., 1998). Since no stabilizer was added for the synthesis, an increase in dose leads to an increase in the average particle size.

By further increasing the concentration of perrhenate ions to 5mM the particle size increases from 10 to 30 kGy and decreases at 40 kGy. Apparently, at this high dose a considerable amount of perrhenate ions is consumed during the nucleation process leading to a decrease in the particle size at 40 kGy. The measured particle sizes at various concentrations and doses of 10, 20, 30, and 40 kGy are summarized in Table 2.

The 3mM $NaReO_4$ sample irradiated at 40 kGy was evaluated with TEM to better verify the particle size and assess the crystalline structure of the nanoparticles. Figure 4 shows the TEM image obtained at 200KV in bright field mode. By means of electron diffraction analysis the nanoparticles were found to be amorphous. EDX analysis carried out in the TEM owing to the small interaction volumes that can be achieved with the instrument. Spectra were collected in different regions showing that the nanoparticles are oxygen rich with an atomic ratio of O/Re varying between 2.1 and 3.2. EDX spectrum obtained from the 3mM $NaReO_4$ sample irradiated at 40 kGy with the respective region of interest is shown in Figure 5. Note that the presence silicon (Si), aluminum (Al), chromium (Cr) and iron (Fe) peaks are due to internal components of the equipment.

UV-vis spectra of the 3mM $NaReO_4$ solution before irradiation (0 kGy dose) and after 10, 20, 30, and 40 kGy doses are shown in Figure 7. In the spectrum of the non irradiated sample, there is a prominent peak at 228 nm which is characteristic of perrhenate ions. After irradiation, an absorption peak appears at around 350 and the absorbance increases with increasing radiation dose from 10 to 40 kGy.

Nanoparticles synthesized by gamma irradiation were found to be stable in the suspension for a period of about 3 weeks. Afterwards, the suspension color changed slowly from yellow-brown back to transparent. This event could be an evidence of reoxidation of the reduced species. According to the stability of the rhenium oxides Re_2O_3 may undergo oxidation to ReO_2 in acid or neutral solutions and to ReO_4^- in alkaline solutions. Likewise, ReO_2 can be oxidized to ReO_3 or perrhenic acid in very acid

solutions or to ReO_4^- in less acidic conditions. However, this needs to be studied in more detail to evaluate the stability of the synthesized nanoparticles.

Instability in water of reduced $ReCl_6^-$ with hydrazine has been previously reported. It was found that that hydrazine-generated "rhenium hydrosols" are unstable in water and slowly dissolve over time in aqueous media to form the highly stable perrhenate ion (Mucalo and Bullen, 2001). The stability of rhenium based nanoparticles has to be considered when being used in aqueous systems and developing advanced applications of this material.

4. Conclusions

In this work, the synthesis of rhenium based nanoparticles through radiolytic reduction of perrhenate ions in a water-isopropanol solution is described. The nanoparticles were synthesized without any surfactant/stabilizer in a dose range from 10 to 40 kGy at various concentrations of sodium perrhenate (1, 3, 5mM). The nanoparticles size was found to increase with increasing dose between 10 and 40 kGy for concentrations of sodium perrhenate of 1mM and 3mM. The average particle size increased from 10 to 15 nm and from 23 to 39 nm for the sodium perrhenate 1 and 3 mM solutions respectively. For the 5mM solution the particle size increased from 10 to 30 kGy and a decrease is observed at 40 kGy. The synthesized nanoparticles were found to be amorphous. Calcination of the nanoparticles will be conducted in order to evaluate crystalline phase's formation.

Acknowledgements

The authors would like to thank Dr. Stoyan Toshkov at the Nuclear, Plasma, and Radiological Engineering Department at the University of Illinois for his help in irradiating the samples. Thanks to Carlos E. Castano for his technical assistance in electron microscopy. Thanks to the Materials Research Center (MRC) for partial funding provided for the analysis and, to the Energy Research and Development Center (ERDC) for their financial support.

This work was supported by NRC radiochemistry grant PPR-NRC-38-10-966

References

Alrehaily, L. M., Joseph, J. M., Musa, A. Y., Guzonas, D. A., Wren, J. C., 2013. Gamma-radiation induced formation of chromium oxide nanoparticles from dissolved dichromate. Phys. Chem. Chem. Phys. 15, 98-107

Alrehaily, L. M., Joseph, J. M., Biesinger, M. C., Guzonas, D. A., Wren, J. C., 2013. Gamma-radiolysis-assisted cobalt oxide nanoparticle formation. Phys. Chem. Chem. Phys. 15, 1014-1024

Appleby, A., Schwarz, H. A., 1969. Radical and molecular yields in water irradiated by gamma rays and heavy ions. J. Phys. Chem. 73 (6), 1937–1941.

Babu, K. M., Mucalo, M. R., 2003. XPS studies of freshly prepared rhenium nanoparticle dispersions from hydrazinium hydrate and borohydride reduction of hexachlororhenate solutions. J. Mater. Sci. Lett. 22, 1755 – 1757.

Bard, A. J., Parsons, R., & Jordan, J. CRC Press. 1985. Standard potentials in aqueous solution. Chapter 15.

Belloni J., Mostafavi. Jonah C.D., Rao, B.S. M., 2001. Radiation chemistry of nanocolloids and clusters. Radiation Chemistry: Present status and future trends. Elsevier, 411-452.

Belloni J., Mostafavi, M., Remita, H., Marignier, J.-L., and Delcourt, M.-O., 1998. Radiation-induced synthesis of mono- and multi-metallic clusters and Nanocolloids. New J. Chem. 1239-1255.

Biswas K., Rao, C. N. R., 2006. Metallic ReO_3 Nanoparticles. J. Phys. Chem. B. 110, 842-845.

Boneta, F., Delmasa, V., Grugeona, S., Herrera U. R., Silverta, P-Y., Tekaia-Elhsissena, K. 1999. Synthesis of monodisperse Au, Pt, Pd, Ru and Ir nanoparticles in ethylene glycol. Nanostructured Materials. 11 (8), 1277–1284

Broadbent, H. S., Johnson, J. H., 1962. Rhenium Catalysts. IV. Rhenium (III) Oxide from Perrhenate via Borohydride Reduction. J. Org. Chem. 7 (12), pp 4400–4402

Bryskin, B. D. 1992. Rhenium and its alloys. Advanced Materials and Processes;(United States), 142(3).

Carlen, J. C., Bryskin, B. D., 1994. Rhenium-a unique rare metal. Material and manufacturing process. 9(6), 1087-1104.

Cazzanelli, E., Castriota, M., Marino, S., Scaramuzza, N., Purans, J., Kuzmin, A., Kalendarev, R., Mariotto, G., Das, G., 2009. Characterization of rhenium oxide films and their application to liquid crystal cells. J. of appl. phys. 105, 114904.

Chong, Y. Y., Chow, W. Y., Fan, W. Y., 2012. Preparation of rhenium nanoparticles via pulsed-laser decomposition and catalytic studies. J. Colloid Interf. Sci. 369, 164–169.

Conzone, S. D., Haefeli, U. O., Day, D. E., Ehrhardt, G. J., 1998. Preparation and properties of radioactive rhenium glass microspheres intended for in vivo radioembolization therapy. J. Biomed. Mater. Res. 42(4), 617-625.

Grzelczak, M., Pérez-Juste, J., Mulvaney, P., and Liz-Marzán, L. M., 2008. Shape control in gold nanoparticle synthesis. Chem Soc. Rev. 37, 1783-1791

Häfeli, U. O., Roberts, W. K., Pauer, G. J., Kraeft, S. K., Macklis, R. M., 2001. Stability of biodegradable radioactive rhenium (Re-186 and Re-188) microspheres after neutron-activation. Appl. Radiat. Isot. 54(6), 869-879.

Hoefelmeyer, J. D., Liu, H. Somorjai, G. A., Tilley, T. D., 2007. Reverse micelle synthesis of rhodium nanoparticles. J. Colloid Interface Sci. 309(1), 86–93.

James, C., 2012. The Preparation of Palladium Nanoparticles. Platinum Metals Review. 56 (2), 83-98(16)

Kim, S. C., Shim, W. G., Lee, M. S., Jung, S. C., Park, Y-K. 2011. Preparation of Platinum Nanoparticle and Its Catalytic Activity for Toluene Oxidation. J. Nanosci. Nanotechnol. 11 (8), 7347-7352.

King, J. P., & Cobble, J. W. 1957. Thermodynamic Properties of Technetium and Rhenium Compounds. VI. The Potential of the ReO3/ReO4-Electrode and the Thermodynamics of Rhenium Trioxide1, 2. J. Amer. Chem. Soc. *79*(7), 1559-1563.

Mucalo, M. R., Bullen, C. R., 2001. Rhenium-Based Hydrosols: Preparation and Properties J. Colloid Interf. Sci. 239, 71–77.

Pourbaix M., 1974. Atlas of electrochemical equilibria in aqueous solutions. 2nd ed. Houston: National Association of Corrosion Engineers.

Remita, H., Remita, S. Metal cluster and Nanomaterials: Contribution on radiation chemistry, in James F. Wishart, BSM Rao (Eds.), 2010. Recent trends in radiation chemistry. World Scientific publishing Co., Singapure. 347-383.

Rojas, J., Castano, C. H. (2011, April). Production and characterization of supported transition metal nano-particles on multi-walled carbon nanotubes functionalized by gamma irradiation and chemical processes. In TMS 2011 140th Annual Meeting and Exhibition, Materials Processing and Energy Materials, 1, 237-244. Wiley-TMS.

Rojas, J.V., Castano, C.H., 2012. Production of palladium nanoparticles supported on multiwalled carbon nanotubes by gamma irradiation. Rad. Phys. and Chem. 81 (1), 16-21.

Rojas, J.V., Castano, C. H., 2013. Production of Metal Nanoparticles on Carbon Nanotubes by Gamma Irradiation. Chapter 22 in Radiation Synthesis of Materials and Compounds, Kharisov, B. I. Kharissova, O. V., Mendez, U.

Sun, Y., 2013. Controlled synthesis of colloidal silver nanoparticles in organic solutions: empirical rules for nucleation engineering. Chem. Soc. Rev. 42, 2497-2511.

Vargas-Uscateguia, A., Mosquera, E., Cifuentes, L., 2013. Analysis of the electrodeposition process of rhenium and rhenium oxides in alkaline aqueous electrolyte. Electrochim. Acta. 109 283– 290

Vijaya Kumar, R., Diamant, Y., Gedanken, A.,2000. Sonochemical Synthesis and Characterization of Nanometer-Size Transition Metal Oxides from Metal Acetates. Chem. Mater, 12, 2301-2305

Wang, C-C., Chen, D-H, Huang, T-C., 2001. Synthesis of palladium nanoparticles in water-in-oil microemulsions. Colloids and Surfaces A: Physicochemical and Engineering Aspects. 189, 145–154

Zhao P., Li, N. Astruc, D., 2013. State of the art in gold nanoparticle synthesis. Coordination Chemistry Reviews. 257 (3-4), 638–665.

Table 1. Reactions of Scavenger and radicals and redox potentials of the radical products (Belloni et al., 1998)

Scavenger	Radical	Products	Redox potential
$(CH3)_2CHOH$	OH•	$(CH3)_2C•OH + H_2O$	$E°((CH3)_2CO/(CH3)_2C•OH)$= -1.8VNHE
	H•	$(CH3)_2C•OH + H_2$	
HCOO-	OH•	$COO- + H_2O$	$E°(CO_2/ COO-)$= -1.9VNHE
	H•	$COO- +H_2$	

Table 2. Measured average particle sizes at various NaReO4 concentrations, and doses of 10, 20, 30 and 40 kGy.

$NaReO_4$ concentration	**Nanoparticle size (nm)±St.Dev. at different doses (kGy)**			
	10	**20**	**30**	**40**
1mM	9.6±2.2	11.1±1.2	13.7±1.6	15.9±2.3
3 mM	23.3±5.1	28.5±6.1	33.1±5.1	38.4±13.0
5 mM	39.5±5.4	45.9±9.1	56.4±10.4	31.2±6.8

Figure 1. Photograph the sample vials containing sodium perrhenate in water-isopropanol (3mM) a) before gamma irradiation and b) after irradiation with absorbed doses of 10, 20, 30, 40 kGy

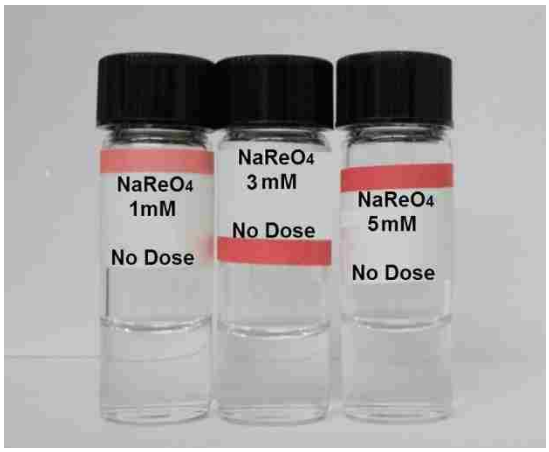

(a)

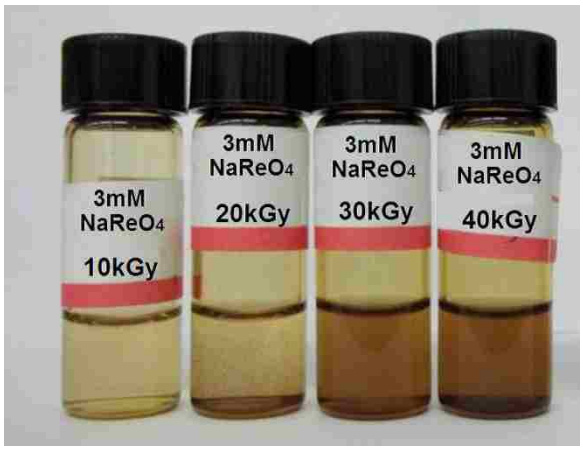

(b)

Figure 2. STEM images of resulting nanoparticles after irradiation of aqueous solution 0.1M sodium perrhenate with absorbed doses of a) 10 kGy b) 20 kGy c) 30 kGy and d) 40 kGy.

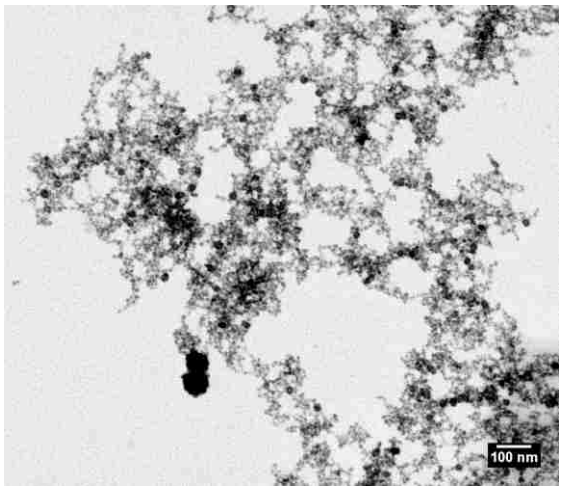

(a)

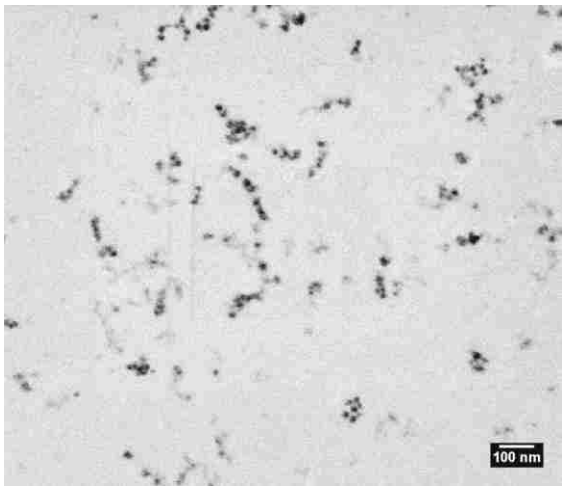

(b)

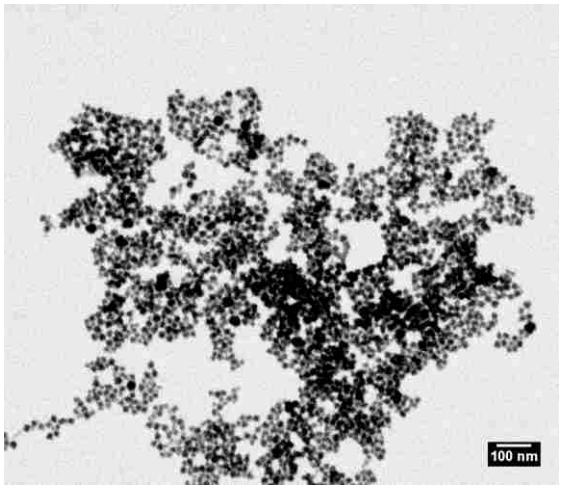

(c)

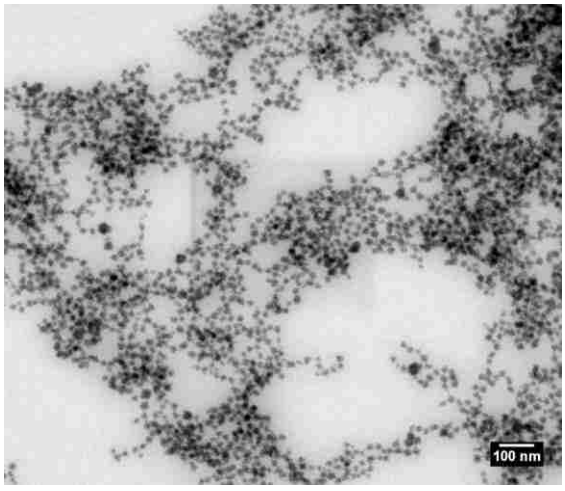

(d)

Figure 3. Particle size Re_xO_y nanoparticles as a function of absorbed dosed between 10 and 40 kGy. Solution 1mM, 3mM and 5 mM of $NaReO_4$

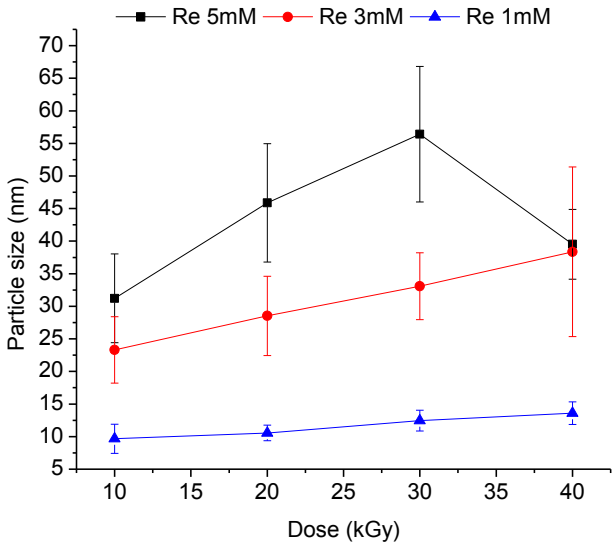

Figure 4. TEM image Re_xO_y nanoparticles formed after irradiation of solution 3mM of $NaReO_4$ at 40 kGy.

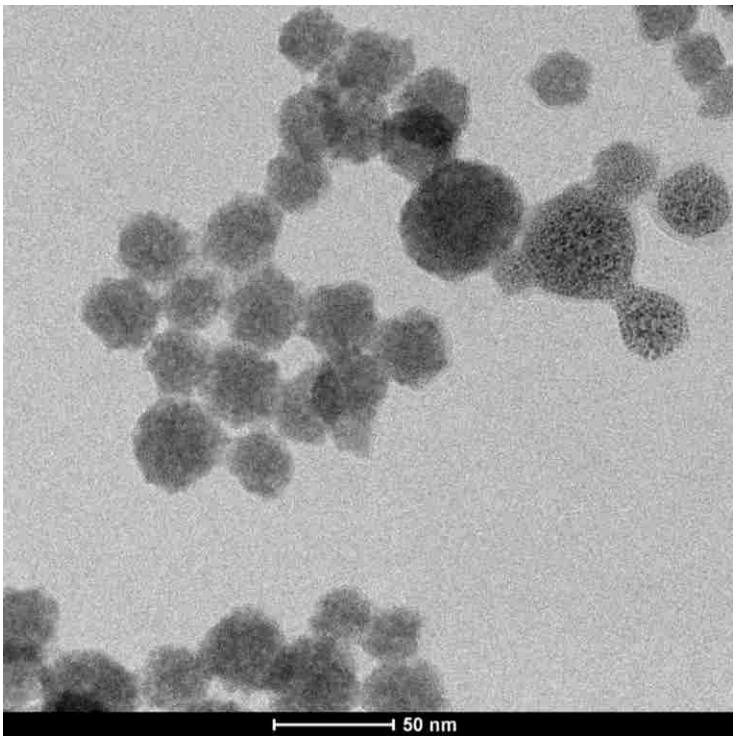

Figure 5.EDX of nanoparticles obtained from solution 3 mM of $NaReO_4$ at 40 kGy.

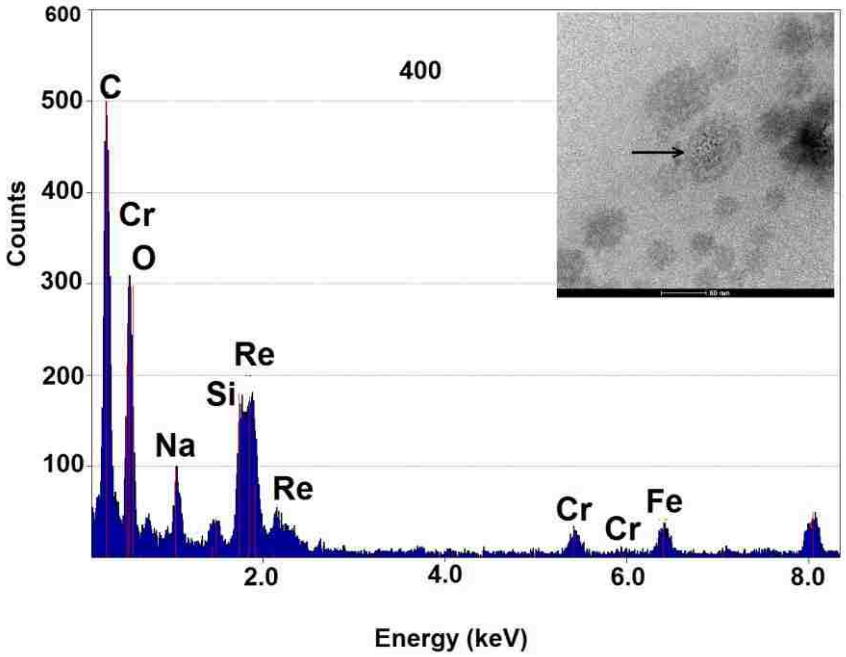

Figure 6. UV-VIS spectra of solution 3 mM of $NaReO_4$ after irradiation at 0 (no dose), 10, 20, 30 and 40 kGy.

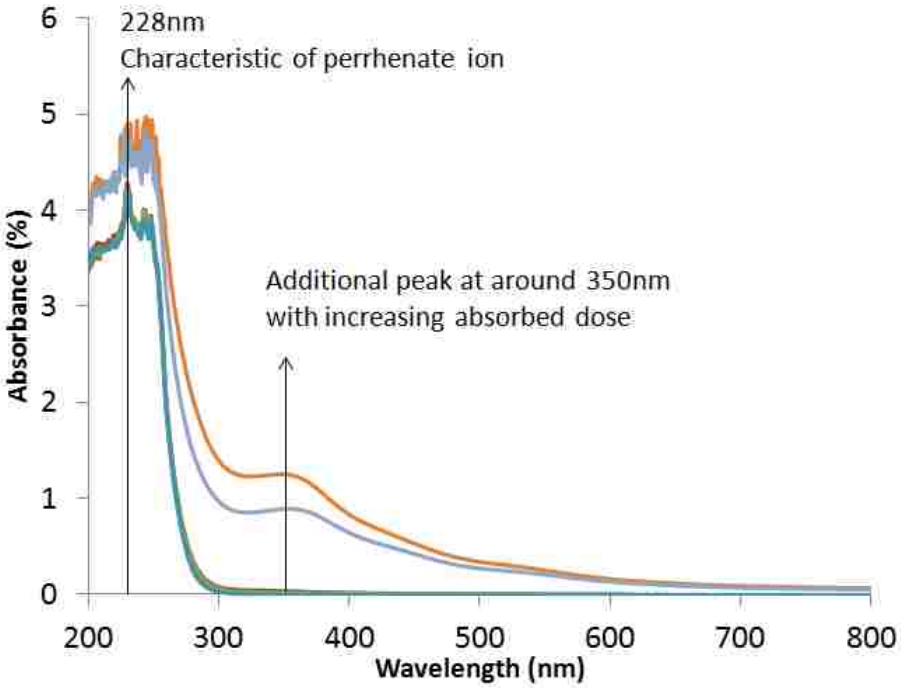

III. RADIATION-ASSISTED SYNTHESIS OF IRIDIUM AND RODIUM NANOPARTICLES SUPPORTED ON POLYVINYLPYRROLIDONE

J. V. Rojas [a], C. H. Castano [a*]

[a] Department of Mining and Nuclear Engineering, Missouri University of Science and Technology. jvr45d@mst.edu.

[a*] Corresponding author. Department of Mining and Nuclear Engineering, Missouri University of Science and Technology, 301 W. 14th St. Rolla MO 65409 USA. castanoc@mst.edu. Tel: +1 – (573) 341 – 6766. Fax: +1 – (573) 341 – 6309

Abstract

The controlled synthesis of rhodium and iridium nanoparticles carried out by gamma irradiation of aqueous solutions of metal precursor salts in the presence of PVP as stabilizer is reported in this work. Gamma irradiation served as a method to generate the reducing agents from radiolysis of water. The nanoparticles were synthesized at precursor concentrations of 3mM and 6mM and PVP concentrations of 0.3mM and 0.6mM at doses of 20, 40 and 60 kGy. Irradiation of the solutions at 60 kGy evidenced a complete reduction of the ionic species. Nanoparticles with narrow particle size distributions were obtained at metal precursor/PVP concentrations of 6mM/0.3mM and 6mM/3mM for iridium and rhodium nanoparticles irradiated at 60 kGy. This process led to the formation of iridium and rhodium nanoparticles with average sizes of 2.4 nm and 2.6 nm respectively. The interaction of the nanoparticles surfaces with both of the functional

groups on PVP, C-N and C=O, accounts for the high stability of the nanoparticles in suspension and the control over the particle size.

Keywords: Iridium nanoparticles, Rhodium nanoparticles, radiolytic synthesis, gamma irradiation, radiation induced chemistry.

1. Introduction

The controlled synthesis of transition metal nanoparticles has become a subject of growing interest [1, 2]. The physical and chemical properties of such elements at the nanoscale level can be tailored for specific applications by modifying their size, shape and crystalline structure [1, 3, 4]. Transition metals nanoparticles and its alloys are being investigated for applications in medicine, optoelectronics, sensing and catalysis [5-10]. Among these materials, iridium (Ir) and rhodium (Rh) have gained significant attention for catalytic applications [2, 6, 11-13]. Iridium has been studied for hydrogenation [6, 12], dehydrogenation, hydrazine decomposition [14], selective naphthene ring opening, and reduction of imines to the corresponding amines [2]. Diverse methods have been employed to synthesize iridium nanoparticles such as precipitation, impregnation, grafting and atomic layer deposition [15-17]. These approaches have included the use of supports to avoid agglomeration of the nanoparticles after synthesis. L.I. Kuznetsova et al. and H. Bernas et. al. studied the synthesis of Ir nanoparticles on carbon supports using the impregnation and precipitation methods [12, 15]. The reduction of the precursor was achieved either with the addition of $NaBH_4$ or under flowing hydrogen at high temperatures (400 °C to 500 °C). The use of γ-Al_2O_3, silica and β-zeolite to support Ir

nanpoparticles has also been investigated by H. Vuori et. al and A. Djeddi [16, 17]. Other supports such as TiO_2, MgO, CeO_2, have been also used for this purpose [11]. Furthermore, the synthesis of Ir nanoparticles in metal organic frameworks[18] and imidazolium ionic liquids [13] has been reported. Rhodium, similar to iridium, has been used for applications in hydrogenation, carbonylation, hydroformylation, and oxidation reactions [19]. The nanoparticles have been synthesized in water-in-oil microemulsions [20], and using solid supports such as Al_2O_3 [21], SiO_2, ZrO_2 [19] and carbon nanotubes [22-24].

With the advances in radiation chemistry, the use of ionizing radiation has become a potential method to not only modify the properties of the materials but to synthesize them [25]. Irradiation of aqueous solution with α, β, γ generates homogeneously distributed species such as solvated electrons (e_{aq}^-), OH and H that are highly reactive [26]. The species e_{aq}^- and H are powerful reducing agents and can bring metal ions to zero valence state. The OH being highly oxidizing specie can be scavenged by secondary alcohols or formate ions, which results in additional reducing species [27]. This method has shown to provide several advantages for the synthesis of nanostructures: it is carried out at ambient temperature, does not require the use of additional chemicals at it creates a reducing environment and parameters such as dose and dose rate can be controlled. This allows control over the particle size and shape [3, 27, 28].

The synthesis of gold nanoparticles, platinum [29], ruthenium, silver [30], palladium [31] among other inorganic nanostructures, using gamma irradiation has been previously reported. Herein, we report a method to synthesize well distributed Ir and Rh

nanoparticles stabilized by PVP using gamma irradiation. A complete characterization of the final nanostructure is presented here.

2. Experimental Procedure

The synthesis of iridium and rhodium nanoparticles was carried out using hydrogen hexachloroiridate (IV) hexahydrate ($H_2IrCl_6*6H_2O$) and sodium hexachlororhodate (III) ($Na_3RhCl_6*6H_2O$) as metal precursor, polyvinylpyrrolidone (PVP Mw~10000 g/mol) as capping agent and 2-propanol (> 99.5% purity) as radical scavenger. Also, deionized water (18.2 MΩ.cm at 25 °C) from a Barnstead nanopure water purification system was used to prepare the solutions. Initially, mixtures of water-isopropanol (2:1 v/v) with $H_2IrCl_6*6H_2O$ (or Na_3RhCl_6) in concentrations of 3mM and 6 mM were prepared. Then, PVP was added to obtain concentrations of 0.03 mM and 0.06 mM. Finally, the solutions were transferred to glass vials and degassed with argon to remove oxygen. Gamma irradiation of the solutions was carried out in a Cobalt-60 Gammacell 220 Excel (MDS, Nordion) with absorbed doses of 20, 40 kGy and 60 kGy (dose rate ~10 KGy/hr).

The nanoparticles were characterized using a Helios NanoLab 600 in STEM mode at 30kV, a PANalytical X'Pert Pro MPD X- ray diffractometer operating at 45 kV and 40 mA with a copper anode (Cu Kα λ = 1.5401Å) and an X-ray photoelectron spectrometer (XPS) Kratos Axis 165 using a monochromated aluminum X-ray source. Also, a Thermo Scientific *GENESYS 10S* UV-vis spectrophotometer was used to acquire the optical absorption spectra of the suspensions. The suspensions were diluted 20 times

in order to obtain accurate results and the measurements were carried out using quartz square spectrophotometer cuvettes, with 10mm pathlength. For electron microscopy analysis, the samples were prepared by depositing a drop of the diluted suspension on a formvar-carbon coated copper grid and allowed to dry. Samples for XRD and XPS were prepared by air drying the suspension on a silicon wafer. Image processing and particle size measurements were carried out using the software Image J 4.1 and XPS spectra were analyzed using the software CASA XPS version 2.3.16. NIST XPS Standard Reference Database 20, Version 4.1 was used for the analysis.

3. Results and Discussion

Gamma irradiation of solutions containing various concentrations of $H_2IrCl_6*6H_2O$ and $Na_3RhCl_6*6H_2O$ and PVP was carried out at doses of 20, 40 and 60 kGy. After irradiation, the appearance of the solutions, initially dark yellow at the selected concentrations, turned dark brown. Irradiation of the solutions under the same conditions and in the absence of PVP resulted in a black precipitate. The suspensions irradiated in the presence of PVP were stable for at least 2 months. The solutions were analyzed with UV-vis spectroscopy and the spectra are shown in Figure 1. Optical absorbance spectra of the metal precursor salts in water-isopropanol before irradiation show the characteristic peaks of $IrCl_6^{-2}$ between 400 nm and 500 nm which correspond to the legand-to-metal charge transfer (LMCT) and a weak peak around 300 nm that corresponds to d-d ligand-field transitions [32]. Similarly, $RhCl_6^{-3}$ shows an absorption band at 450 nm. After irradiation at 20 kGy the characteristic absorption peaks disappeared, which indicates the reduction of the species to lower oxidation states. In the

case of the iridium suspensions, there is a drastic increase of absorbance when the dose increases from 20 to 40 kGy. Likewise, rhodium suspensions show a similar trend in absorbance in the UV-vis region. Although the absorbance increases with irradiation dose from 20 to 40 kGy, the change is not as drastic as it is in the case of iridium. By increasing the dose up to 60 kGy for both, iridium and rhodium suspensions, the absorbance further increases. However this variation is not significant. This indicates a complete reduction of the ionic species when the dose reaches 60 kGy.

The suspensions were analyzed with electron microscopy after irradiation. Rhodium and iridium nanoparticles were obtained with concentrations of metal precursor of 3 mM and 6 mM and PVP of 0.3 mM and 0.6 mM. Among the different samples, a uniform particle size and shape was obtained with a combination of metal precursor and PVP concentration of 6 mM and 0.3 mM and 3 mM and 0.6 mM for iridium and rhodium respectively, when irradiated with 40 and 60 kGy. The STEM micrographs of these samples with their particle size histogram are shown in Figure 2. The mean particle size as measured from STEM images was found to be 2.6 ± 0.4 nm and 2.6 ± 0.6 nm for iridium (Figure 2.a) and rhodium (Figure 2.a) nanoparticles respectively. In the case of rhodium, few bigger clusters of approximately 5 nm were observed.

Figure 3 shows the X-ray diffraction patterns of the Ir and Rh suspensions. The peaks in the diffraction pattern from the iridium sample (Figure 3 a) appeared at 2 theta angles of 44.12, 46.78, 69.67 and 76.57. These peaks correspond to metallic Iridium (Ir PDF 00-006-0598) with a face centered cubic (FCC) crystalline structure. Similarly, in the diffraction pattern from the suspension containing rhodium the peaks appear at 2 theta degrees of 40.78, 47.87, 69.87 and 89.45. They correspond to Metallic rhodium (Rh PDF

0050685) with an FCC structure. In addition, a set of peaks in the diffraction pattern at 2 theta angles of 22.23, 31.67, 45.44, 56.51, 66.36, 75.30 and 83.97 were identified as NaCl (Halite PDF001-0994). This was identified as a subproduct from the reaction.
The peak broadening in both of the patterns also evidenced nanometric size of the particles. Using the Scherrer equation with the Ir and Rh 111 peak, the crystallite size (average) was found to be 2.4 nm and 2.6 nm respectively which are comparable with the values obtained with electron microscopy.

The stability of the metallic nanoparticles in the suspension strongly depends on their interaction with the media and capping agent. Some polymeric materials have been previously used as stabilizers due to their ability to interact with the nanoparticle surface trough their functional groups. They do not only serve as diffusion barriers to the growth species but also avoid agglomeration of the particles. Furthermore, it has been previously reported that the presence of stabilizers may affect their catalytic properties. Thus, understanding the interaction mechanism of the polymer with the metallic nanoparticles is important when the particles are intended to be used in such applications. The interaction of iridium and rhodium nanoparticles with the polymer PVP was studied with XPS. For this purpose, high resolution (HR) spectra for the N, O, and Ir and Rh peaks from the polymer alone and in the presence of the nanoparticles were collected. The position of the C 1s peak at 284.5 eV was used to calibrate the spectra. The HR XPS for Ir and Rh nanoparticles in PVP are shown in Figure 4 a) and b) respectively. In the case of iridium, the peaks at 60.24 and 63.24 eV correspond to $4f_{7/2}$ and $4f_{5/2}$ from Ir(0). The peaks fitted at higher binding energies are due to shake-up like events following core electron photoemission that causes a tail on the higher binding energy side of the main

peak. XPS spectrum was also collected from the black precipitate obtained after irradiation of the Ir solution at 40 kGy (information not shown). In this case the peaks from Ir(0) were observed at 60.77 and 63.77 eV (comparable with the values reported in NIST database). Therefore, the peaks from Ir(0) in the presence of PVP shifted towards lower binding energies (Δ~0.5eV) compared with bulk iridium. In the case of bulk rhodium, the peaks of $3d_{5/2}$ and $3d_{3/2}$ were observed at binding energies of 306.65 and 311.41 eV, respectively. However, the same peaks were observed at 305.55 and 310.41 eV for Rh nanoparticles in PVP (Figure 4 b). Thus, these peaks are also shifted towards lower binding energies compared to the ones from bulk rhodium. Two additional peaks are observed in the HR XPS of Rh 3d that can be attributed to unreduced $RhCl_x$ species. The peak shift observed in both samples of iridium and rhodium in PVP, is due to an increase in electron density around the atoms caused by the surrounding environment. The HR XPS spectra of the functional groups, O and N, in the amide carbonyl moieties of PVP are shown in Figure 5. Nitrogen peak, in Figure 4 a, was observed in the binding energy interval from 393eV to 405 eV and deconvoluted into two peaks. The first at 397.16 eV that corresponds to the C-N bond and the second at 399.16 eV that corresponds to the N-C=O group. The oxygen peak was also deconvoluted into two peaks, one 530.63 eV that corresponds to the C=O interaction and another at 528.51 eV that may be due to polar interactions. The HR XPS for N and O collected from the Ir-PVP and Rh-PVP are presented in Figure 5 a-d. The results revealed that both, N and O, shifted to higher binging energies compared to the observed in PVP alone. This occurs as a result of a decrease in the electron density of such atoms.

The peak shift observed for Ir, Rh, N and O evidence an interaction between the metallic nanoparticles and both of the functional groups in the PVP polymer. This accounts for the highly stable suspension obtained after gamma irradiation. The interaction of N and O with metallic nanoparticles such as Pd and gold has been previously reported [4, 9, 33]. The understanding of this type of interactions is essential when evaluating surface-mediated properties of these metallic nanoparticles, such as catalysis.

4. Conclusions

In this study, rhodium and iridium nanoparticles were successfully synthesized though a radiolytic assisted method. A homogeneous particle size distribution for both, iridium and rhodium, was obtained at the concentrations of Rh precursor / PVP of 6 mM /0.3 mM and Ir precursor / PVP of 3 mM / 0.6 mM. It was found that the particle size distribution can be controlled by changing the absorbed dose. At higher doses more homogeneous particle size distribution is obtained. Additionally, the amount of precursor species that are reduced to zero valence state increases with increasing the dose, making the synthesis process more efficient. The nanoparticles in PVP were found to be stable for more than 3 months. This stability was explained bases on the interaction of iridium and rhodium with the PVP chains. XPS elucidated that such interactions take place between both nitrogen and oxygen with the metallic nanoparticles.

Acknowledgements

The authors thank Dr. Stoyan Toshkov at the Nuclear, Plasma, and Radiological Engineering Department at the University of Illinois for sample irradiation. Also, to the Materials Research Center (MRC) and Energy Research Development Center (ERDC) at Missouri S&T for their financial support. This work was supported by NRC radiochemistry grant PPR-NRC-38-10-966

References

[1] Guisbiers G, Abudukelimu G, Hourlier D. Size-dependent catalytic and melting properties of platinum-palladium nanoparticles. Nanoscale research letters. 2011;6:396.

[2] Rueping M, Koenigs RM, Borrmann R, Zoller J, Weirich TE, Mayer J. Size-Selective, Stabilizer-Free, Hydrogenolytic Synthesis of Iridium Nanoparticles Supported on Carbon Nanotubes. Chemistry of Materials. 2011;23:2008-10.

[3] Misra N, Biswal J, Gupta A, Sainis JK, Sabharwal S. Gamma radiation induced synthesis of gold nanoparticles in aqueous polyvinyl pyrrolidone solution and its application for hydrogen peroxide estimation. Radiation Physics and Chemistry. 2012;81:195-200.

[4] Xian J, Hua Q, Jiang Z, Ma Y, Huang W. Size-dependent interaction of the poly(N-vinyl-2-pyrrolidone) capping ligand with Pd nanocrystals. Langmuir. 2012;28:6736-41.

[5] Shim JH, Kim JE, Cho YB, Lee C, Lee Y. Oxidation-state dependent electrocatalytic activity of iridium nanoparticles supported on graphene nanosheets. Phys Chem Chem Phys. 2013;15:15365-70.

[6] Sharif MJ, Maity P, Yamazoe S, Tsukuda T. Selective Hydrogenation of Nitroaromatics by Colloidal Iridium Nanoparticles. Chemistry Letters. 2013;42:1023-5.

[7] Gniewek A, Trzeciak A, Ziolkowski J, Kepinski L, Wrzyszcz J, Tylus W. Pd-PVP colloid as catalyst for Heck and carbonylation reactions: TEM and XPS studies. Journal of Catalysis. 2005;229:332-43.

[8] Evangelisti C, Panziera N, Pertici P, Vitulli G, Salvadori P, Battocchio C, et al. Palladium nanoparticles supported on polyvinylpyridine: Catalytic activity in Heck-type reactions and XPS structural studies. Journal of Catalysis. 2009;262:287-93.

[9] Borodko Y, Humphrey SM, Tilley TD, Frei H, Somorjai GA. Charge-Transfer Interaction of Poly(vinylpyrrolidone) with Platinum and Rhodium Nanoparticles. J Phys Chem C. 2007.

[10] Ichikuni HTN, Sakurai H, Tsukuda T. Effect of Electronic Structures of Au Clusters Stabilized by Poly(N-vinyl-2-pyrrolidone) on Aerobic Oxidation Catalysis. J Am Chem Soc. 2009;131:7086–93.

[11] Lu J, Aydin C, Browning ND, Wang L, Gates BC. Sinter-Resistant Catalysts: Supported Iridium Nanoclusters with Intrinsically Limited Sizes. Catalysis Letters. 2012;142:1445-51.

[12] Bernas H, Simakova I, Prosvirin IP, Mäki-Arvela P, Leino R, Murzin DY. Hydrogenation of Citral Over Carbon Supported Iridium Catalysts. Catalysis Letters. 2012;142:690-7.

[13] Fonseca GS, Machado G, Teixeira SR, Fecher GH, Morais J, Alves MC, et al. Synthesis and characterization of catalytic iridium nanoparticles in imidazolium ionic liquids. J Colloid Interface Sci. 2006;301:193-204.

[14] Cho S, Lee J, Lee Y, Kim D. Characterization of Iridium Catalyst for Decomposition of Hydrazine Hydrate for Hydrogen Generation. Catalysis Letters. 2006;109:181-6.

[15] Kuznetsova LI, Kuznetsova NI, Koscheev SV, Zaikovskii VI, Lisitsyn AS, Kaprielova KM, et al. Carbon-supported iridium catalyst for reduction of chlorate ions with hydrogen in concentrated solutions of sodium chloride. Applied Catalysis A: General. 2012;427-428:8-15.

[16] Djeddi A, Fechete I, Garin F. Selective ring opening of methylcyclopentane over Pt/γ-Al2O3, Ir/γ-Al2O3 and Pt-Ir/γ-Al2O3 catalysts with hydrogen at atmospheric pressure. Applied Catalysis A: General. 2012;413-414:340-9.

[17] Vuori H, Pasanen A, Lindblad M, Valden M, Niemelä MV, Krause AOI. The effect of iridium precursor on oxide-supported iridium catalysts prepared by atomic layer deposition. Applied Surface Science. 2011;257:4204-10.

[18] Zahmakiran M. Iridium nanoparticles stabilized by metal organic frameworks (IrNPs@ZIF-8): synthesis, structural properties and catalytic performance. Dalton Trans. 2012;41:12690-6.

[19] Yuan Y, Yan N, Dyson PJ. Advances in the Rational Design of Rhodium Nanoparticle Catalysts: Control via Manipulation of the Nanoparticle Core and Stabilizer. ACS Catalysis. 2012;2:1057-69.

[20] Hoefelmeyer JD, Liu H, Somorjai GA, Tilley TD. Reverse micelle synthesis of rhodium nanoparticles. J Colloid Interface Sci. 2007;309:86-93.

[21] Hayeka K, Gollerb H, Penner S, Rupprechterc G, Zimmermannd C. Regular alumina-supported nanoparticles of iridium, rhodium and platinum under hydrogen

reduction: structure, morphology and activity in the neopentane conversion. Catalysis Letters. 2004;92:1-9.

[22] Yoon B, Wai CM. Microemulsion-Templated Synthesis of Carbon Nanotube-Supported Pd and Rh Nanoparticles for Catalytic Applications. Journal of the Americal Chemical Society. 2005;127:17174-5.

[23] Pan H-B, Wai CM. Sonochemical One-Pot Synthesis of Carbon Nanotube-Supported Rhodium Nanoparticles for Room-Temperature Hydrogenation of Arenes. J Phys Chem C. 2009;113:19782–8.

[24] Suarez-Martinez I, Ewels CP, Wolfgang Drube AF, IMN U, Ke X, Pireaux J-J, et al. Study of the Interface between Rhodium and Carbon Nanotubes. ACS nano. 2010;4:1680-6.

[25] Rojas JV, Castano CH. Production of metal nanoparticles on carbon nanotubes by gamma irradiation. In: Kharisov BI, Kharissova OV, Mendez UO, editors. Radiation Synthesis of Materials and Compounds: CRC Press; 2013. p. 491-503.

[26] Appleby A, Schwarz HA. Radical and Molecular Yields in Water Irradiated by y Rays and Heavy Ions. J Phys Chem. 1969;79:1937-41.

[27] Belloni J, Mostafavi M. Radiation chemistry of nanocolloids and clusters. In: Jonah CD, Rao BSM, editors. Radiation chemistry: present status and future trends: Elsevier; 2001. p. 411-52.

[28] Belloni J. Nucleation, growth and properties of nanoclusters studied by radiation chemistry. Catalysis Today. 2006;113:141-56.

[29] Zhang X, Ye Y, Wang H, Yao S. Deposition of platinum–ruthenium nano-particles on multi-walled carbon nano-tubes studied by gamma-irradiation. Radiation Physics and Chemistry. 2010;79:1058-62.

[30] Naghavi K, Saion E, Rezaee K, Yunus WMM. Influence of dose on particle size of colloidal silver nanoparticles synthesized by gamma radiation. Radiation Physics and Chemistry. 2010;79:1203-8.

[31] Rojas JV, Castano CH. Production of palladium nanoparticles supported on multiwalled carbon nanotubes by gamma irradiation. Radiation Physics and Chemistry. 2012;81:16-21.

[32] Glebov EM, Kolomeets AV, Pozdnyakov IP, Plyusnin VF, Tkachenko NV, Lemmetyinen H. Ultrafast pump-probe spectroscopy of IrCl6(2-) complex in alcohol solutions. Photochemical & photobiological sciences : Official journal of the European Photochemistry Association and the European Society for Photobiology. 2011;10:1709-14.

[33] Habib Ullah M, Hossain T, Ha C-S. Kinetic studies on water-soluble gold nanoparticles coordinated to poly(vinylpyrrolidone): isotropic to anisotropic transformation and morphology. Journal of Materials Science. 2011;46:6988-97.

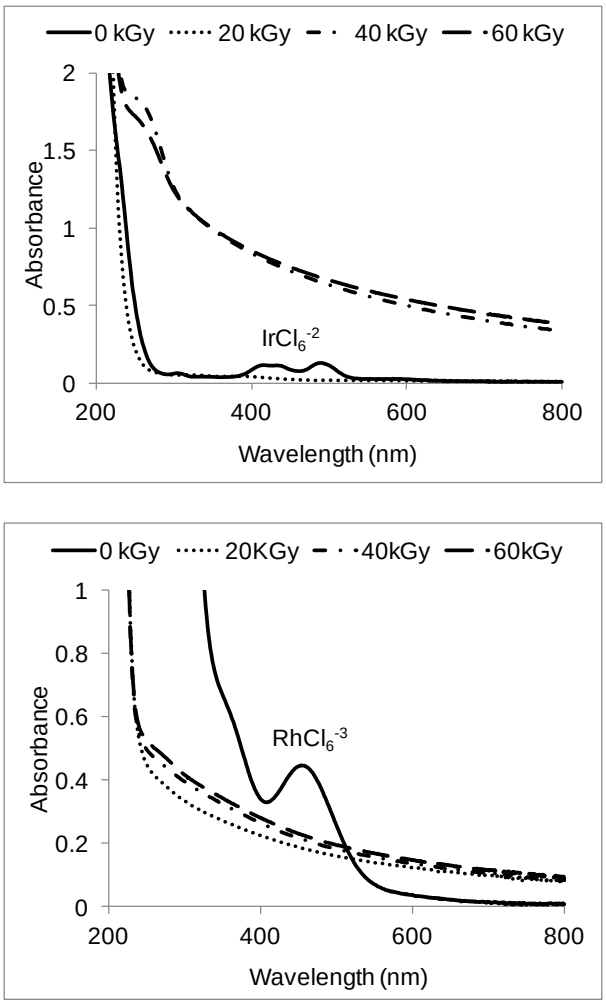

Figure 1. UV-Vis spectra of a) Ir nanoparticles with concentrations $HIrCl_6$ and PVP of 6 mM and 0.3 mM respectively and b) Rh nanoparticles with concentrations $NaRhCl_6$ and PVP of 3 mM and 0.6 mM respectively, irradiated with 0, 20, 40 and 60 kGy. Samples diluted 20 times.

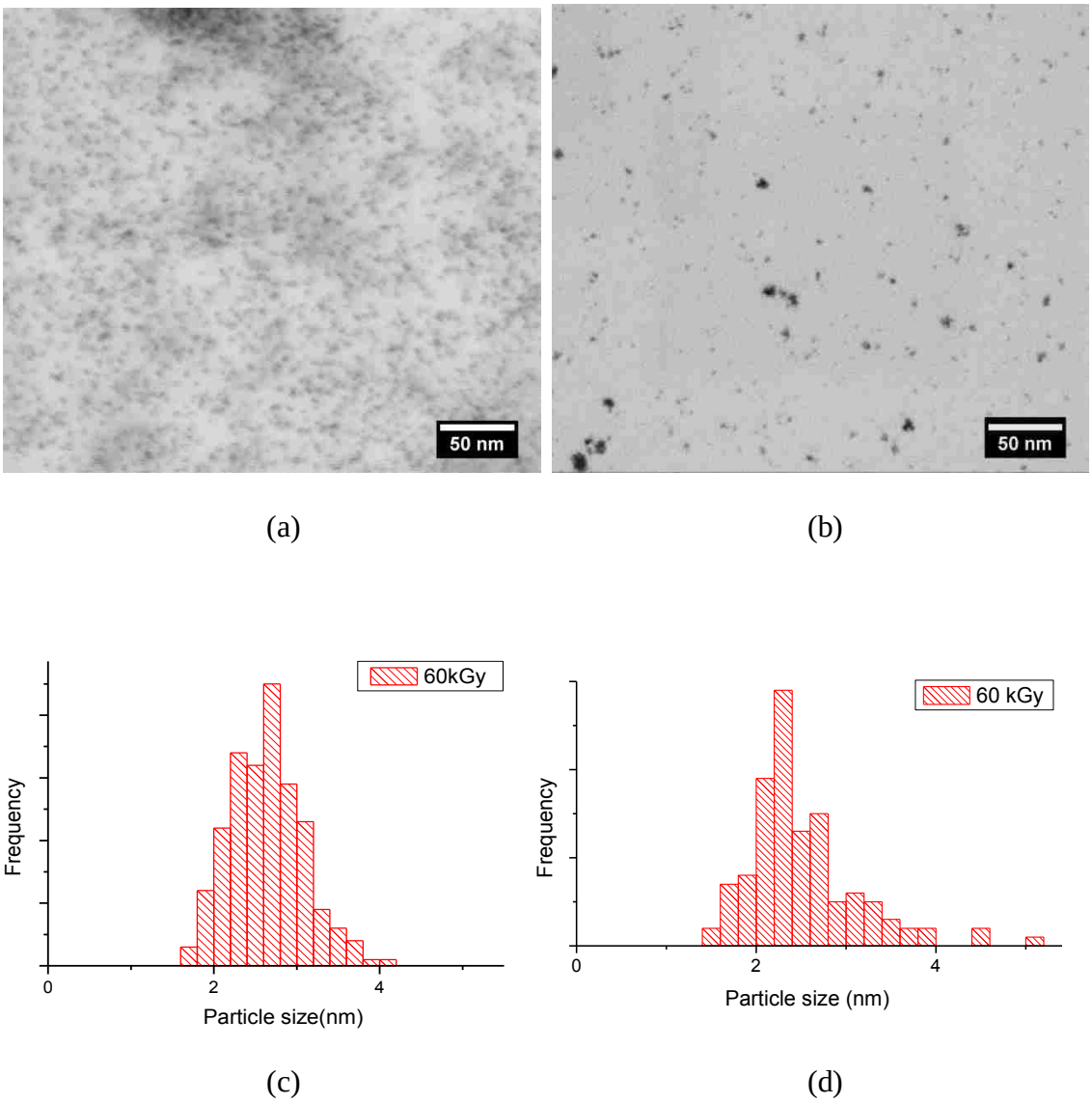

Figure 2. STEM images of a) Ir nanoparticles with concentrations $HIrCl_6$ and PVP of 6 mM and 0.3 mM respectively and b) Rh nanoparticles with concentrations $NaRhCl_6$ and PVP of 3 mM and 0.6 mM respectively, irradiated with 60 kGy c) Histogram of particle size for image (a) and d) Histogram of particle size for image (b).

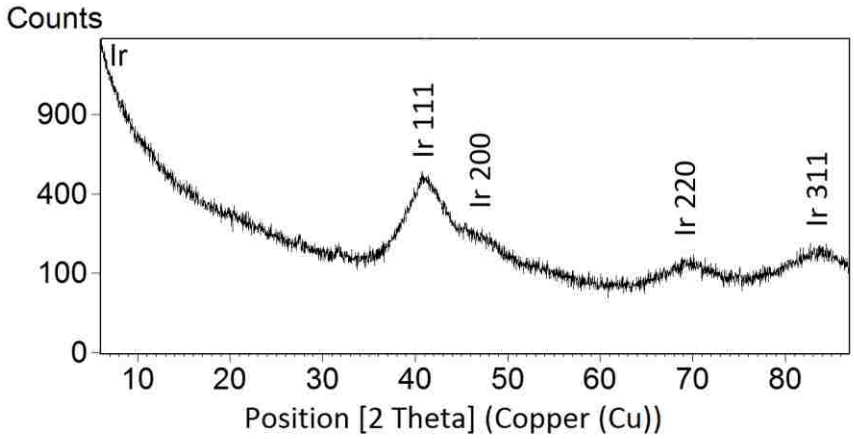

(a)

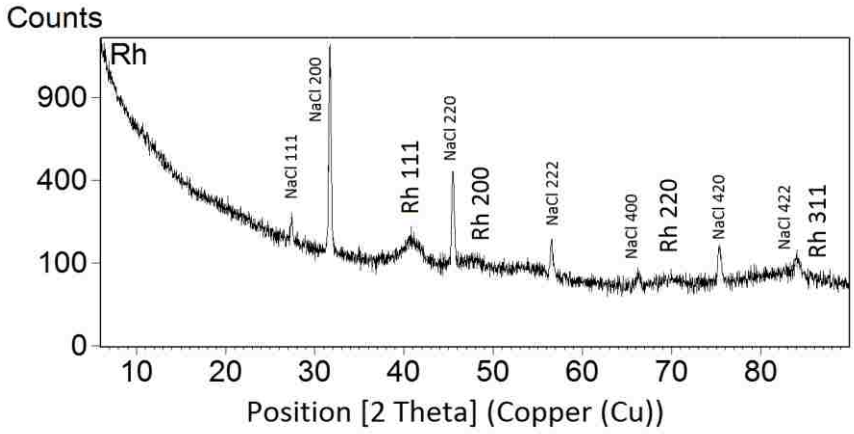

(b)

Figure 3. XRD pattern of a) Ir nanoparticles with concentrations $HIrCl_6$ and PVP of 6 mM and 0.3 mM respectively and b) Rh nanoparticles with concentrations $NaRhCl_6$ and PVP of 3 mM and 0.6 mM respectively, irradiated at 60 kGy.

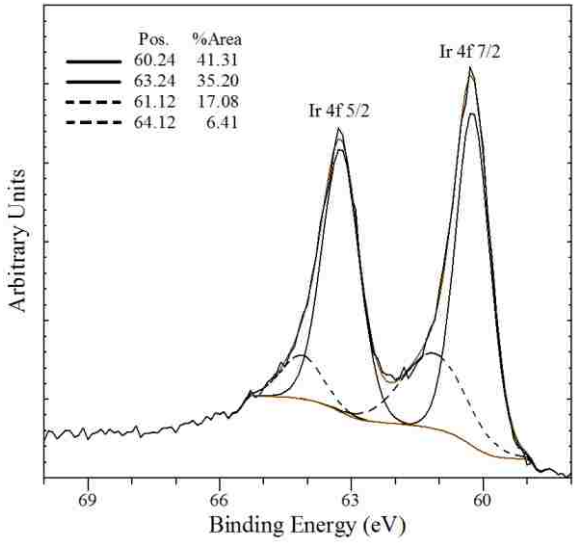

(a)

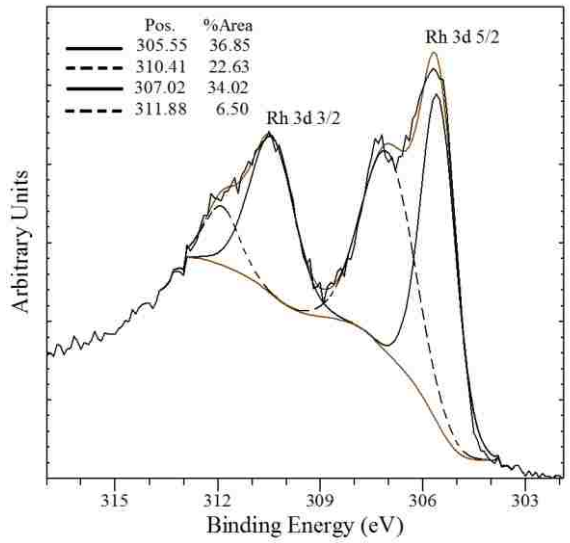

(b)

Figure 4. High resolution XPS for peaks Ir a) Ir and b)Rh nanoparticles in PVP.

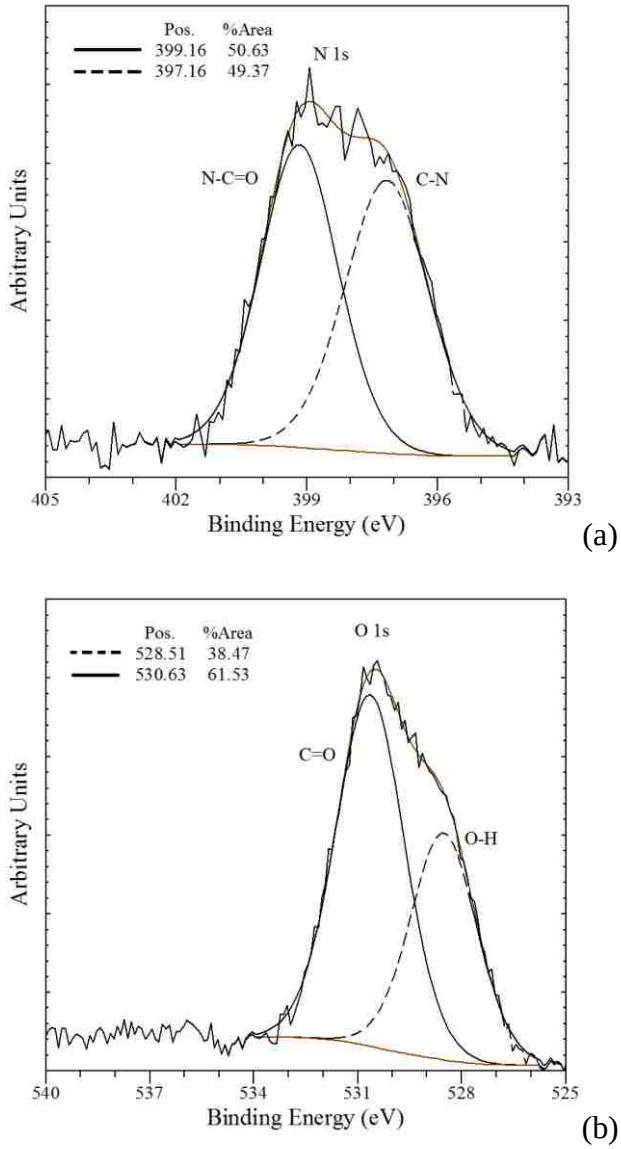

Figure 5. High resolution XPS for peaks of a) N 1s and b)O 1s in PVP.

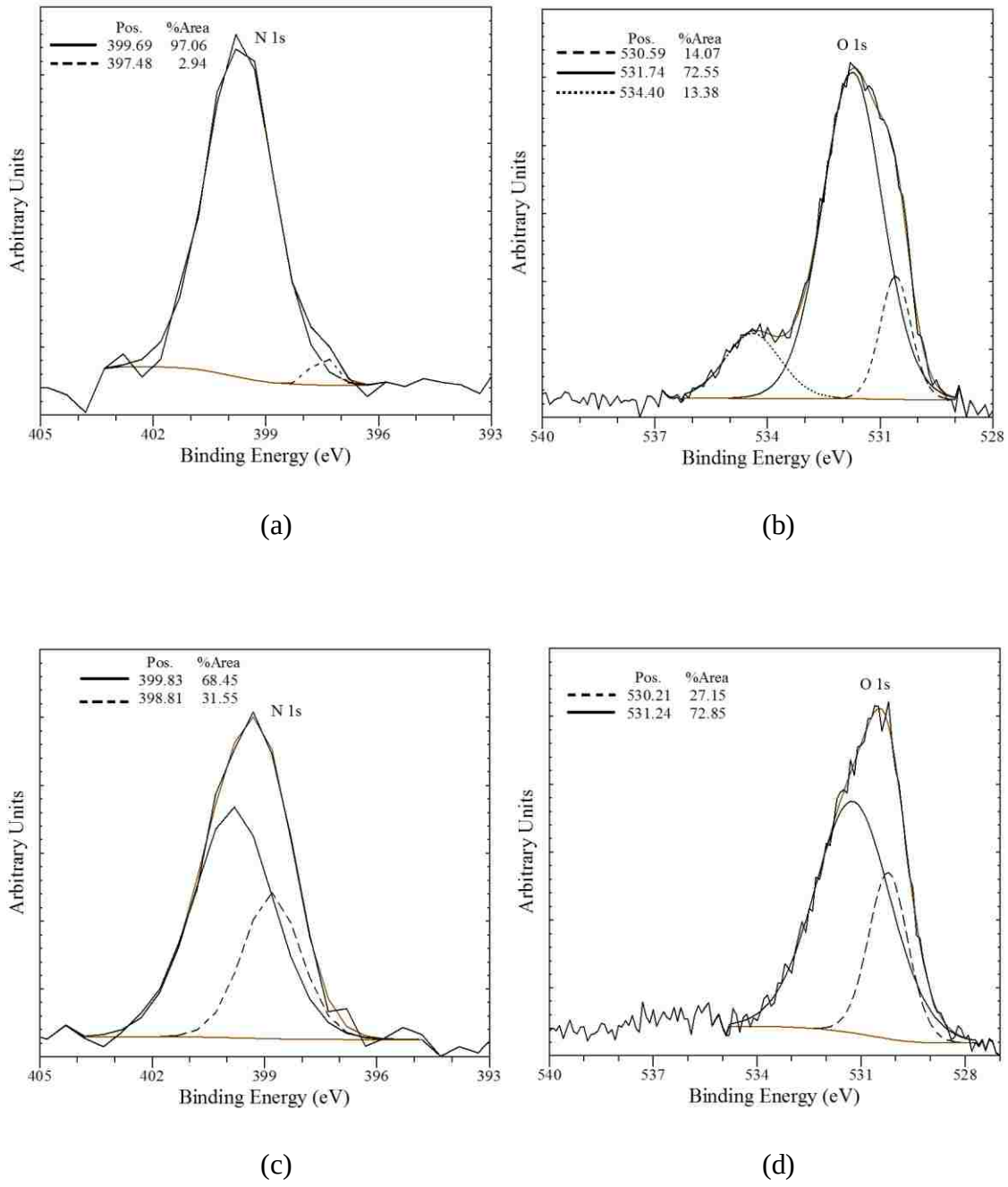

Figure 6. High resolution XPS for peaks of a) N 1s and b) O 1s in Ir-PVP nanoparticles and c) N 1s and d) O 1s in Rh-PVP nanoparticles.

IV. RADIOLYTIC SYNTHESIS OF IRIDIUM NANOPARTICLES ONTO CARBON NANOTUBES

J. V. Rojas [a], C. H. Castano [a*]

[a] Department of Mining and Nuclear Engineering, Missouri University of Science and Technology. jvr45d@mst.edu.

[a*] Corresponding author. Department of Mining and Nuclear Engineering, Missouri University of Science and Technology, 301 W. 14th St. Rolla MO 65409 USA. castanoc@mst.edu. Tel: +1 – (573) 341 – 6766. Fax: +1 – (573) 341 – 6309

Abstract

Iridium nanoparticles on multiwalled carbon nanotubes were synthesized in a single step process by gamma irradiation from a cobalt-60 source. These particles were prepared at various absorbed doses, precursors, and surfactant concentrations. The nanoparticles were homogeneously distributed onto the nanotubes' surface with average particle sizes between 2 nm and 5 nm. The particle size was found to decrease from 4.5 nm to 3.4 nm, when the absorbed dose increased from 20 kGy to 60 kGy. An increase in the surfactant concentration also reduced the particle size from 3.8 nm to 2.5 nm. No significant variation in particle size was observed when the precursor concentration was increased. No Ir-C bonds were detected by X-ray photoelectron spectroscopy (XPS), but Iridium-oxygen bonds were. The interaction between the nanoparticles and the nanotubes seems to occur through oxygenated sites on the nanotubes' surface.

Keywords: Iridium nanoparticles, radiolytic synthesis, gamma irradiation, radiation-induced chemistry, carbon nanotubes.

1. Introduction

Control over the particle size and shape of nanomaterials plays an important role on their final physical and chemical properties [1]. In the case of metallic nanoparticles, variations in their morphology lead to changes in their electrical, optical, and catalytic properties [2, 3]. These properties are also affected by the tendency of nanomaterials to aggregate due to their high surface energies [4].

Among the transition metals, Iridium (Ir) is of great interest for catalytic applications such as hydrogenation, dehydrogenation, selective naphthene ring opening, and reduction of imines to the corresponding amines [4-7]. Therefore, it is important to not only develop methods to synthesize iridium nanoparticles with a uniform particle size but also avoid agglomeration after synthesis. It is also essential to adequately select synthesis media, reducing agents and/or stabilizers as they may affect the nanoparticles' efficiency thereby reducing their catalytic activity [8, 9].

Supports are often used to synthesize of nanoparticles, which lead to a better distribution of the nanoparticles and avoid aggregation [4]. They may also provide mechanical strength and offer additional desired properties for certain applications. Within this context, various methods have been reported to synthesize iridium nanoparticles with sizes between 1-10 nm on various supports such as γ-Al2O3, TiO2, MgO, CeO2, and carbon. [4-6]. Among the various types of substrates, single walled and multiwalled carbon nanotubes (SWCNTs and MWCNTs) have several advantages such

as chemical and thermal stability over a wide temperature range. They can also be synthesized with a high purity level [7]. The decoration of CNTs with nanoparticles has been carried out by a number of diverse methodologies including electroless deposition, thermal decomposition, impregnation using an aqueous solution, electrodeposition, and radiation [8].

Ionizing radiation (β and γ) has shown promise as a method to synthesize different nanomaterials that have a controlled particle size and shape [9-11]. The irradiation of aqueous solutions causes radiolysis of water. This process results in the production of highly reactive species that are homogeneously distributed throughout the solution [12]. The simple physicochemical conditions of this process lead to the homogeneous reduction and nucleation of nanoparticles. This synthesis is conducted at room temperature and, because no reducing agents are required, it typically does not produce unwanted residues [9, 10].

The work presented here suggests that gamma irradiation can be used to synthesize well distributed Ir nanoparticles onto MWCNTs. A complete characterization of the final nanostructure is also presented here.

2. Experimental Procedure

All of the chemical reagents in this study were used as purchased without additional purification. Deionized water from a nanopure water purification system was used to prepare the solutions. The supported iridium nanoparticles on MWCNTs were produced by a modification of a procedure previously explained elsewhere [11]. Briefly, MWCNTs (with an outside diameter between 3 nm and 20 nm, an inside diameter

between 1 nm and 3 nm, and a purity of 95.5%) were mixed with sodium dodecylsulfate (SDS, C12H25SO4Na) in a solution of water-isopropanol (2:1 v/v); this solution contained the metal precursor hydrogen hexachloroiridate (IV) hexahydrate. The concentration of MWCNT in the solution was 0.5 mg/ml. Concentrations of both SDS of 0.03 M and 0.06 M, and precursor salt concentrations of 3 mM and 6 mM were used to evaluate the effect of these parameters in the final product. The suspension was homogenized by placing it in an ultrasonic bath for 30 minutes. It was then distributed in 2ml glass vials and degassed with argon. The samples were irradiated in a Cobalt 60 Gammacell 220 Excel (MDS, Nordion) with absorbed doses of 20, 40, and 60 kGy. After irradiation the samples were washed with water to remove excess of surfactants.

Both the morphology and the crystalline structure of the nanomaterial were evaluated with a Helios NanoLab 600 in STEM mode at 30kV, by TEM TECNAI F20 at 200kV and by XRD PANalytical X'Pert Pro MPD with a copper anode. X-ray photoelectron spectroscopy (XPS) was also conducted with a Kratos Axis 165 X-ray photoelectron spectrometer (XPS) using a monochromated aluminum X-ray source. A drop of the sample was deposited on a formvar-carbon coated copper grid for the electron microscopy analysis. Samples were prepared for XRD and XPS by air drying the suspension on a silicon wafer.

3. Results and Discussion

The iridium nanoparticles, synthesized by gamma irradiation at various absorbed doses, were uniformly deposited onto the surface of MWCNT (as presented Figure 1). These nanoparticles were firmly attached to the nanotubes, as they were not removed

during the washing, sonication, and centrifugation steps used to remove the excess of surfactant. No nanoparticles were found on the MWCNT before irradiation (see Figure 1 a)). Iridium nanoparticles with an average size of 4.5 ± 1.0 nm where obtained after irradiation at 20 kGy. Additional nanoparticles were deposited on the nanotubes and the mean particle size decreased down to 3.4 ± 0.7 nm when the dose was increased from 20 kGy to 60 kGy. We hypothesize that the sequence of events to obtain Ir metallic nanoparticles is as follows: strong reducing agents such as electrons in aqueous solution (e_{-aq}) and $H^{\cdot}$ were homogeneously generated in the solution during the gamma irradiation. This was accompanied by the production of $OH^{\cdot}$ species, which are strong oxidizing agents. This radical was scavenged in our experiments using isopropanol, which results in the formation of the radical $(CH_3)_2\dot{C}OH$, a powerful reducing agent. Thus, the $(IrCl_6)^{-2}$ ions in the solution are subjected to a reducing environment that brings Ir(IV) to Ir(0) valence state. As the Ir(0) atoms were produced, they become deposited on the MWCNTs surface, creating seeds for subsequent nanoparticle growth. A significant amount of precursor was consumed during the nucleation process when the irradiation dose was increased. As a result, a large number of nanoparticles was generated and fewer ions contributed to the nanoparticle growth.

The influence of both precursor and surfactant concentrations on the final MWCNT/Ir production was studied. Figures 2 a) and b) reveal Ir nanoparticles on MWCNT that were synthesized using concentrations of Ir/SDS of 3 mM / 0.03 M and 6 mM / 0.03 M, respectively. An increase in precursor concentration from 3 to 6 mM led to a higher concentration of nanoparticles on the nanotubes. The particles size was not significantly affected, i.e. 3.8± 0.4 nm and 3.4±0.7 nm respectively. Additionally, some Ir

nanoparticle aggregates were observed at higher concentrations of SDS. Figure 2 c) reveals Ir nanoparticles obtained with an Ir/SDS concentration of 3 mM / 0.06 M, this increment in surfactant resulted in a reduction of the particle's size down to 2.5 ±0.4 nm.

An X- ray diffraction of the MWCNT/Ir is illustrated in Figure 2 d). The diffraction pattern in this image reveals that the peaks at 2θ = 40.9, 45.8, 69.0 and 83.0 correspond to Metallic Iridium (Ir PDF 00-006-0598) with a face centered cubic structure. Peak broadening in the XRD pattern was produced by the nanocrystalline structure of the metallic The 002 graphite peak from the MWCNT was also present at 2θ = 25.9. In the high resolution TEM (HRTEM) image presented in Figure 2 e), the lattice parameter was measured giving d_{111}=0.22 ± 0.02 nm, which correspond to metallic iridium. This confirmed the XRD results.

High resolution XPS for C, O and Ir is presented in Figure 3. For C1s, the first two peaks at a low binding energy (BE) correspond to C1s sp2 and C sp3 hybridizations. The BE around 286 and 290 eV corresponds to hydroxyl (C-OH), and carboxyl (COOH) groups, respectively. No additional peaks were detected from Ir-C interaction. The O1s exhibits BE at approximately 533 eV indicating O–C bonds in ethers and phenols. The BE at about 532 eV corresponds to the O=C bonds in quinines, ketones and aldehydes [13]. An additional low intensity peak observed at 529.9 eV was found to be associated to Ir-O interaction. The Ir 4f was fitted for the 4f7/2 and 4f5/2 states, where the two components Ir(0) at both 61.3 and 64.2 eV and Ir(IV) at both 62 and 64.2 eV were present.

4. Conclusions

Iridium nanoparticles were synthesized and deposited on MWCNT using gamma irradiation. The nanoparticles were found to be well distributed on the nanotubes. The concentration of nanoparticles was found to increase as the absorbed dose increased from 0 kGy to 60 kGy. The particle size did not change when the precursor concentration was increased from 3 mM to 6 mM. However, an increase of both absorbed dose from 20 to 60kGy and surfactant concentration from 3 mM to 6 mM led to a reduction in particle size. No evidence of Ir-C interaction from the XPS spectra was identified, but a weak Ir-O peak was observed. This may imply that the interaction of the Ir nanoparticles with the nanotubes occurs through oxygenated sites on their surface.

Acknowledgements

The authors thank Dr. Stoyan Toshkov at the Nuclear, Plasma, and Radiological Engineering Department at the University of Illinois for sample irradiation. Thanks to the Materials Research Center (MRC) and Energy Research Development Center (ERDC) at Missouri S&T for their financial support. This work was supported by NRC radiochemistry grant PPR-NRC-38-10-966

References

[1] Menezes, W.G., Zielasek, V., Thiel, K., Hartwig, A, Bäumer, M. Journal of Catal. 299 (2013), pp. 222-231.

[2] Grégory Guisbiers, Gulmira Abudukelimu, Djamila Hourlier. Nanoscale Res. Lett. (2011) 6:396.

[3] Hills, Charles W., Nathan H. Mack, and Ralph G. Nuzzo. The J. of Phys. Chem. B 107.12 (2003). pp. 2626-2636.

[4] Lu, J., Aydin, C., Browning N. D., Wang L., Gates, B. C. Catal. Lett. 142 (2012), pp. 1445–1451.

[5] Kuznetsovaa, L. I., Kuznetsovaa N. I., Koscheeva, S. V., Zaikovskiia, V. I., Lisitsyn, A. S., Kaprielovaa, K. M., Kirillova, N. V., Twardowskib Z. Appl. Catal. A: General 427– 428 (2012), pp. 8– 15.

[6] Bernas, H., Simakova, I., Prosvirin, I. P., Maki-Arvela, P., Leino, R., Murzin, D. Yu. Catal Lett. 142 (2012), pp. 690–697

[7] Rueping, M., Koe nigs, R. M., Borrmann, R., Zoller, J., Weirich, T. E., Mayer, J. Chem. Mater. 23 (2011), 2008–2010

[8] Georgakilas, V., Gournis D., Tzitzios, V. Pasquato, L. Guldie, D. M., Prato, M. J. Mater. Chem. 17 (2007), 2679–2694.

[9] Belloni J., Mostafavi, M., Remita, H., Marignier, J.-L., and Delcourt, M.-O. New J. Chem. 1998. pp. 1239-1255.

[10] Rojas, J.V., Castano, C.H. Rad. Phys. and Chem. 81 (2012), pp. 16-21.

[11] Rojas, J.V., Castano, C. H. In Radiation Synthesis of Materials and Compounds. CRC Press, (2013). pp. 491 -503. Kharisov, B. I. Kharissova, O. V., Mendez, U (Eds.).

[12] Appleby, A., Schwarz, H. A. 1969. J. Phys. Chem. 73 (6), pp. 1937–1941.

[13] Stobinski, L., Lesiak, B., Kövér, L., Tóth, J., Biniak, S., Trykowski, G. Judek, J. J. Alloy. Compd. 501 (2010), pp. 77–84.

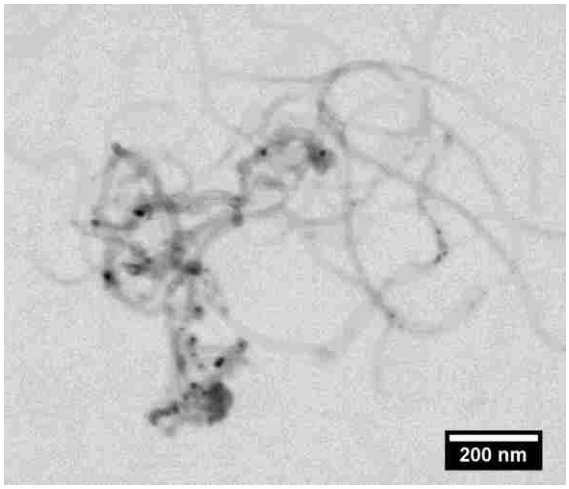

(a)

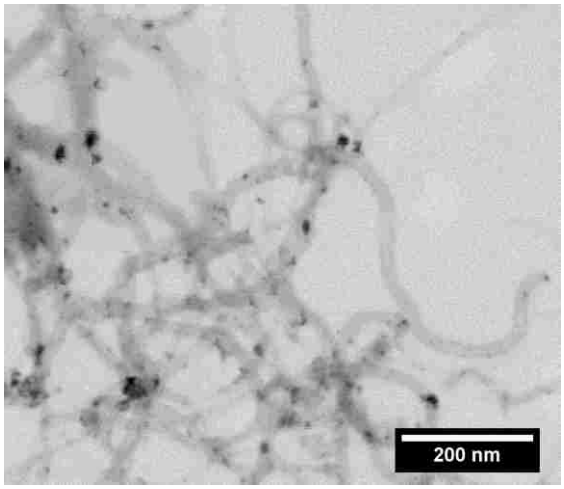

(b)

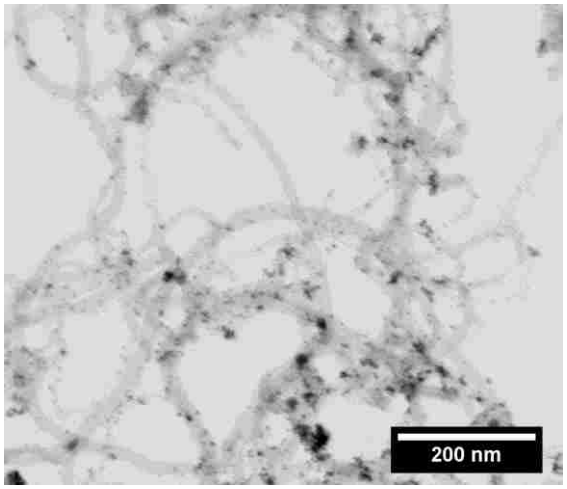

(c)

Figure 1. STEM images of MWCNT/Ir with concentrations of $HIrCl_6$ and SDS of 3 mM and 0.03 M, respectively. Each was irradiated with a) 0 kGy, b) 20 kGy, and c) 60 kGy.

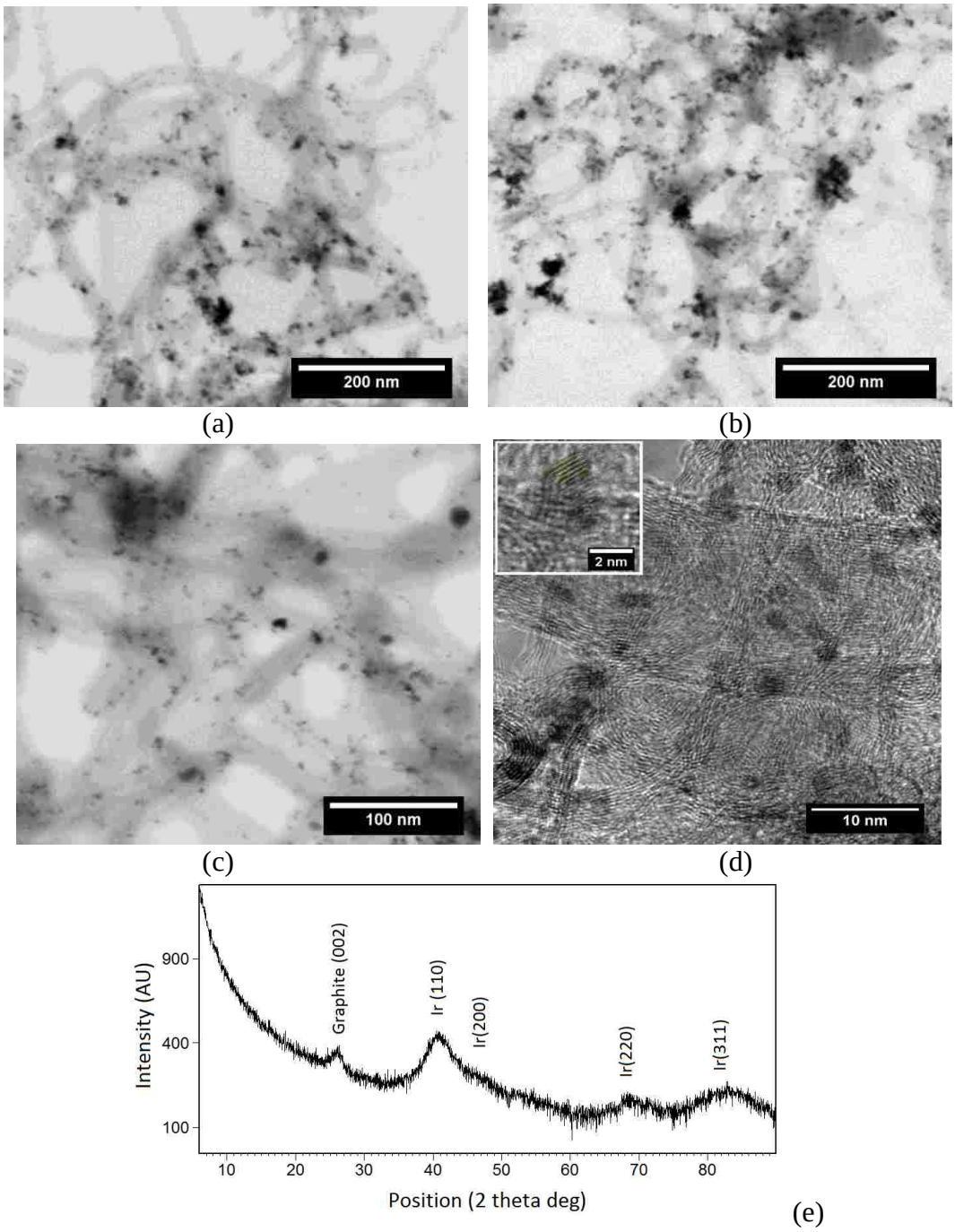

Figure 2. (a-c) STEM images of MWCNT/Ir with concentrations of Ir/SDS at a) 3 mM / 0.03 M, b) 6 mM / 0.03 M, and c) 3 mM / 0.06 M. d) and e) XRD pattern and HRTEM of MWCNT/Ir with Ir/SDS 6 mM / 0.03 M, respectively. The samples were irradiated with 60 kGy.

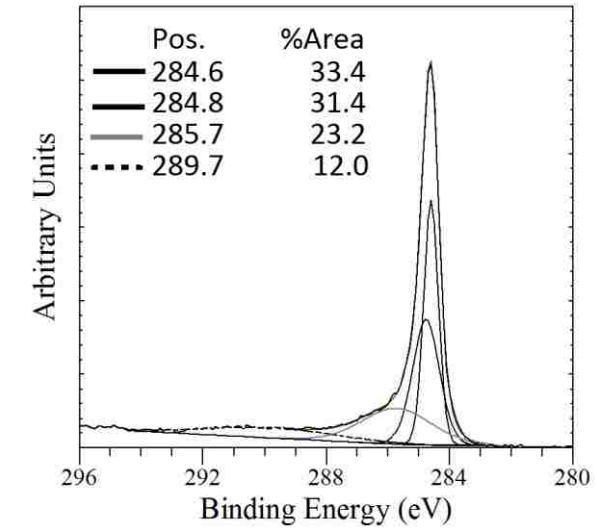

(a)

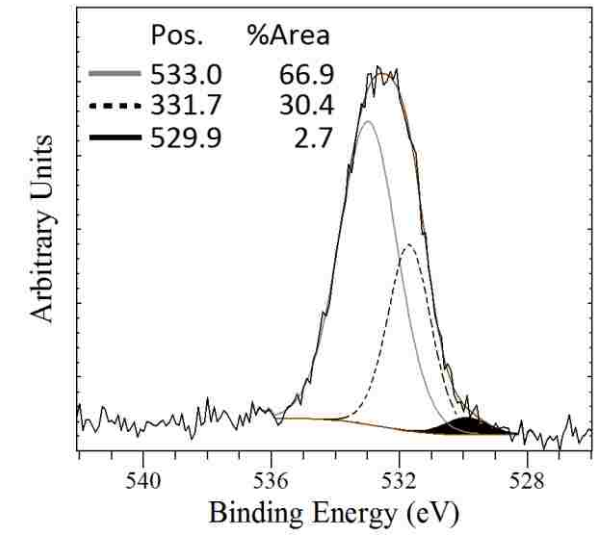

(b)

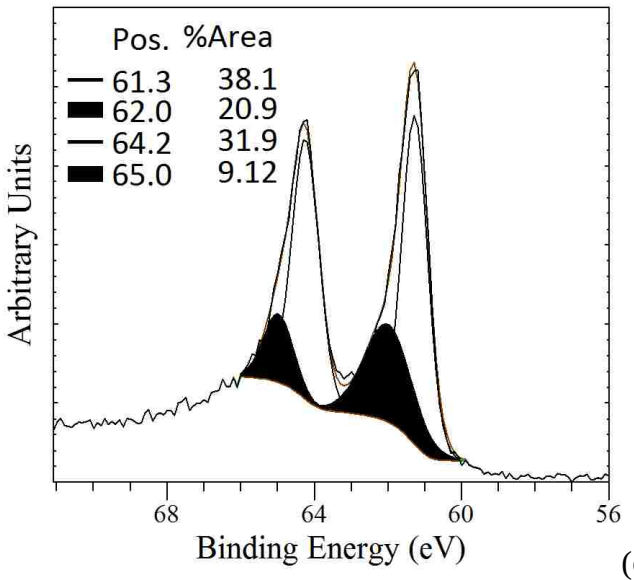

(c)

Figure 3. High resolution XPS for peaks a)C1s, b)O1s and c)Ir4f.

V. SYNTHESIS AND CHARACTERIZATION OF LANTHANUM PHOSPHATE NANOPARTICLES AS CARRIERS FOR RADIUM ISOTOPES

(Manuscript in preparation)

Abstract

Targeted alpha therapy has the potential for killing specific tumor cells with minimum damage to surrounding tissue. Radionuclides such as ^{225}Ra and ^{223}Ra are of special interest for this purpose as they emit multiple alpha particles during their decay. The use of appropriate carriers that are able to retain not only the parent isotope but their daughter products is important for the isotope delivery to the tumor site. In this work, core and core-shell nanoparticles of $LaPO_4$ were used to encapsulate the radium isotopes ^{223}Ra and ^{225}Ra. The synthesis of lanthanum phosphate containing ^{223}Ra and ^{225}Ra isotopes was carried out in aqueous media using a precipitation method. The NPs crystallized in rhabdophane structure with a mean particle size of 3.4 nm and 6.3 nm for core and core-2shells, respectively. The ability of $LaPO_4$ NPs to retain the isotopes within their structure was investigated. It was found that core NPs retained up to 88% of the activity over a period of 35 days. It was also found that the addition of two $LaPO_4$ shells to the core NPs increased the retention ability up to 99.9%. This fact suggests that $LaPO_4$ NPs are potential carriers of radium isotopes for targeted alpha therapy.

1. Introduction

Recent advances in nanotechnology have shown the potential use of nanomaterials as carriers for radioisotopes in targeted radioimmunotherapy (RIT),

targeted alpha therapy (TAT), and medical diagnostic imaging [1]. This approach aims to overcome the global radiotoxicity of the radionuclides and associated daughters, one of the main limitations of TAT [2-5]. Synthesis of biocompatible nanomaterials has become essential for the design and fabrication of drug delivery and imaging systems [6]. Inorganic nanomaterials are of special importance due to their size-shape dependent properties that make them suitable for a variety of applications. In this group of nanomaterials, lanthanide phosphates possess remarkable physical and chemical properties that are well-suited for biomedical applications [7-9].

Lanthanide phosphates, besides their favorable luminescent properties, are stable in aqueous media and relatively non-toxic [9]. These materials are also known for their high resistance to radiation damage [10, 11]. Lanthanide phosphate NPs are therefore promising candidates as carriers of α and β emitters in RIT, TAT, and imaging applications [1-4, 8, 9]. Recent investigations have been conducted to sequester decay products of the α-emitter ^{225}Ac using $LnPO_4$ (Ln = La, Gd) in core-shell nanostructures [2-4]. The results [5] showed that core NPs of approximately 5 nm in diameter retained more than 99.9% of ^{225}Ac and about 50% of the decay daughters (^{221}Fr and ^{213}Bi). Further work on this system [2-4] has shown that the addition of shells to the NPs improves the retention of the daughters. Adding four shells of $GdPO_4$, increased the retention of the ^{221}Fr daughter from 50% to 98% initially. Daughter retention (for both ^{221}Fr and ^{213}Bi) then stabilized at 88% over the course of a week. This retention is a tremendous improvement over conventional chelation approaches where a radionuclide is coupled to a monoclonal antibody through a chelating molecule such as linear or cyclic polyamino carboxylate ligands (eg. diethylene triamine pentaacetic acid (DTPA) or

1,4,7,10-tetraazacyclododecane-1,4,7,10-tetraacetic acid (DOTA)), which releases all daughters from α -emitting radionuclides *in vivo* [12-14].

The isotopes ^{223}Ra, ^{224}Ra, ^{225}Ra are also promising candidates for alpha therapy [15-21] . During their decay, a total energy of about 28 MeV is released and about 94% of this energy is associated to four sequentially emitted alpha particles (Figure 1). The US Food and Drug Administration (FDA) recently approved the use of ^{223}Radium, marketed as Alpharadin® or Xofigo®, for the treatment of patients with prostate cancer and symptomatic bone metastases [22]. The effectiveness of this treatment is due to the high affinity of radium with calcium, the main constituent of bone tissue but limits the usefulness to target other tissues. Thus, the selection of appropriate carriers for ^{223}Ra is required. Investigations on the potential usefulness of liposomes with an approximate diameter of 120 nm showed retention of ^{223}Ra up to 93% after 100 hours in serum [15, 16]. Also, recent work on the use of the NaA nanozeolite particles of approximately 100 nm, to carry radium radionuclides has been reported [18]. In this work, the ability of core and core-shell lanthanum phosphate nanoparticles to retain both ^{223}Ra and ^{225}Ra radium isotopes within their lattice structure was studied.

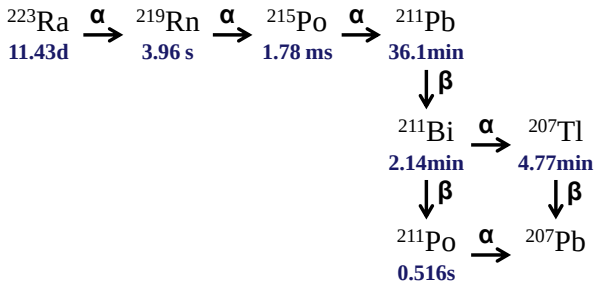

Figure 1. a) ^{223}Ra decay scheme and b) ^{225}Ra decay scheme.

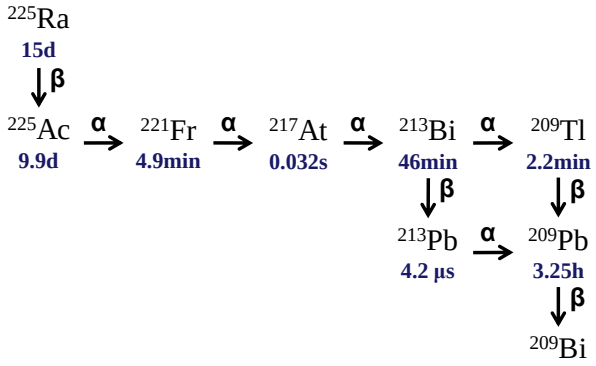

Figure 1. a) 223Ra decay scheme and b) 225Ra decay scheme (cont).

2. Materials and methods

2.1. Materials

Lanthanum nitrate ($La(NO_3)_3$) and sodium tripolyphosphate ($Na_5P_3O_{10}$) were purchased from Sigma-Aldrich. The chemicals were of analytical chemical grade and were used without any further purification. Deionized water from an 18MΩ MilliQ system was used to prepare the solutions. A Spectra/Por 10 kDa molecular weight cutoff (MWCO) regenerated cellulose dialysis membrane was used purify the nanoparticles after the synthesis process. The membranes were previously soaked in water for 10 min to remove the glycerine. Then, it was rinsed thoroughly in DI water.

2.2. Samples preparation

Radioactive core lanthanum phosphate nanoparticles

The synthesis of lanthanum phosphate ($LaPO_4$) nanoparticles containing the radioisotope ^{223}Ra (or ^{225}Ra) was carried out by adapting an aqueous route reported elsewhere [7, 8]. Initially, a solution containing the specific isotope was allowed to dry

under mild conditions in a 5 ml V-bottom glass vial. Next, 500µL of 0.1M lanthanum nitrate was added into the vial and vortexed to disperse radioactive species in the solution followed by the addition of 500 µL of 0.1M sodium tripolyphosphate. The mixture was vortexed until it appeared clear and colorless. The solution was then heated at 90 °C for 3 hours under continuous stirring. The resulting white and turbid colloidal suspension of lanthanum phosphate was cooled and dialyzed for 1 day against deionized water to remove the excess of ions and phosphate species.

Radioactive core-shell lanthanum phosphate nanoparticles

The suspension of core $LaPO_4$ nanoparticles were collected after dialysis and dispersed into a solution containing 500 µL 0.1 M of lanthanum nitrate and 1 mL of tripolyphosphate (molar ratio La:TPP of 1:2) . The solution was vortexed and heated at 90 °C for 3 h. The addition of a second shell was done following the same process. Finally, the core-2 shells nanoparticles were collected via centrifugation and purified by dialysis. The supernatant was saved and assayed for radioactivity.

Non-radioactive core, core-1 shell and core-2 shells $LaPO_4$ nanoparticles were synthesized by following the same procedure in the absence of the radioisotope for characterization purposes.

2.3. Characterization

The morphology and crystalline structure of the resulting nanoparticles were evaluated with a transmission electron microscope TEM Zeiss Libra 120 at 120 kV. The suspensions were initially diluted in deionized water and sonicated for 30 minutes.

Subsequently, a drop of the suspension was directly deposited a formvar-carbon coated copper grid. The sample was allowed to dry at room temperature.

X-Ray diffraction (XRD) was used to characterize the crystalline structure of the resulting nanoparticles. A Panalytical x pert pro MPD diffractometer with Cu Kα radiation operated at 45 kV and 40 mA, with the PW 3071 sample stage and X'celerator detector was used for analysis.

2.4. Radioactivity measurements

Gamma-ray spectroscopy was carried out using a high purity germanium detector (HPGe). In order to determine the amount of each radioactive species and their daughters leaking from the $LaPO_4$ nanoparticles, they were dialyzed against deionized water (18MΩ) under continuous stirring. Then, a 5 ml aliquot from the dialysate was collected periodically and assayed for radioactivity. Activity measurements were corrected for radioactive decay and volume lost due to previous aliquot removals from the dialysate. The gamma-rays energies and intensities used to determine the activities of ^{223}Ra and ^{225}Ra were 269.46 keV with 13.9% and 40.23 keV with 30.0%, respectively. The activity of ^{221}Fr was determined by its 218 keV gamma-ray with an intensity of 11.6%. The aliquot was measured 2 h after removal from the dialysate and the ^{221}Fr gamma ray was also used to calculate the activity of ^{225}Ac.

2.5. Preliminary analysis of the radioactive samples

Three different solutions containing the radioisotopes ^{223}Ra were used for the synthesis of the radioactive core and core-2 shells nanoparticles. The solutions were

initially characterized with gamma-ray spectroscopy to determine the activities of the main components; for this purpose, 5 µL were taken from the stock solution and counted for 5 minutes. The calculated activities are listed in Table 1, where sample 1 was used for the synthesis of the core nanoparticles, 2 and 3 were used for the core-2 shells and its replica respectively.

Table 1. Activity of main isotopes in 5 µL of the stock solutions (ND: not detected)

Isotope	Energy KeV (%Intensity)	Type of decay	Average activity (µCi) ± %error		
			Sample 1	Sample 2	Sample 3
^{223}Ra	154.208 (5.70) 269.463(13.90) 323.871 (3.99)	α: 100%	2.11 ± 3.89	2.04 ± 1.62	3.52 ± 1.66
^{140}Ba	162.66 (6.22) 537.26 (24.39) 304.84 (4.29)	β^- : 100%	1.84±1.9	1.27±1.83	2.14±1.48
^{140}La	328.76 (20.3) 487.021 (45.5) 1596.21 (95.4)	β^- : 100%	2.17±1.99	1.30±1.19	0.15±3.66
^{136}Cs	340.547 (42.2) 818.514 (99.704) 1048.07 (80)	β^- : 100%	1.29±2.74	ND	ND
^{134}Cs	569.33 (15.37) 604.721(97.62) 795.864 (85.46)	β^- : 100%	0.562±4.92	ND	ND

3. Results

Size and size distribution of lanthanum phosphate nanoparticles

Figures 2 a) b) and c) show the TEM micrographs of lanthanum phosphate nanoparticles with core, core-1 shell and core-2 shells structure with their respective size distribution histogram. The core nanoparticles were found to have a diameter of 3.4 nm. Subsequent addition of $LaPO_4$ shells caused growth of the nanoparticles, as it can be seen from the histograms the mean size of the nanoparticles increases from 3.4 nm to 6.3 nm with the addition of two shells.

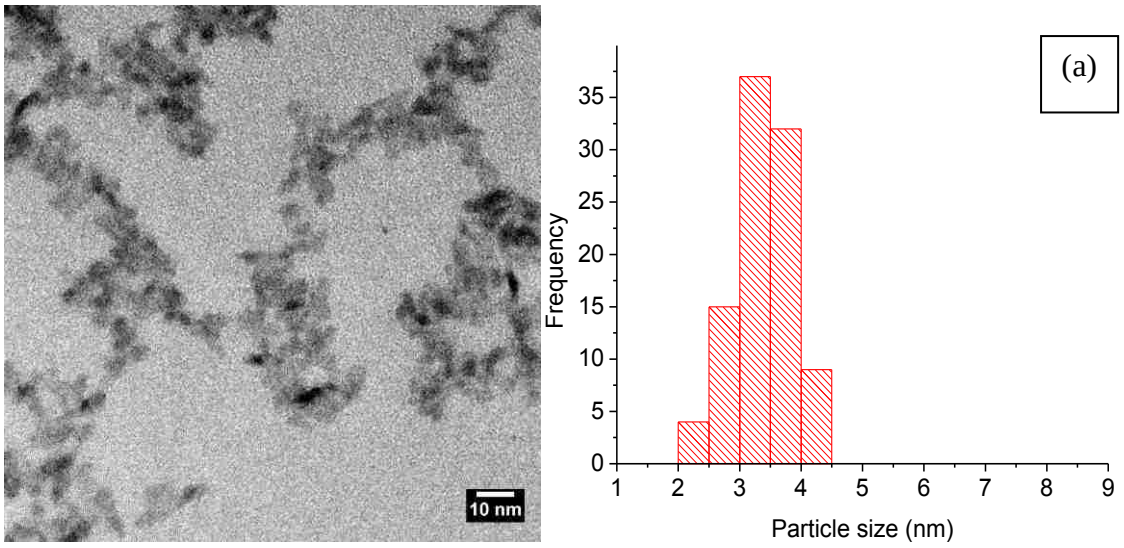

Figure 2. TEM micrographs of LaPO4 nanoparticles with their corresponding histograms for a) Core, b) Core-1 shell and c) Core-2 shells.

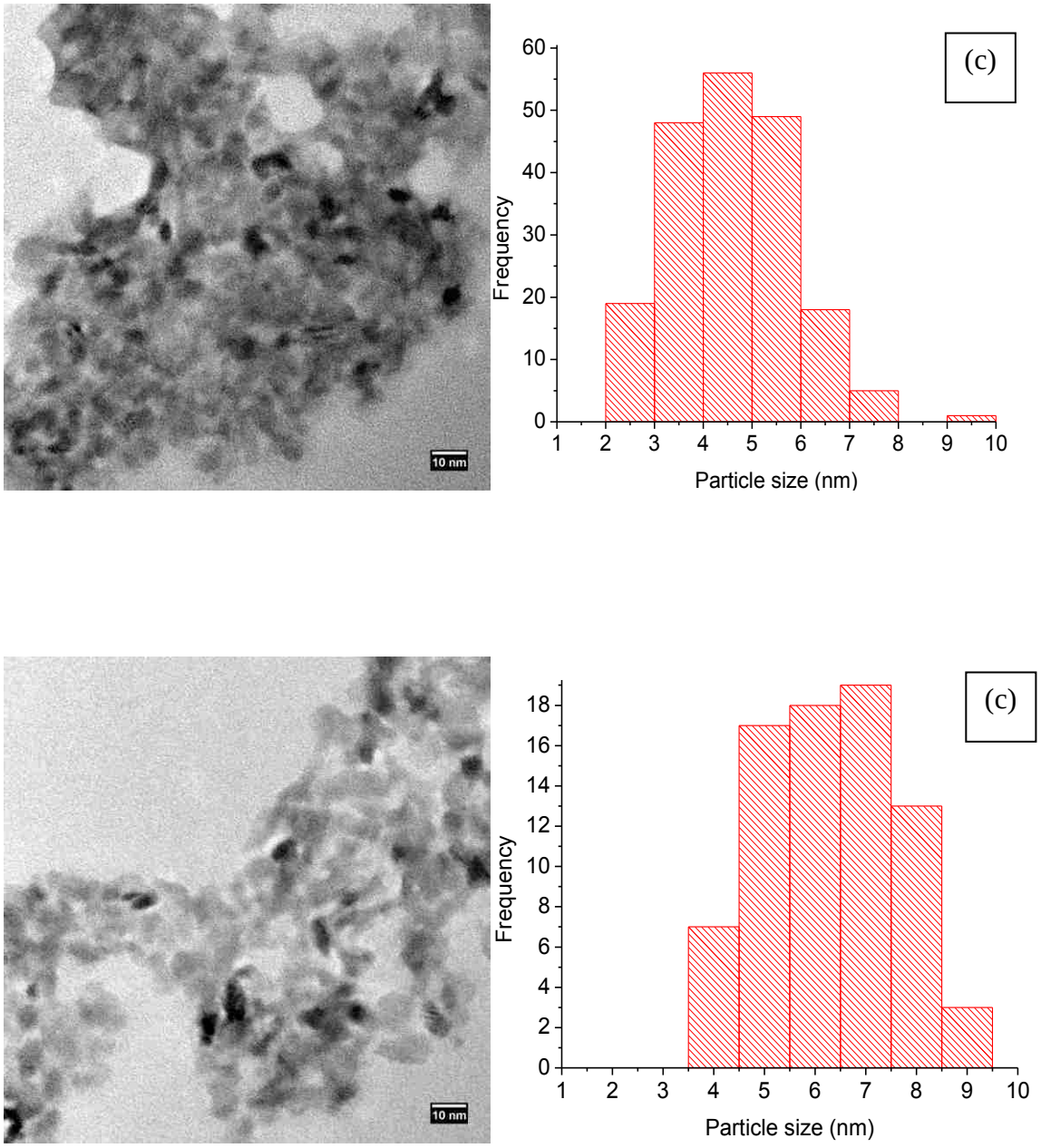

Figure 2 (cont). TEM micrographs of $LaPO_4$ nanoparticles with their corresponding histogram a) Core, b) Core-1 shell and c) Core-2 shells.

X-ray diffraction patterns for the core $LaPO_4$ nanoparticles aged at 90 °C for 3 h and 9 h are shown in Figure 3. The analysis revealed that the nanoparticles crystallized in rhabdophane phase (Powder Diffraction File (PDF) of the International Center of

Diffraction Data, reference number 46-1439, $LaPO_4.xH_2O$) that corresponds to the hydrated form of lanthanum phosphate. Longer reaction time (> 3 h) caused an improvement in the crystallinity of the nanoparticles and a small increase of the particle size. The successive addition of $LaPO_4$ shells to the core nanoparticles resulted in an increase of the average particle size which is observed from the peak sharpening in the diffraction patterns (Figure 4). The particle size estimated by the Scherrer equation were 3.8, 6.2 and 7.1 nm for core, core-shell and core-2 shells $LaPO_4$ nanoparticles, respectively. These values are in good agreement with the mean particle size found with TEM.

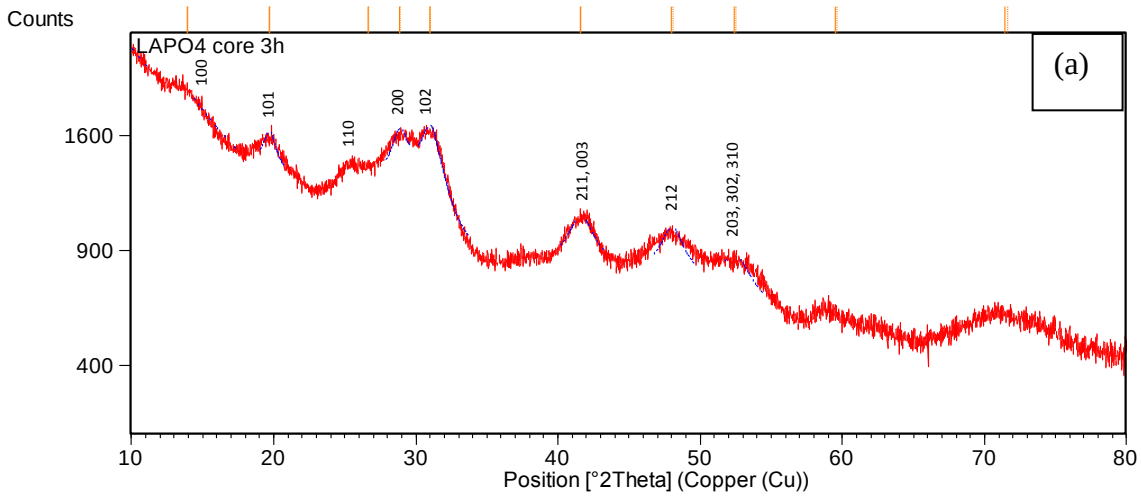

Figure 3. XRD pattern for core $LaPO_4$ nanoparticles aged for a)3 hours and b) 9 hours

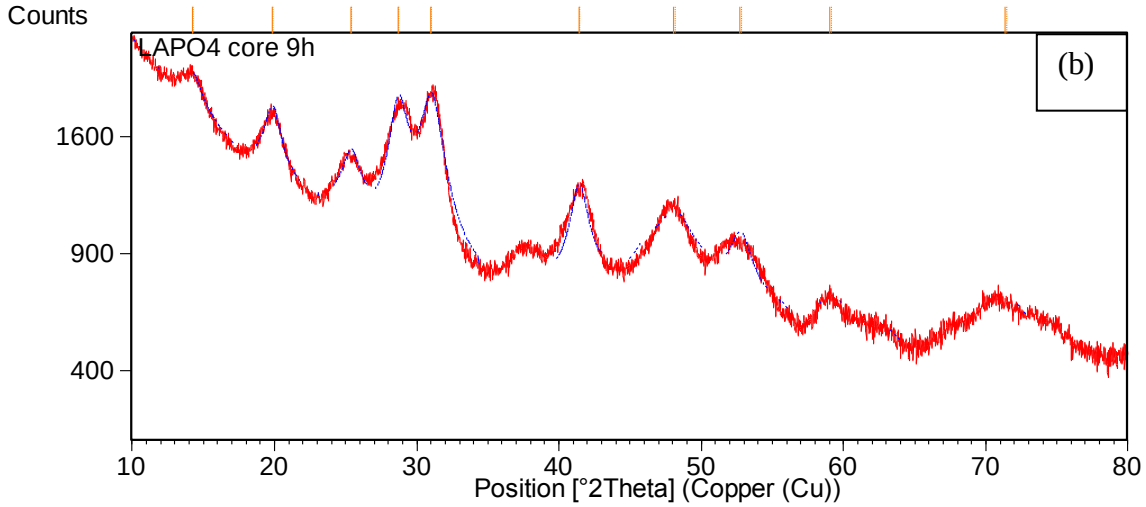

Figure 3. XRD pattern for core $LaPO_4$ nanoparticles aged for a)3 hours and b) 9 hours (cont).

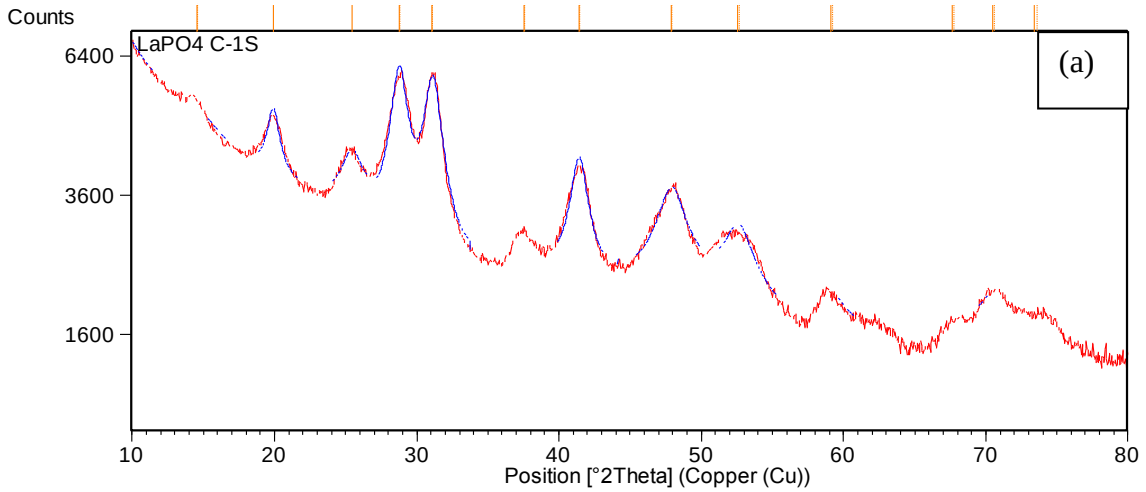

Figure 4. XRD pattern for a) core-1 shell $LaPO_4$ nanoparticles b) core-2 shells $LaPO_4$ nanoparticles

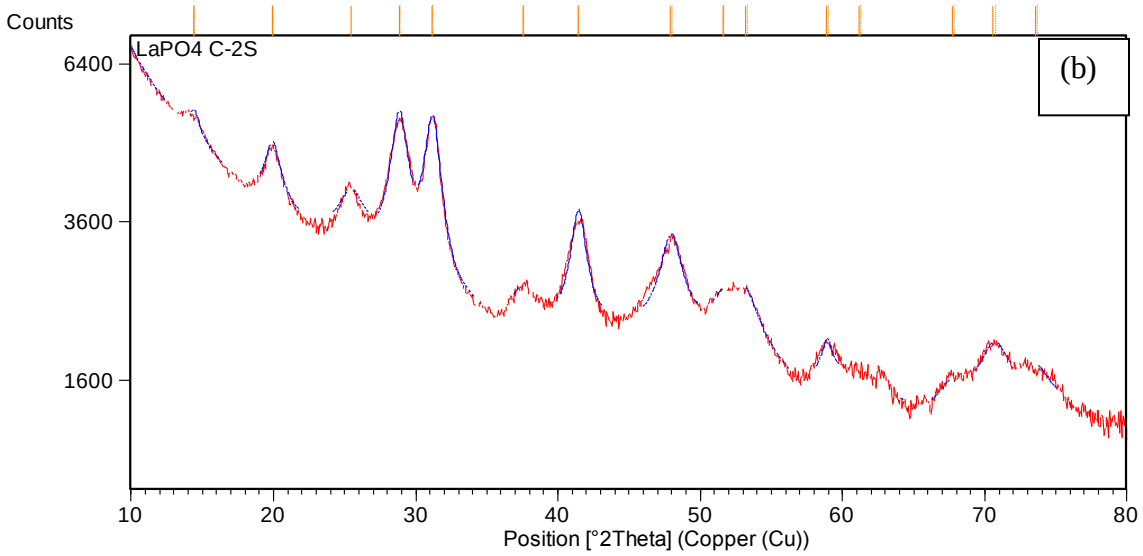

Figure 4. XRD pattern for a) core-1 shell $LaPO_4$ nanoparticles b) core-2 shells $LaPO_4$ nanoparticles (cont).

In-vitro release of ^{223}Ra, ^{211}Pb, ^{140}Ba, ^{140}La and ^{225}Ra from the lanthanum phosphate core and core-2 shells nanoparticles.

For the synthesis of the core $LaPO_4$ nanoparticles 10 µL from the stock solution 1 were used. This amount corresponds to ^{140}Ba and ^{223}Ra activities of 3.7 and 4.2µCi respectively. During the transferring process to the dialysis membrane 9% of the activity was lost between pipettes and synthesis vial. Thus, the final activity was found to be 3.3 and 3.8 µCi of ^{140}Ba and ^{223}Ra respectively. Aliquots collected periodically from the dialysate were measured and the activities of the different components were calculated. ^{140}Ba and ^{223}Ra in the dialysate were found to have a similar trend over time as shown in Figure 5. The activity percent of these isotopes in the dialysate increase gradually and, after 35 days reached a value of 11.5 and 12.7% of ^{140}Ba and ^{223}Ra respectively. ^{140}La

also increased up to 2.85%, this value was found to be a consequence of the decay of ^{140}Ba already present in the dialysate. Thus, leakage of ^{140}La form the core $LaPO_4$ nanoparticles is not appreciable. ^{211}Pb was found to be in equilibrium with ^{223}Ra in the dialysate as shown in Figure 5.

The isotopes ^{136}Cs and ^{134}Cs were also tracked in the dialysate and it was found that they are not retained in the nanoparticles lattice. After the first day of dialysis 89% and 97% of ^{136}Cs and ^{134}Cs activities were found in the dialysate.

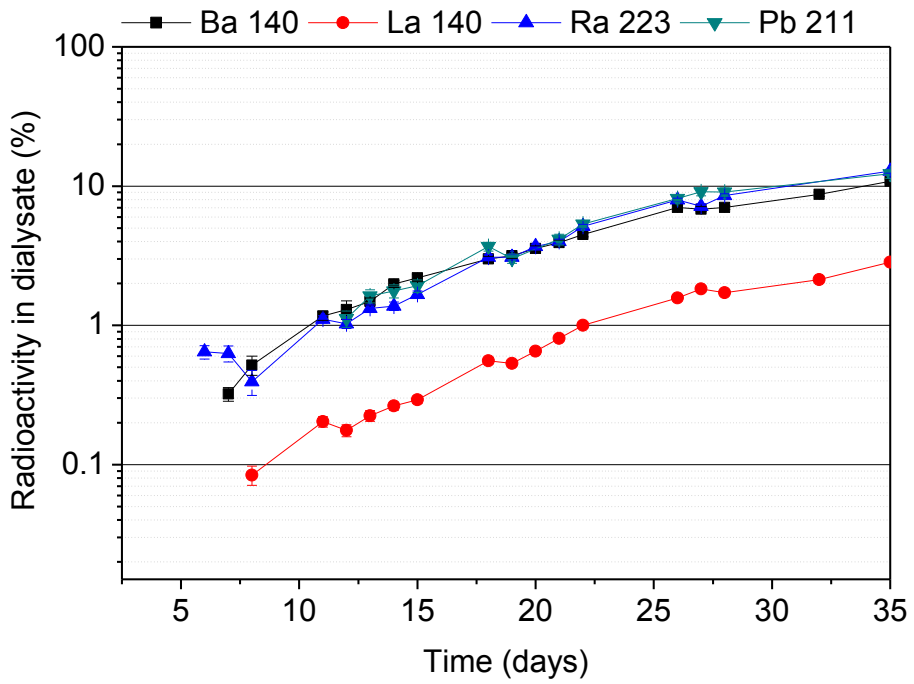

Figure 5. *In*-vitro release of ^{223}Ra, ^{211}Pb, ^{140}Ba, ^{140}La from the $LaPO_4$ core nanoparticles

Synthesis of the core-2 shells nanoparticles was carried out with a total activity ^{140}Ba and ^{223}Ra of 76.4 and 122 μCi respectively. During the synthesis process ~15% of the initial activity is lost distributed among dialysis bags, pipettes, synthesis vials, and centrifuge vials. The addition of 2 shells on the surface of the core nanoparticles reduced the leakage of the isotopes to less than 1.5% for ^{223}Ra and 0.6% for ^{140}Ba after 30 days (Figure 6). During the synthesis of the radioactive core nanoparticles used in this experiment, a white precipitate was observed when the lanthanum and phosphate precursors were mixed with the dried radioactive material, presumably due to presence of impurities in the radioactive solution. Thus larger particles might have formed which could lead to a non-uniform growth of the shells, leading to overrated values of isotopes leakage from the nanostructure.

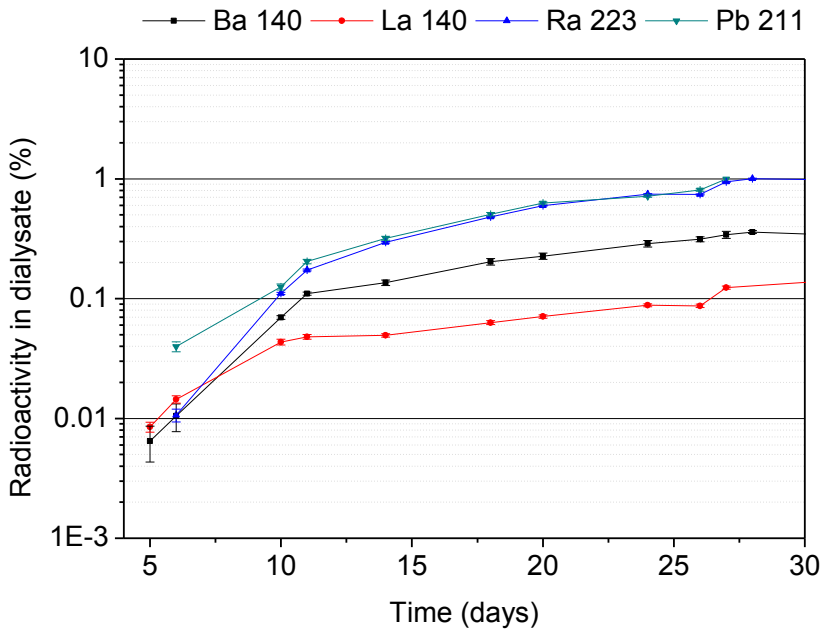

Figure 6. *In*-vitro release of ^{223}Ra, ^{211}Pb, ^{140}Ba, ^{140}La from the $LaPO_4$ core-2shells nanoparticles

In order verify the measurements obtained in the first experiment, a replica of the radioactive core- 2 shells was carried out. In this case a total activity ^{140}Ba and ^{223}Ra of 42.7 and 70.3 μCi, respectively, was used. During the synthesis ~20% of the initial activities were lost. As it can be observed in Figure 7, the fraction of ^{140}Ba and ^{223}Ra was found to be less than 0.04% over a period of 27 days. The evident reduction of isotope release from the core-2 shells nanoparticles compared with the first experiment could be associated to a well-controlled synthesis process that lead to a uniform growth of the $LaPO_4$ shells.

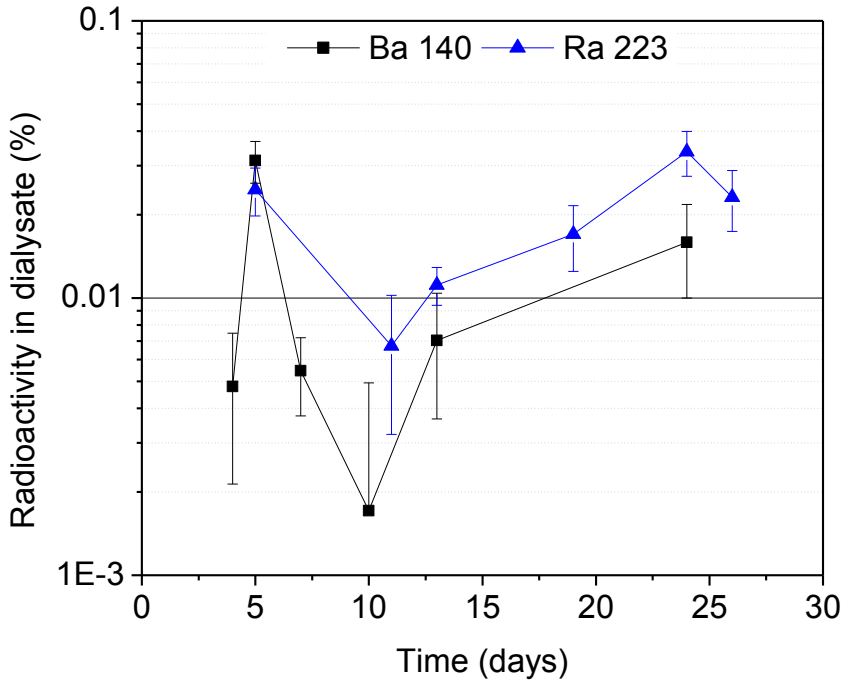

Figure 7. *In*-vitro release of ^{223}Ra, and ^{140}Ba, from the $LaPO_4$ core-2shells nanoparticles (replica)

Core-2 shells nanoparticles containing $^{225}Ra/^{225}Ac$ were also synthesized in order to evaluate the behavior or ^{225}Ra in nanostructure. During the synthesis process approximately 15% of the initial activity was lost and the final activities of the isotopes $^{225}Ra/^{225}Ac$ in the core-2 shells nanostructure were found to be 44.4 and 53.4 μCi respectively. The behavior of ^{225}Ra and ^{225}Ac in the dialysate is shown in Figure 8; the fractions of ^{225}Ra and ^{225}Ac isotopes were less than 0.02% over a period of 35 days.

The isotope ^{221}Fr, decay products of ^{225}Ac was also tracked during the process. For quantification purposes, the time duration between withdrawal of the sample from the dialysate and the start of the measurement was recorded. Subsequently a set of measurements were collected every minute. This information was fed into the software CLSQ (*least squares decay*-curve analysis program routine) [9] to determine the activity of ^{221}Fr and ^{213}Bi in the dialysate. The fraction of this isotope released from the nanoparticles reached a value of 20% (80% retention) after 35 days as shown in Figure 8. Previous work on the retention of ^{225}Ac, ^{221}Fr and ^{213}Bi on lanthanum/gadolinium phosphate nanoparticles ($\{La_{0.5}Gd_{0.5}\}PO_4$) have reported an increase in the retention ^{221}Fr daughter with the addition of $GdPO_4$ shells; 2 shells increased retention from 50% (for the $LaPO_4$ core) to 70% and, with four shells of $GdPO_4$, the initial retention of the ^{221}Fr daughter was 88% after the course of a week.

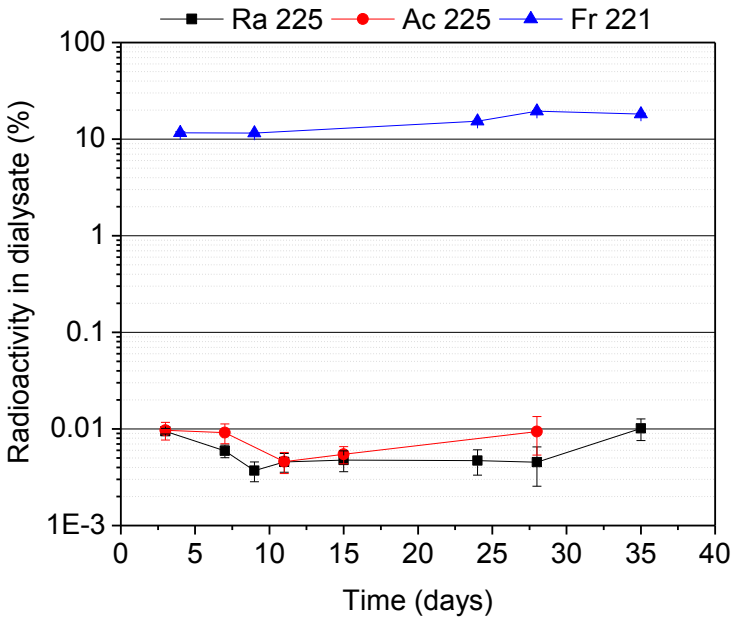

Figure 8. *In*-vitro release of ^{225}Ra and ^{225}Ac and ^{221}Fr.

This work makes evident the potential use of lanthanum phosphate nanoparticles to encapsulate radium isotopes. The addition of two shells to the surface of core lanthanum phosphate nanoparticles reduced the release of radium to less than 0.1%. This system could, therefore, become a potential candidate for targeted alpha therapy.

4. Conclusions

In this work lanthanum phosphate core and core-shells nanoparticles were doped with ^{223}Ra and ^{225}Ra in order to evaluate their ability to retain the isotopes. The $LaPO_4$ nanoparticles crystallized in rhabdophane structure with a mean particle size of 3.4 nm and 6.3 nm for core and core-2shells respectively. Core nanoparticles were found to retain in ~88% of the activity over a period of 35 days. The addition of two shells

reduced notoriously the release of the isotopes over time. Surface functionalization of the nanostructures and *in vivo* studies would be needed to further evaluate the potential use of radium-containing $LaPO_4$ nanoparticles for targeted alpha therapy.

References

[1] Zhang L, Chen H, Wang L, Liu T, Yeh J, Lu G, et al. Delivery of therapeutic radioisotopes using nanoparticle platforms: potential benefit in systemic radiation therapy. Nanotechnol Sci Appl. 2010;3:159-70.

[2] McLaughlin MF, Robertson D, Pevsner PH, Wall JS, Mirzadeh S, Kennel SJ. LnPO4 nanoparticles doped with Ac-225 and sequestered daughters for targeted alpha therapy. Cancer Biother Radiopharm. 2014;29:34-41.

[3] McLaughlin MF, Woodward J, boll RA, Rondinone AJ, Mirzadeh S, Robertson JD. Gold-coated lanthanide phosphate nanoparticles for an 225Ac in vivo alpha generator. Radiochim Acta 2013;101:595-600.

[4] McLaughlin MF, Woodward J, Boll RA, Wall JS, Rondinone AJ, Kennel SJ, et al. Gold Coated Lanthanide Phosphate Nanoparticles for Targeted Alpha Generator Radiotherapy. Plos One. 2013;8:1-8.

[5] Woodward J, Kennel SJ, Stuckey A, Osborne D, Wall J, Rondinone AJ, et al. LaPO4 nanoparticles doped with actinium-225 that partially sequester daughter radionuclides. Bioconjug Chem. 2011;22:766-76.

[6] Barreto JA, O'Malley W, Kubeil M, Graham B, Stephan H, Spiccia L. Nanomaterials: applications in cancer imaging and therapy. Adv Mater. 2011;23:H18-40.

[7] Buissette V, Moreau M, Gacoin T, Boilot JP. Luminescent Core/Shell Nanoparticles with a Rhabdophane LnPO4-xH2O Structure: Stabilization of Ce3+-Doped Compositions. Advanced Functional Materials. 2006;16:351-5.

[8] Buissette V, Moreau M, Gacoin T, Boilot JP, Chane-Ching J-V, Mercier TL. Colloidal Synthesis of Luminescent Rhabdophane LaPO4:Ln3+,xH2O (Ln) Ce, Tb, Eu; x ≈ 0.7) Nanocrystals. Chem Mater. 2004;16:3767-73.

[9] Meiser F, Cortez C, Caruso F. Biofunctionalization of fluorescent rare-earth-doped lanthanum phosphate colloidal nanoparticles. Angew Chem Int Ed Engl. 2004;43:5954-7.

[10] Grechanovsky AE, Eremin NN, Urusov VS. Radiation resistance of LaPO4 (monazite structure) and YbPO4 (zircon structure) from data of computer simulation. Physics of the Solid State. 2013;55:1929-35.

[11] Picot V, Deschanels X, Peuget S, Glorieux B, Seydoux-Guillaume AM, Wirth R. Ion beam radiation effects in monazite. Journal of Nuclear Materials. 2008;381:290-6.

[12] Davis IA, Glowienka KA, Boll RA, Deal KA, Brechbiel MW, Stabin M, et al. Comparison of 225Actinium Chelates: Tissue Distribution and Radiotoxicity. Nuclear Medicine & Biology. 1999;26:581–9.

[13] Henriksen G, Hoffa P, Larsen RH. Evaluation of potential chelating agents for radium. Applied Radiation and Isotopes. 2002;56:667-71.

[14] Miederer M, Scheinberg DA, McDevitt MR. Realizing the potential of the Actinium-225 radionuclide generator in targeted alpha particle therapy applications. Adv Drug Deliv Rev. 2008;60:1371-82.

[15] Henriksen G, Schoultz BW, Michaelsen TE, Bruland OS, Larsen RH. Sterically stabilized liposomes as a carrier for alpha-emitting radium and actinium radionuclides. Nucl Med Biol. 2004;31:441-9.

[16] Jonasdottir TJ, Fisher DR, Borrebaek J, Bruland OS, Larsen RH. First In Vivo Evaluation of Liposome-encapsulated 223Ra as a Potential Alpha-particle-emitting Cancer Therapeutic Agent. Anticancer Research. 2006:2841-8.

[17] Larsen RH, Saxtorph H, Mikala Skydsgaard, Borrebaek J, Jonasdottir TJ, Bruland OS, et al. Radiotoxicity of the Alpha-emitting Bone-seeker 223Ra Injected Intravenously into Mice: Histology, Clinical Chemistry and Hematology. in vivo. 2006;20:325-32.

[18] Piotrowska A, Leszczuk E, Bruchertseifer F, Morgenstern A, Bilewicz A. Functionalized NaA nanozeolites labeled with Ra for targeted alpha therapy. J Nanopart Res. 2013;15:2082.

[19] Gjermund H, Fisher DR, Roeske JC, Bruland ØS, Larsen aRH. Targeting of Osseous Sites with alpha emitting 223Ra- comparison with B emitter 89Sr in mice. The Journal of Nuclear Medicine. 2003;44.

[20] Kennel SJ, Lankford T, Garland M, Sundberg JP, Mirzadeh S. Biodistribution of 225Ra citrate in mice: retention of daughter radioisotopes in bone. Nucl Med Biol. 2005;32:859-67.

[21] Mulford DA, Scheinberg DA, Jurcic JG. The promise of targeted alpha particle therapy. The Journal of Nuclear Medicine. 2005;46:199-204.

[22] Kluetz PG, Pierce W, Maher VE, Zhang H, Tang S, Song P, et al. Radium Ra 223 dichloride injection: U.S. Food and Drug Administration drug approval summary. Clin Cancer Res. 2014;20:9-14.

[23] Cumming JB. CLSQ, the brookhaven decay curve analysis program. In: O'Kelly GD, editor. Application of computers to nuclear and radiochemistry. Washington: NAS-NRC; 1963.

SECTION

3. CONCLUSIONS

The main goal of this work was to study the synthesis of non radioactive and radioactive nanoparticles (NPs) through radiolytic and wet chemistry. Gamma irradiation was implemented as a single step method to synthesize non radioactive transition metal nanoparticles such as rhenium, iridium and rhodium unsupported or supported on polymeric matrices or carbon nanotubes. Wet chemistry was used to synthesize lanthanum phosphate ($LaPO_4$) nanoparticles containing radium isotopes. The synthesis or transition metal nanoparticles was carried out by irradiating solutions of water-isopropanol with a volume ratio of 2:1 containing the metal salt precursor in a specific concentration and, either polyvinyl-pyrrolidone (PVP) or multiwalled carbon nanotubes. During gamma irradiation of water, strong oxidizing and reducing species are produced. Thus, isopropanol was primarily added to scavenge the oxidizing species, generating an appropriate environment for the reduction of ionic metal precursors.

Irradiation of the solutions containing sodium pherrhenate as the rhenium precursor led to the nucleation and growth of amorphous rhenium oxide nanoparticles. Nanoparticles with average sizes ranging from 10 to 55 nm were obtained. In this case since no stabilizer was used, the average size of the nanoparticles was found to increase with the precursor concentration. The binding energy between two reduced species is stronger than the atom-solvent or atom-ligand bond energy, as a result the species tend to dimerize when they encounter or associate with an excess of ions. This effect contributed to the growth of the nanoparticles.

The synthesis of metallic iridium and rhodium nanoparticles through a radiolytic assisted method was carried out in the presence of polyvinyl-pyrrolidone (PVP). A homogeneous particle size distribution for both, iridium and rhodium, was obtained at the concentrations of Rh precursor / PVP of 6 mM / 0.3 mM and Ir precursor / PVP of 3 mM / 0.6 mM. It was found that at higher doses more homogeneous particle size distribution is obtained. At higher absorbed doses the majority of the metal ions would be consumed during the nucleation process which would lead to a narrow particle size distribution. The nanoparticles in PVP were found to be stable for more than 3 months. This stability was explained based on the interaction of iridium and rhodium with the PVP functional groups C-N and C=O.

Multiwalled carbon nanotubes were found to be a suitable support for iridium nanoparticles synthesized using gamma irradiation. This method of synthesis led to well distributed nanoparticles on the nanotubes with a narrow particle size distribution. The nanoparticle yield increased with increasing the concentration of the Ir precursor salt which is the result of more metal ions contributing to the nucleation process. In addition the concentration of nanoparticles also was found to increase with increasing absorbed dose from 0 to 60 kGy. At higher doses a larger concentration of reducing species was obtained which resulted in more metal ions being reduced to zero valence state and contributing to nucleation and growth of the nanoparticles on the nanotubes surface. The interaction between the Ir nanoparticles with the nanotubes occurs through oxygenated sites on their surface.

The synthesis of lanthanum phosphate containing ^{223}Ra and ^{225}Ra isotopes was carried out in aqueous media using lanthanum nitrate and sodium tripolyphosphate (TPP)

as sources of lanthanum and phosphate ions. The reaction was carried out at 90 °C for 3 hours. Sodium tripolyphosphate served as both, source of phosphate species and stabilizer agent to control the growth of the $LaPO_4$ nanoparticles. Layering of the nanoparticles was carried out by dispersing the nanoparticles in a mixture of La-TPP and heated for 3 hours. This process resulted in nanoparticles with rhabdophane crystalline structure having a mean particle size of 3.4 nm and 6.3 nm for core and core-2shells, respectively. The ability of $LaPO_4$ NPs to retain the isotopes within their structure was investigated. The core NPs retained up to 88% of the radium activity over a period of 35 days. The retention of the isotopes was further increased up to 99.99% by the addition of two $LaPO_4$ shells to the core NPs. The ability of $LaPO_4$ NPs to retain the radioisotopes within their structure positions this material as potential carrier of radium isotopes for targeted alpha therapy.

4. SUGGESTIONS FOR FUTURE WORK

This work evidenced the potential of gamma irradiation as single step method to synthesize transition metal nanoparticles with controlled particle size. It also demonstrated the ability of $LaPO_4$ NPs to retain up to 99.9% of radium isotopes within their structure making this material a promising option as carrier for targeted alpha therapy. There are two main points that may be further explored from this work. The first one is the synthesis of rhodium nanoparticles on carbon nanotubes using gamma irradiation. Preliminary work was carried out following the procedure explained in the manuscript "Radiolytic synthesis of iridium nanoparticles onto carbon nanotubes" and using sodium hexachlororhodate (Na_2RhCl_6) as source of rhodium ions. Using this method a bimodal distribution of rhodium nanoparticles with a mean size of 40 ± 9.6 nm and 12.2 ± 2 nm was obtained as shown in Figure 4.1. In order to obtain a more uniform particle size distribution different surfactants or stabilizers need to be explored.

The second point is to explore and develop the surface chemistry of lanthanum phosphate nanoparticles loaded with the ^{225}Ra or ^{223}Ra. While the methods to synthesize $LaPO_4$ NPs in aqueous media have been previously reported and their ability to retain the isotopes has been addressed, their surface chemistry and process for antibody conjugation are yet to be studied. In addition, further work on the comparison of the radiotoxicity of free vs. NP-bound $^{225}Ra/^{225}Ac$ and ^{223}Ra needs to be done.

Previous studies on the biodistribution of intravenously administered ^{225}Ra acetate demonstrate its toxicity from the daughter isotopes that relocate from the target organ (bones). Hence, binding of a radionuclide within an inorganic nanoparticle that possesses

multiple strong metal-oxide bonds should significantly reduce the unintentional release making the system a much less toxic alternative.

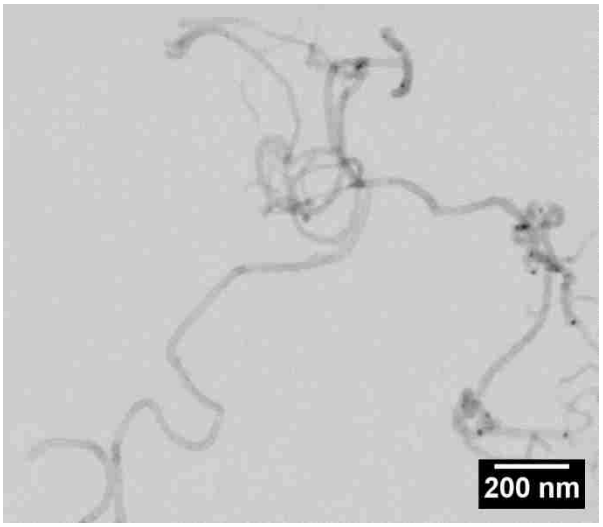

(a)

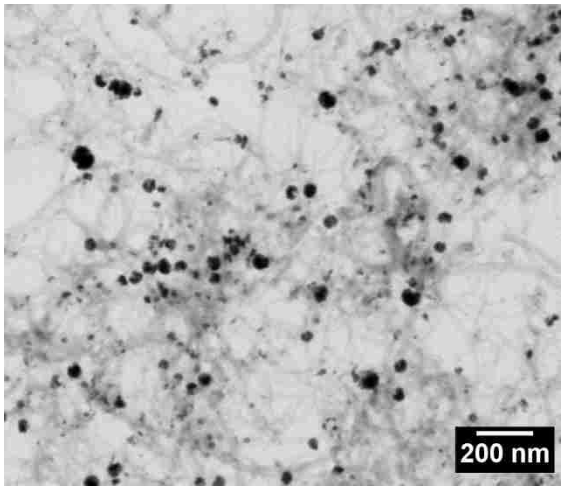

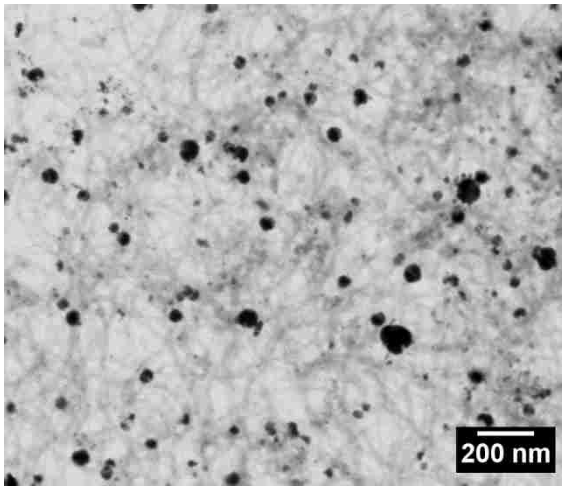

(b) (c)

Figure 4.1. STEM images of MWCNT/Rh with concentrations of Rh / SDS of a) 6 mM / 0.06 M after irradiation at 0 kGy, b) Rh / SDS 3 mM / 0.03 M 60 kGy and b) Rh / SDS 3 mM / 0.06 M 60 kGy

VITA

Jessika V. Rojas Marin was born in Medellin, Colombia. She was accepted into the Physics School at the National University of Colombia in 2001 and graduated in July 2006 with a Bachelors of Science in Engineering Physics. During her undergraduate, Jessika was a member of the Radiology group where she developed her thesis entitled "Dose quantification in mammography studies". In 2007, Jessika started a master in the School of Materials Engineering at the same University, and became a member of the Tribology and Surfaces group (GTS). Her research was focus on the identification and quantification of phases of ASTM A743 grade CA6NM cast martensitic stainless steel through high-temperature X-ray diffraction. Jessika graduated in 2009 with a Master in Engineering- Materials and processes. She then pursued a second Master degree in Nuclear Engineering at the Missouri University of Science and Technology, which was awarded in December 2011. In January of 2013, Jessika participated in a DOE funded internship program in Nuclear Engineering, at Oak Ridge National Laboratory (ORNL). While at ORNL, Jessika's research focused on the synthesis and evaluation of nanoparticles as carriers of therapeutic radionuclides, specifically on the synthesis of lanthanum phosphate nanoparticles containing medically useful isotopes of radium-223 and radium-225. In May 2014, Jessika graduated with her PhD in Nuclear Engineering.